ALMA MATER STUDIORUM
UNIVERSITÀ DEGLI STUDI DI BOLOGNA

DEPARTMENT OF ELECTRONICS, COMPUTER SCIENCES AND SYSTEMS

SCUOLA DI DOTTORATO IN BIOINGEGNERIA - CICLO XXIV
SETTORE CONCORSUALE: 09/G2
SETTORE SCIENTIFICO DISCIPLINARE DI AFFERENZA:
ING-INF/06

MODELS FOR THE STUDY OF CORTICAL ACTIVITY DURING COGNITIVE AND MOTOR TASKS

Filippo Cona

Supervisor

Prof. Mauro Ursino

Reviewers

Prof. Serenella Salinari

Dr. Rosalyn Moran

Ph.D. Coordinator

Prof. Angelo Cappello

Esame Finale Anno 2012

ALMA MATER STUDIORUM
UNIVERSITÀ DEGLI STUDI DI BOLOGNA

DEPARTMENT OF ELECTRONICS, COMPUTER SCIENCES AND SYSTEMS

SCUOLA DI DOTTORATO IN BIOINGEGNERIA - CICLO XXIV
SETTORE SCIENTIFICO DISCIPLINARE DI AFFERENZA:
ING-INF/06

MODELS FOR THE STUDY OF CORTICAL ACTIVITY DURING COGNITIVE AND MOTOR TASKS

Filippo Cona

Supervisor

Prof. Mauro Ursino

Reviewers

Prof. Serenella Salinari

Dr. Rosalyn Moran

Ph.D. Coordinator

Prof. Angelo Cappello

Esame Finale Anno 2012

ACKNOWLEDGEMENTS

Al termine di un percorso come quello del dottorato è normale, ritengo, sentirsi grati, se non addirittura debitori, verso una gran quantità di persone e volerle ringraziare per il loro supporto. Tuttavia in questa sede io non voglio stilare una lista di nomi con allegati più o meno grandi meriti che hanno avuto. Preferisco dire perché voglio ringraziare queste persone, non elencarle, voglio dire il peccato, non il peccatore, perché non c'è bisogno, penso, di ribadire l'ovvio. Coloro cui va il mio ringraziamento lo sanno.

Credo invece sia più significativo focalizzarmi sui motivi che mi spingono a scrivere questi ringraziamenti, forse perché questi motivi sono un po' meno banali, forse un po' meno ovvi.

Io sono sempre stato una persona piuttosto inconcludente, la mia vita è costellata di quadri incompleti, progetti abbandonati. Forse è normale sentirsi inadeguati in molte situazioni della vita, al punto da non volerne più sapere, da desiderare solo di lasciar perdere per rimettersi alla ricerca di qualcos'altro, qualcosa di più idoneo alle nostre capacità, al nostro gusto. Certo è che io sono un campione in questo genere di attività, il nuovo, l'esotico, il diverso, ha sempre avuto per me un fascino disarmante in confronto alla noia dell'attuale, del presente, sempre troppo parco di soddisfazioni. Preferisco la continua promessa dello sconosciuto, alla delusione che sempre ne consegue quando diventa noto.

È chiaro che questo tipo di atteggiamento nei confronti della vita può portare fortuna forse ad un artista, non di certo ad uno studente, men che meno ad un aspirante ricercatore, attività che richiede piuttosto caparbietà, fiducia anche di fronte alle più cocenti delusioni, voglia di rimettersi in sella, sempre.

Per questo voglio, devo ringraziare le persone che mi sono state più o meno vicine in questi anni. Perché se ora sto scrivendo questa tesi non posso di certo attribuire il merito a me stesso. Io posso averci messo il tempo, le competenze tecniche, posso aver impostato linee di ricerca, cercato conferme sperimentali, pubblicato risultati. La forza per farcela fino in fondo la avete messa voi.

Grazie.

When we are no more than babies,
we stare at our hand while it moves at our will,
stupefied by such a wonder.

A life later, we cease to be
and still don't have a satisfying answer
to that first, unsaid mystery.

SUMMARY

I. INTRODUCTION

The interest in the genesis, the meaning and the function of the cerebral rhythms and, more generally, in the neural dynamics, has grown rapidly in the last years due to the essential role that such dynamics seems to play in many processes of elaboration in the cortex, including phenomena such as perception, attention, learning, memory, motion, maybe consciousness. This issue will likely become increasingly prominent in the proximate future involving different but correlated disciplines such as neurosciences, cognitive sciences, psychology, neurology.

The rhythmic activity is an essential property of neural groups and it is known since the first electroencephalographic recordings made by Berger in the twenties [Berger, 1929]. It is organized in complex patterns not yet completely known, that depend on the brain state (e.g. sleep/waking, relaxation/excitation), on the task (cognitive or motor) and on the subject who performs it during the measurement. Due to the limited temporal resolution of metabolic neuroimaging techniques (such as functional magnetic resonance (fMRI) and positron emitting tomography (PET)), human neural dynamics are studied in a non-invasive way through techniques based on the recording of electromagnetic fields on the scalp: electroencephalography (EEG) and magnetoencphalography (MEG). For this reason, this thesis is focused almost exclusively on data recorded through EEG.

The study of the neural rhythms consists of two main aspects: the spatial location and the frequency band. However, these aspects do not fully cover the quantity of information carried by the EEG signal. Recent studies concentrated on connectivity indices between signals, in order to highlight the correlation between the signals themselves, their synchronization or, more generally, the presence of connections between the cerebral areas involved.

The variety of mechanisms that drive the cortical dynamics, the complexity of their mutual interactions and the lack of analysis techniques universally accepted, have boosted the interest in computational, biologically inspired models. As is stressed in recent works [Kiebel et al., 2008] currently there's not only uncertainty on which is the most convenient way for analyzing EEG data, but also on the mechanisms that generate the cortical rhythms, on their role in the cerebral elaboration and on the information that they carry.

In the scientific literature there are essentially two main typologies of mathematical models inspired by biology, that can be used to study the cortical dynamics and the behavior of neural populations. The first uses networks consisting of a huge number of neurons, in which each unit is represented in a realistic manner and, when excited, is able to generate a train of spikes. Such models can greatly differ from one another depending on the way the single neuron Is modeled.

The most complex models describe each neuron by means of compartments, distinguishing between soma, axon, dendrites, and explicitly consider the ionic channels dynamics responsible for the generation of the action potential [Traub et al., 2005]. In less complex models, the single neuron can be modeled with the "integrate and fire" formalism, in which the action potential is represented by a stereotyped waveform [Dayan & Abbott, 2001]. Though these models play a relevant role for the analysis of the genesis of cortical rhythms and of the biophysical mechanisms

that induce neural populations' synchronism, they are not suitable for studying superior cognitive functions, such as sensorial elaboration, memory, learning, language, because of the extraordinary high number or parameters and variables involved. This intrinsic complexity makes very difficult to synthesize the results and to develop new high level theories [Wilson & Cowan, 1972].

Nowadays, it is universally accepted that the brain performs its tasks through the interaction of connected regions that can share information. The number of neurons involved is excessively high to try and analyze them individually and it is very unlikely that an approach based on the local properties of each neuron could catch the essential aspects of the emergent properties of the whole system. Finally, it is worth noting that neurons tend to have random dynamics, so in this context the statistical behavior of many neurons is more meaningful than the single realization.

An alternative approach is based on the use of neural mass models (NMM). In these models the dynamics of whole cortical columns, or even brain areas, is modeled through a limited number of state variables, and thus by a limited number of differential equations and parameters. This is achieved by collapsing the variables of a great number of neurons, that belong to the same population, and by substituting them with their mean values. Despite their simplicity, these models can catch the most relevant phenomena emerging from the interaction of brain regions with thousands of neurons, and thus have become very useful tools for the study of the rhythmic activity recorded with the EEG or the MEG. Recently, they have also been employed to try and connect the information coming from different recording techniques (e.g. EEG and fMRI).

Last but not least, the EEG signal is the result of the current flows produced by populations of pyramidal neurons, whose post-synaptic potentials are synchronized in such a way to sum their activity. This characteristic makes the NMM particularly suitable to simulate the EEG signal since it is intrinsically insensible to the dynamics of single neurons, and to catch the most prominent collective behaviors.

This thesis is mainly devoted to show how EEG data and related phenomena can be reproduced using mathematical models of neural masses. The aim is to describe some of these phenomena, to show in which ways the design of the models architecture is influenced by such phenomena, point out the difficulties of tuning the dozens of parameters of the models in order to reproduce the activity recorded with EEG systems during different kinds of experiments, and suggest some strategies to cope with these problems. In particular the chapters are organized as follows: in chapter II the main characteristics of the cortical column, of the EEG signal and of the neural mass models will be presented, in order to show the relationships that hold between these entities; chapter III describes a study in which a NMM from the literature has been used to assess brain connectivity changes in tetraplegic patients; in chapter IV a modified version of the NMM is presented, which has been developed to overcomes some of the previous version's intrinsic limitations; chapter V describes a study in which the new NMM has been used to reproduce the electrical activity evoked in the cortex by the transcranial magnetic stimulation (TMS); chapter VI presents some preliminary results obtained in the simulation of the neural rhythms associated with memory recall; finally, some general conclusions are drawn in chapter VII.

II. PRELIMINARY CONCEPTS

1. THE CORTICAL COLUMN

The cerebral cortex is organized in elementary units of elaboration, known as cortical columns. Such structures were firstly described by Vernon Mountcastle, more than half a century ago [Horton & Adams, 2005]. Mountcastle, while examining the cortex, hypothesized the existence of an unit of elaboration, consisting of a vertical group of neurons, that crosses all the six layers of the cortex. These cortical blocks, which are no more than 500 μm wide, contains neurons that process together the same piece of information (e.g., in the case of the somatosensory cortex, they may respond to the same skin receptor). Later, different examples of cortical columns have been discovered in different regions of the cortex, e.g. the cortical columns of the primary visual cortex, that process the light stimuli coming from a specific area of the retina, and the original concept has been extended to cover different structures and functions.

The role and the real importance of these elementary units is a topic of debate and is not in the scope of this chapter to examine this issue (the interested reader can refer to [Horton & Adams, 2005]). Here we are interested in what the structure of the cortical columns can tell us about the neural populations the are present in the cortex and how they interact. In other words, I will use the concept cortical column to identify which neural populations are essential to develop NMMs and to describe the synaptic contacts that exists inside a cortical area or between different cortical areas.

As said before the cortex is constituted of up to six horizontal layers, each of which has a different composition in terms of neurons and connectivity. The number and the architecture of these layers can vary from region to region. The most typical structure is made of six layers, progressively numbered from the outer layer to the inner one. Pyramidal excitatory neurons are found in layer III and V and project their axons vertically with respect to the cortex surface and are responsible for the long range connections between different cortical areas (for this reason they are also known as projection neurons). Other neural cells do not project their axons toward far areas of the brain, but their connections are rather limited to local neurons (for this reason they are also known as interneurons). In particular stellate excitatory cells are mainly found in layer IV, while inhibitory cells that employ the GABA neurotransmitter (e.g., chandelier and basket cells) are mainly found in the other layers.

It is believed that the cortex is organized in a laminar structure because it is an efficient way to manage the input-output relationships between neurons and between cortical areas. Thus, knowing this structure can greatly help in developing NMMs that try to identify dynamic properties the emerge from links between neural populations and between cortical regions. In particular, it is very important to distinguish between bottom-up, top down and lateral connections [Felleman & Van Essen, 1991]. Bottom-up connections typically go from the pyramidal cells in layer III towards excitatory interneurons in layer IV. Instead, top-down and lateral connections generally originates from pyramidal cells in deeper layers (V and VI) and target a great variety of

neurons in layers I, II and VI. It is very important to keep these conditions in mind when developing a NMM, since the model has to be as physiologically plausible as possible.

In what follows the terms cortical column, cortical area and cortical region, will be used interchangeably.

2. THE EEG SIGNAL

Electroencephalography is the recording of electrical activity along the scalp. EEG measures voltage fluctuations resulting from ionic current flows within the neurons of the brain. In clinical contexts, EEG refers to the recording of the brain's spontaneous electrical activity, as recorded from multiple electrodes placed on the scalp. In neurology, the main diagnostic application of EEG is in the case of epilepsy, as epileptic activity can create clear abnormalities on a standard EEG study. A secondary clinical use of EEG is in the diagnosis of coma, encephalopathies, and brain death. Moreover the EEG signal is used to distinguish between the states of consciousness, such as wakefulness, rapid eyes movement (REM) sleep and different stages of deep sleep.

Derivatives of the EEG technique include evoked potentials (EP), which involves averaging the EEG activity time-locked to the presentation of a stimulus of some sort (visual, somatosensory, or auditory). Event-related potentials (ERPs) refer to averaged EEG responses that are time-locked to more complex processing of stimuli; this technique is used in cognitive science, cognitive psychology, and psychophysiological research.

2.1. Source of EEG activity

The brain's electrical charge is maintained by billions of neurons. Neurons are electrically charged (or "polarized") by membrane transport proteins that pump ions across their membranes. Neurons are constantly exchanging ions with the extracellular milieu, for example to maintain resting potential and to propagate action potentials. Ions of like charge repel each other, and when many ions are pushed out of many neurons at the same time, they can push their neighbors, who push their neighbors, and so on, in a wave. This process is known as volume conduction. When the wave of ions reaches the electrodes on the scalp, they can push or pull electrons on the metal on the electrodes. Since metal conducts the push and pull of electrons easily, the difference in push or voltage between any two electrodes can be measured by a voltmeter. Recording these voltages over time gives us the EEG.

The electric potentials generated by single neurons are far too small to be picked by EEG. EEG activity therefore always reflects the summation of the synchronous activity of thousands or millions of neurons that have similar spatial orientation. If the cells do not have similar spatial orientation, their ions do not line up and create waves to be detected. Pyramidal neurons of the cortex are thought to produce the most EEG signal because they are well-aligned and fire together. Because voltage fields fall off with the square of distance, activity from deep sources is more difficult to detect than currents near the skull.

2.2. EEG activity in the frequency domain

Scalp EEG activity shows oscillations at a variety of frequencies. Several of these oscillations have characteristic frequency ranges and spatial distributions, and are associated with different states of brain functioning (e.g., waking and the various sleep stages). They represent synchronized activity over a network of neurons. The neuronal networks underlying some of these oscillations are understood (e.g., the thalamocortical resonance underlying sleep spindles), while many others are not (e.g., the system that generates the posterior basic rhythm).

The rhythmic activity is divided into bands by frequency. To some degree, these frequency bands are a matter of nomenclature (i.e., any rhythmic activity between 6–12Hz can be described as "alpha"), but these designations arose because rhythmic activity within a certain frequency range

was noted to have a certain distribution over the scalp or a certain biological significance. These bands are commonly subdivided as follows:

1. Delta is the frequency range up to 4Hz. It tends to be the highest in amplitude and the slowest wave. It is seen normally in adults in slow wave sleep. It is also seen normally in babies.
2. Theta is the frequency range from 4Hz to 8Hz. Theta is seen normally in young children. It may be seen in drowsiness or arousal in older children and adults; it can also be seen in meditation.
3. Alpha is the frequency range from 8Hz to 12Hz. Hans Berger named the first rhythmic EEG activity he saw as the "alpha wave". This was the "posterior basic rhythm", seen in the posterior regions of the head on both sides, higher in amplitude on the dominant side. It emerges with closing of the eyes and with relaxation, and attenuates with eye opening or mental exertion. In addition to the posterior basic rhythm, there are other normal alpha rhythms such as the mu rhythm (alpha activity in the contralateral sensory and motor cortical areas that emerges when the hands and arms are idle) and the "third rhythm" (alpha activity in the temporal or frontal lobes). Alpha can be abnormal; for example, an EEG that has diffuse alpha occurring in coma and is not responsive to external stimuli is referred to as "alpha coma".
4. Beta is the frequency range from 12Hz to about 25Hz (sometimes the upper frequency limit is set to 30Hz since there is not a globally accepted value yet). It is seen usually on both sides in symmetrical distribution and is most evident frontally. Beta activity is closely linked to motor behavior and is generally attenuated during active movements. Low amplitude beta with multiple and varying frequencies is often associated with active, busy or anxious thinking and active concentration. It is the dominant rhythm in subjects who have their eyes open.
5. Gamma is the frequency range approximately 25-100Hz. Gamma rhythms are thought to represent binding of different populations of neurons together into a network for the purpose of carrying out a certain cognitive or motor function.
6. Mu ranges 8-13Hz, and partly overlaps with other frequencies. It reflects the synchronous firing of motor neurons in rest state. Mu suppression is thought to reflect motor mirror neuron systems, because when an action is observed, the pattern extinguishes, possibly because of the normal neuronal system and the mirror neuron system "go out of sync", and interfere with each other.

3. INTRODUCTION TO NEURAL MASS MODELS

The first NMMs were developed in the mid seventies by Freeman [Freeman, 1978, 1987] and Lopes da Silva [Lopes da Silva et al., 1974] and were later modified by Jansen and Rit [Jansen & Rit, 1995]. As was shown in section 1. the EEG signal is generated mainly by the activity of pyramidal neurons, which communicate with several other types of neural groups inside a cortical column. So, in these models the dynamics of a cortical column is described through the interaction of different neural populations. Generally there is a population of pyramidal cells that generates the output of the model, and that is interconnected through a feedback loop with populations of excitatory and inhibitory interneurons.

3.1. Model of a single neural population

Each neural population is modeled through two blocks. The first block is a non-linear static activation function, that transforms the membrane potential of the neural population into the average spike density. This function is typically sigmoidal of the type $z(v) = \frac{A}{1+e^{s(v_0-v)}}$, where z is the spike density, which depends on the membrane potential v, A is the maximum firing rate, v_0 is the threshold between inactivation and activation, and s is the slope in the linear range. The second block represents the synapse kinetics and is usually a dynamic linear function that transforms the firing rate into the postsynaptic potential (PSP) variation. It is typically a second order differential equation with impulse response $h(t) = \frac{G}{\tau} t e^{-\frac{t}{\tau}}$, where G determines the maximum amplitude of the PSP, and τ is the time constant.

Each of these neural populations simulates a group of neurons described in the previous section (pyramidal cells, excitatory stellate cells, GABAergic inhibitory interneurons). Their interaction gives rise to the dynamics of the whole cortical column, as discussed in sub-section 3.2. .

3.2. Model of a cortical column

Each cortical column typically consists of at least two neural populations, one excitatory and one inhibitory in order to generate an oscillatory activity. For example, Jansen and Rit's model has three populations, one representing the pyramidal cells, whose membrane potential is taken as the simulated EEG, one representing excitatory interneurons employing glutamate mediated synapses, and one representing inhibitory interneurons employing $GABA_A$ mediated synapses. However, in what follows, I will always refer to a more complex model developed by Wendling [Wendling et al., 2002], in which there's additional population of inhibitory interneurons. The latter population was added to account for neurons with $GABA_A$ mediated synapses that have a particularly fast dynamics [White et al., 2000], thus, the two populations will be referred to as $GABA_{A,slow}$ and $GABA_{A,fast}$ interneurons. As will be widely discussed in the following chapters, the $GABA_{A,fast}$ interneurons are essential to generate fast oscillatory activity in the gamma band, which is involved in many higher cognitive tasks.

Each neural population communicates with other populations in the same cortical column by sending them its average firing rate, thus generating excitatory or inhibitory PSPs in the target populations. The connections have a gain that is proportional to the mean number of synaptic contacts on the dendritic tree of the target population.

This kind of model is able to generate a wide variety of rhythmic activity that are observed in experimental EEG signals. Different behaviors are obtained by modifying internal parameters of

the populations, such as the gain or the time constant of the synapses or the number of synaptic contacts between different populations. As will be showed later, one of the major difficulties encountered using these models, is to tune the relatively high number of parameters (usually some dozens) so that the model can reproduce experimental EEG signals, both in the time and in the frequency domain.

3.3. Connectivity between cortical columns

One of the most important issues that can be analyzed using NMMs, is the interaction between different cortical areas. Actually, the key feature that makes NMMs so competitive in the field of neural computing is their ability to reproduce the activity of several cortical regions and to study the emergent properties of large neural networks, using a parsimonious description not excessively demanding from a computational point of view.

The implementation of the interaction between different cortical columns is pretty straightforward. The interaction is similar to that of neural populations within the same cortical column, with a few changes:

1. Only pyramidal populations are allowed to send connections to populations in other cortical regions.
2. The connection may employ a finite delay to account for the transmission time between areas which are far away from one another.

The target population of these connections, also known as “long range connections”, depends on the architecture of the network. Bottom-up connections (i.e., from lower to upper hierarchical levels) typically target the population of excitatory interneurons, top-down connections (i.e., from upper to lower levels) target pyramidal neurons, while lateral (i.e., within the same hierarchical level) can target all of the neural populations. However it is not simple to follows these rules, for at least two reasons: sometimes we do not know the hierarchical relationships between cortical areas, with the exception of the easiest perceptive and motor phenomena; not all of the possible connections play a crucial role and it is thus convenient to reduce the number of connections for the sake of parsimony and simplicity.

III. SPECTRAL CHANGES IN TETRAPLEGIC PATIENTS[1]

1. INTRODUCTION

It is well known that the execution of even simple motor and/or cognitive tasks by the brain requires the participation of multiple cortical regions, which are mutually interconnected and exchange their information via plastic long-range synapses. Consequently, knowledge of brain connectivity is becoming an essential aspect of modern neuroscience, especially useful to understand how the brain realizes its basic functions and what the role of the different regions is. Connectivity, however, is an elusive concept, which can have different definitions depending on the emphasis of the investigators [Horwitz, 2003]. In particular, the definition of connectivity is strictly related to the mathematical method used to extract connectivity parameters from data, i.e. it is "model dependent" and should always be used together with the particular method adopted. For instance, most methods presently used to derive connectivity graphs (such as the Direct Transfer Function or the Partial Directed Coherence [Astolfi et al., 2004; Baccalá & Sameshima, 2001; Kaminski & Blinowska, 1991; Kamiński et al., 1995, 1997; Kaminski et al., 2001; Korzeniewska et al., 2003]) are based on the assumption of linearity, whereas neurons are intrinsically non-linear. Moreover, these methods use empirical equations (i.e. they are based on black box models), which do not provide a description of the underpinning physiological mechanisms (for instance, they do not explicitly consider the time constant and strength of synapses, the role of inhibitory interneurons, etc...). On the other hand, the main advantage of these methods is that they provide analytical solutions to the problem, which are not "modeler driven".

As an alternative method to study effective connectivity, a few authors in recent years have employed the so-called "neural mass models". These models were originally proposed in the mid-seventies [Freeman, 1978; Lopes da Silva et al., 1976] and subsequently improved in the late nineties [Jansen & Rit, 1995; Wendling et al., 2002]. They mimic the activity of entire neural populations via the feedback arrangement of excitatory and inhibitory groups, which are assumed to share a similar membrane potential and work in synchronism. The interaction between excitatory and inhibitory groups can produce oscillatory rhythms, either via an intrinsic instability of the model (like a limit cycle) or by a resonance amplification of an external noise. In particular, similar models have been used to simulate alpha rhythms [Jansen & Rit, 1995], dynamics in the olfactory cortex [Freeman, 1987], or paradoxical epileptic discharges [Wendling et al., 2000, 2002]. A few recent studies used these models to study effective connectivity among different regions of interest (ROIs), to analyze the dependence of cortical EEG on connectivity patterns [David & Friston, 2003; Sotero et al., 2007] and to evaluate the EEG power spectral density [Moran et al., 2008]. Recently, we also used neural mass models, including fast inhibitory dynamics, to simulate the power spectral density of cortical EEG [Ursino et al., 2006; Zavaglia et

[1] The contents of this chapter are published in Computational Intelligence and Neuroscience (Cona et al., 2009).

al., 2006, 2008a] during simple motor tasks. The main indication of these studies is that neural populations with a different dynamics (for instance, different time constants of excitatory and inhibitory synapses) suitably interconnected, can produce EEG rhythms similar to those measured in human subjects via high-resolution EEG methods.

Application of neural mass models to estimate effective connectivity is, however, a very hard task, due to the elevated number of parameters involved and the presence of non-linear terms, which preclude the use of analytical solutions. For instance, in a recent paper [Zavaglia et al., 2008b] we derived some connectivity patterns between three cortical regions (the cyngulate, and the primary and supplementary motor cortices) during a simple foot-movement task, by minimizing a least-square criterion function of the difference between model and data spectral densities. However, just a few exemplary cases could be analyzed, since the minimization algorithm often converges to a sub-optimal solution (i.e., a local minimum) which may exhibit just a poor fitting and, moreover, may be characterized by unphysiological parameter values. Furthermore, also the metrics used to compare model and patient spectral densities may be questionable and affect the final minimization results.

For this reason, in the present work we designed a new method, based on a genetic algorithm, to provide an automatic fitting between model and real data. The method tries to find absolute minima of alternative cost functions within the same procedure. Genetic algorithms have already been used to estimate the parameters of a neural mass model in order to fit real data (see for example [Wendling et al., 2005]). The algorithm has been applied to high-resolution scalp EEG data measured during a simple foot-movement task; scalp EEG was preliminarily propagated to the cortex via a propagation model, to infer cortical electrical activity in three Regions of Interest (ROIs). The model [Zavaglia et al., 2008a] assumes that each ROI is characterized by an intrinsic rhythm (established by the time constants of synapses) and can receive additional rhythms from other connected ROIs. Results have been applied to a group of normal subjects and a group of tetraplegic patients to establish simple patterns of connectivity between the cyngulate, motor and pre-motor cortices, and to look for possible differences in the two populations.

2. METHOD

2.1. Model of a single population

The model of a single population was obtained by modifying equations proposed by Wendling et al. [Wendling et al., 2002]. It consists of four neural groups which communicate via excitatory and inhibitory synapses: pyramidal cells, excitatory interneurons, inhibitory interneurons with slow synaptic kinetics, and inhibitory interneurons with faster synaptic kinetics. Each neural group simulates a pool of neurons which are lumped together and which are assumed to receive similar input and to behave in a similar manner. One lumped circuit communicates with another through the average firing rate corresponding to what that given population of cells is firing on average.

Each neural group receives an average postsynaptic membrane potential from the other groups, and converts the average membrane potential into an average density of spikes fired by the neurons. This conversion is simulated via a static sigmoidal relationship. The effect of the synapses is described via second order linear transfer functions, which convert the presynaptic spike density into the postsynaptic membrane potential. Three different kinds of synapses, with impulse response h_e, h_i and h_g, are used to describe the synaptic effect of excitatory neurons (both pyramidal cells and excitatory interneurons), of slow inhibitory interneurons and of fast inhibitory interneurons, respectively. Model equations can be written as follows:

Pyramidal neurons

$$\frac{dy_p(t)}{dt} = x_p(t) \qquad \text{III.1}$$

$$\frac{dx_p(t)}{dt} = G_e\omega_e z_p(t) - 2\omega_e x_p(t) - \omega_e^2 y_p(t) \qquad \text{III.2}$$

$$z_p(t) = \frac{2e_0}{1 + e^{r(s_0 - v_p)}} \qquad \text{III.3}$$

$$v_p(t) = C_{pe}y_e(t) - C_{ps}y_s(t) - C_{pf}y_f(t) \qquad \text{III.4}$$

Excitatory interneurons

$$\frac{dy_e(t)}{dt} = x_e(t) \qquad \text{III.5}$$

$$\frac{dx_e(t)}{dt} = G_e\omega_e\left(z_e(t) + \frac{u_p(t)}{C_{pe}}\right) - 2\omega_e x_e(t) - \omega_e^2 y_e(t) \qquad \text{III.6}$$

$$z_e(t) = \frac{2e_0}{1 + e^{r(s_0 - v_e)}} \qquad \text{III.7}$$

$$v_e(t) = C_{ep}y_p(t) \qquad \text{III.8}$$

Slow inhibitory interneurons

$$\frac{dy_s(t)}{dt} = x_s(t) \quad \text{III.9}$$

$$\frac{dx_s(t)}{dt} = G_s\omega_s z_s(t) - 2\omega_s x_s(t) - \omega_s^2 y_s(t) \quad \text{III.10}$$

$$z_s(t) = \frac{2e_0}{1 + e^{r(s_0 - v_s)}} \quad \text{III.11}$$

$$v_s(t) = C_{sp} y_p(t) \quad \text{III.12}$$

Fast inhibitory interneurons

$$\frac{dy_f(t)}{dt} = x_f(t) \quad \text{III.13}$$

$$\frac{dx_f(t)}{dt} = G_f\omega_f z_f(t) - 2\omega_f x_f(t) - \omega_f^2 y_f(t) \quad \text{III.14}$$

$$z_f(t) = \frac{2e_0}{1 + e^{r(s_0 - v_f)}} \quad \text{III.15}$$

$$v_f(t) = C_{fp} y_p(t) - C_{fs} y_s(t) \quad \text{III.16}$$

In these equations, the symbols v_i represent the average membrane potentials (i = p, e, s, f for the four groups). These are the input for the sigmoid function which converts them into the average density of spikes (z_i, i = p, e, s, f) fired by the neurons. Then, these outputs enter into the synapses (excitatory, slow inhibitory or fast inhibitory), represented via the second order linear functions. Each synapse is described by an average gain (G_e, G_s, G_f for the excitatory, slow inhibitory and fast inhibitory synapses, respectively) and a time constant (the reciprocal of ω_e, ω_s and ω_f, respectively). The state variables of these equations represent the postsynaptic membrane potentials (y_i, i = p, e, s, f) and their derivatives (x_i, i = p, e, s, f). Interactions among neurons are represented via seven connectivity constants (C_{ij}, where i = p, e, s, f represents the postsynaptic population and j = p, e, s, f represents the presynaptic population). Finally, $u_p(t)$ represents all exogenous contributions, both excitation coming from external sources and the density of action potentials coming from other connected regions.

2.2. Model of connectivity among ROIs

The previous model was used to simulate a single ROI, the dynamic of which ensues from the interactions among the four neural subgroups. In order to study how the ROIs interact, we consider N ROIs which are interconnected through long-range excitatory connections. To simulate this connectivity we assumed that the average spike density of pyramidal neurons (z_p) affects the input $u_p(t)$ in Eq. III.6 via a weight factor, W, and a time delay, T. Hence, the input $u_{p,i}(t)$ in the i-th ROI can be computed as follows

$$u_{p,i}(t) = n_i(t) + \sum_j W_{ij} z_{p,j}\,(t - T) \quad \text{III.17}$$

where W_{ij} is the weight of the synaptic link from the j-th (pre-synaptic) ROI to i-th (post-synaptic) ROI, T is the time delay (assumed equal for all synapses), $n_i(t)$ represents a gaussian white noise with mean value m_i and standard deviation σ_i, and the sum in the right hand member of Eq. V.20 is extended to all ROIs, j, which target into the ROI i.

2.3. Acquisition and processing of EEG data

The experiment took place in the laboratories of the Santa Lucia Foundation, Rome, after the informed consent was obtained. The subject was comfortably seated in an armchair with both arms relaxed, in an electrically shielded, dimly lit room. He was asked to perform a brisk protrusion of the lips (lip pursing) while he was performing a right foot movement. A 58-channel EEG system (BrainAmp, Brainproducts GmbH, Germany) was used to record electrical potentials by means of an electrode cap, accordingly to an extension of the 10-20 international system. A/D sampling rate was 200 Hz. During motor task, subject was instructed to avoid eye blinks, swallowing or any movement other than the required foot movements. Bipolar EMG was recorded from control and spinal cord injury (SCI) subjects, with surface electrodes from the right tibialis anterior muscle and orbicularis oris muscle to detect the onset of foot and lip movements, respectively. The electro-oculograms (EOGs) were recorded to avoid trials with artifacts due to eye-blink movements. The EMG was monitored throughout recordings from electrodes placed as described above to avoid poor quality of the recordings due to muscular artifacts. Artifact rejection was performed on a wide segmentation of the trials (from -4.0 s to +4.0 s) while a narrow segmentation (from -2.5 s to +0.5 s) was used as analysis period.

A 3-shell Boundary Element Model (BEM) of the head was used to estimate the cortical current density (CCD) distribution in some regions of interest (ROI) of the cortex (the cingulate cortex (CMA_L), the primary motor area (M1F_L), and the supplementary motor area (SMAp_L)) starting from activity measured on the scalp. The procedure used is described in previous works [Babiloni et al., 2005; Ursino et al., 2006; Zavaglia et al., 2006]. From the CCD, the average estimated cortical activity in the region has then been evaluated. The latter has been successively subjected to spectral analysis in order to produce the spectra used for the estimation of the model parameters.

Power spectra have been computed by using the Welch's average modified periodogram method [Welch, 1967]. In particular, the model PSD was computed using simulated signal with duration 100 s, and averaging 50% overlapping sections each with duration 1 s. The use of a 100 s simulated signal is justified by the necessity to reduce the variance of the estimated spectrum to an acceptable level. We verified, using a random repetition of the same simulation by changing the input noise, that these spectra are only scarcely affected by the single noise realization. All power spectra have been preliminary normalized to have unitary area in the same frequency range (6-50 Hz). Since the signal beyond 40 Hz may be corrupted, the limit of our investigated gamma range was 30-40 Hz. In particular, we did not investigate the so-called high-gamma range (above 50 Hz).

We examined 5 subjects with spinal cord injury (SCI; 4 males, 1 female, mean age 26.4±2.8 years) and 5 healthy subjects (4 males, 1 female, mean age 25.1± 1.5 years). Informed consent was obtained from all the subjects. The study was approved by the local ethics committee. The SCIs were all of traumatic aetiology and were located at the cervical level (C6 in 3 SCI subjects; C5 and C7 in the remaining 2 subjects); at the time of the study, all the patients had a stabilized lesion (mean time since trauma 19.4 ± 7.2 months). Neurological status was assessed according to

the American Spinal Injury Association (ASIA) standards on the basis of the patients' motor and sensory scores, neurological level and neurological impairment. The completeness of the lesion was defined according to the concept of sacral sparing: sensory preservation of the peri-anal zone and/or motor function of the external anal sphincter (preservation of the lower sacral segments). The lesion was complete in all 5 patients (ASIA-A: complete motor and sensory loss below the lesion level). None of the SCI patients had suffered a head or brain lesion in concomitance with the spinal injury. Neither uncontrollable spasticity-induced body movements nor dysaesthetic pain syndrome were reported by any of the patients. All subjects were right-handed as assessed by the Edinburgh inventory [Salenius & Hari, 2003].

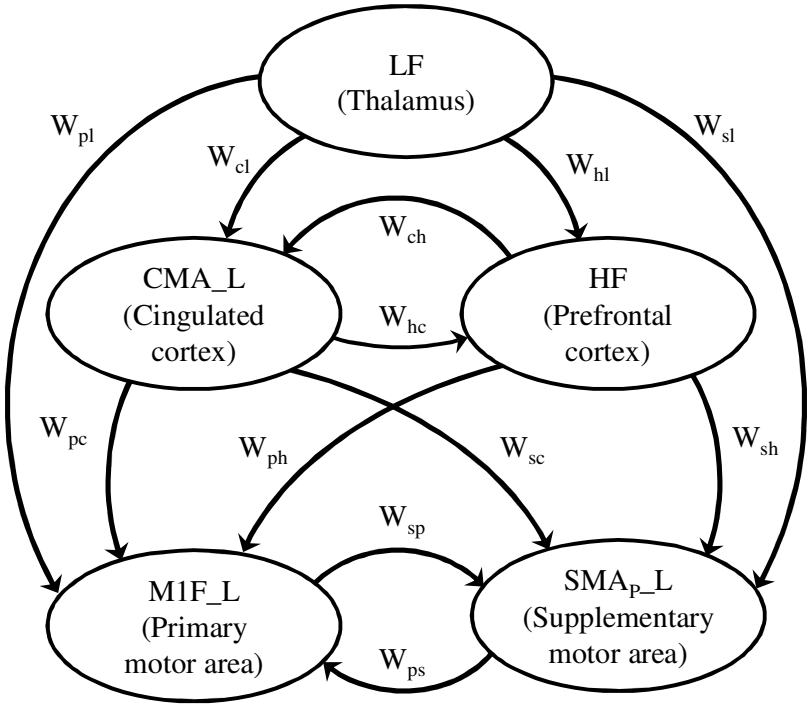

Figure III.1: Model of interconnected ROIs used in this chapter to simulate power spectral densities in pre-frontal regions during a foot-movement task. W_{ij} are connectivity weights, estimated from real data using the genetic algorithm described in the text. The regions CMA_L, M1F_L and SMA_P_L oscillate in the beta range when stimulated with white noise. The LF region oscillates in the alpha range, whereas the HF region generates a rhythm in the gamma band (see Table III.1 for parameter numerical values within the regions).

In order to perform a subsequent fitting, we chose only those EEG tracings for which alpha and gamma rhythms were located at approximately the same frequencies in the three ROIs. This corresponds to model hypothesis (see below) that each of these rhythms is generated by a single external source (limitations of this choice will be discussed at the end). 102 tracings satisfied this criterion. The algorithm was able to fit 59 of these trials: 36 trials on healthy subjects and 23 trials on tetraplegic ones.

2.4. The model of the motor task

Analysis of real EEGs [Zavaglia et al., 2008a, 2008b] demonstrates that power spectral density during the task may exhibit three simultaneous rhythms, in the alpha, beta and gamma ranges, respectively. In order to simulate this behaviour, we assumed that the cortical ROIs involved in

the movement (i.e., the M1F_L, the CMA_L and the SMAp_L), when activated, oscillate with an intrinsic rhythm in the beta range. This hypothesis reflects the frequent idea that, during behavioral activation, beta rhythms are generated locally, perhaps by a recurrent feedback loop involving pyramidal cells and inhibitory interneurons [Salenius & Hari, 2003]. These waves represent excitement of the cortex to a higher state of alertness or tension. Moreover, we assumed that the alpha rhythm is sent to the cortex by an external area (probably located in the thalamus and reticular nucleus). This hypothesis corresponds to the idea [Buzsaki, 2006] that alpha rhythms arise from the endogenous rhythmicity of thalamic populations, which are then transmitted to other thalamocortical populations even in the absence of an external stimulus. Finally, an important problem is how to produce gamma rhythms in the model. A first possibility is that all ROIs can generate not only their intrinsic beta rhythm, but also a gamma oscillation, via a second group of populations with faster kinetics, and that these gamma rhythms are then synchronized via long range synapses. The idea of multiple rhythms in the same ROI was proposed by David and Friston [David & Friston, 2003], and was used by us in a previous model for connectivity estimation [Moran et al., 2008]. A second possibility, which allows PSD to be mimicked with a smaller number of parameters, is that gamma oscillation is generated by a single far region of the cortex, and then transmitted to the other ROIs via long-range synapses.

In the present study we adopted the second hypothesis. First, we assumed that the thalamus receives an external input (simulated as a significant white noise term) and drives the other populations but does not receive any connectivity from them (i.e., any possible feedback from the cortex to the thalamus is neglected). Hence, the motor command originates from the low-frequency region (LF), and spreads toward the cortex. Moreover, the three ROIs in the cortex (CMA_L, M1F_L, and SMA_p_L) can recruit a gamma or high-frequency rhythm from another region (named HF), which may be located in the pre-frontal cortex. This rhythm should reflect the cognitive or conscious aspects of the task. Finally, the cingulate cortex can also modulate the HF region and drives the other two ROIs (i.e. the primary and supplementary motor areas). The latter are linked via a feedback loop. A sketch of the overall model is illustrated in Figure III.1.

It is worth noting that we used the NMM of cortical area to simulate the activity of LF, even if the NMM of a thalamic module would be more appropriate. Thalamic NMMs are much more complicated than cortical ones since they need to account for the dynamics of calcium ions to simulate both the tonic and the burst firing [Pirini & Ursino, 2010]. In this case such a complexity is not necessary, since we just need an alpha wave generator and not to simulate physiological phenomena associated to burst firing (slow waves in sleep). So the use of a thalamic module is not only pointless, but even undesirable for a matter of computational performance.

2.5. The model parameters

The model has a relative large number of parameters, but only a few of them were used as variables for the fitting procedure. It appears that letting the fitting algorithm modulate all of the model parameters leads to incoherent solutions: the same simulated power spectra can be obtained with different sets of parameters. So the parameters estimated by the fitting algorithm were only the reciprocal of time constants of fast inhibitory synapses (to tune power peaks frequencies) and connectivity strengths (to adjust power peaks relative amplitudes). The other parameters have constant values, given in Table III.1. Most of these values are biologically plausible [Jansen & Rit, 1995] and let the model oscillate in the alpha (8-12Hz), beta (12-30Hz), and gamma band (>30Hz) [Ursino et al., 2006; Zavaglia et al., 2006]. Still the input mean m and variance σ^2 have been estimated via the fitting procedure, since no plausible values for these parameters have been

found yet. In fact, as usual in neural mass models [David & Friston, 2003; Wendling et al., 2002; Zavaglia et al., 2008a], this noise simulates all random contributions coming from external sources not included in the model and also accounts for internal neural variability. To do this we run a preliminary set of fittings in which m and σ^2 were used as fitting variables in order to find their optimum values for each trial. The values found were averaged and used as constants (Table III.1) in the following fitting procedures.

Table III.1: Model parameters

Parameters		LF	CMA_L, M1F_L, SMA_p_L	HF
G_e	(mV)	2.67	5.17	5.55
G_s	(mV)	3.15	4.45	3.8
G_f	(mV)	22.3	57.1	173
ω_s	(s^{-1})	20	30	40
ω_f	(s^{-1})	300	350	790
m	(s^{-1})	-103.3	-130.5	-16.1
σ^2	(s^{-2})	27807	10028	23642
			All regions	
C_{ep}			135	
C_{pe}			108	
C_{sp}			33.75	
C_{ps}			33.75	
C_{fp}			40.5	
C_{fs}			13.5	
C_{pf}			108	
r	(mV^{-1})		0.56	
s_0	(mV)		6	
e_0	(s^{-1})		2.5	

2.6. Genetic algorithm and fitting procedure

A Genetic Algorithm (GA) is a search technique that solves optimization problems by simulating the Darwinian natural selection [Holland, 1975]. We used the GA to find the set of model parameters for which the model output fits a given real EEG signal. Parameters used for the fitting procedures are the reciprocal of time constants of fast inhibitory synapses (ω_e), and connectivity strengths.

The GA is divided into generations. Each generation consists of a lot of individuals that are candidate solutions (sets of model parameters) for the fitting. The first generation is typically random. Parameters are represented as bit arrays (chromosomes). Each individual is ranked with a fitting coefficient (FC) in the range [0,1] by calculating the model output and comparing it to the real EEG signal: the better the fitting between the simulated signal and the real one, the higher the FC of the individual. Best ranked individuals (higher FC) have higher probability to reproduce. During reproduction couples of parents are randomly selected according to their FCs. Each couple generates two new individuals whose chromosomes are obtained from applying genetic operators to the parents' ones. Typical genetic operators are crossover and mutation (Figure III.2). Crossover is the exchange of genetic material between parents to generate the sons' chromosomes. Mutation simply switches the values of a low percentage of bits (mutation rate). The worst individuals of the previous generation are replaced with the best newborn individuals.

In this way, each generation tends to preserve the best genetic material. The algorithm converges to a population composed of sets of parameters that fit the real EEG signal well.

The major challenge in implementing a GA is to find an efficient fitting function for determining the FCs and rank the individuals, so that the algorithm is able to converge in reasonable time. To compare the simulated signal to the real one, we used their Power Spectral Densities (PSD).

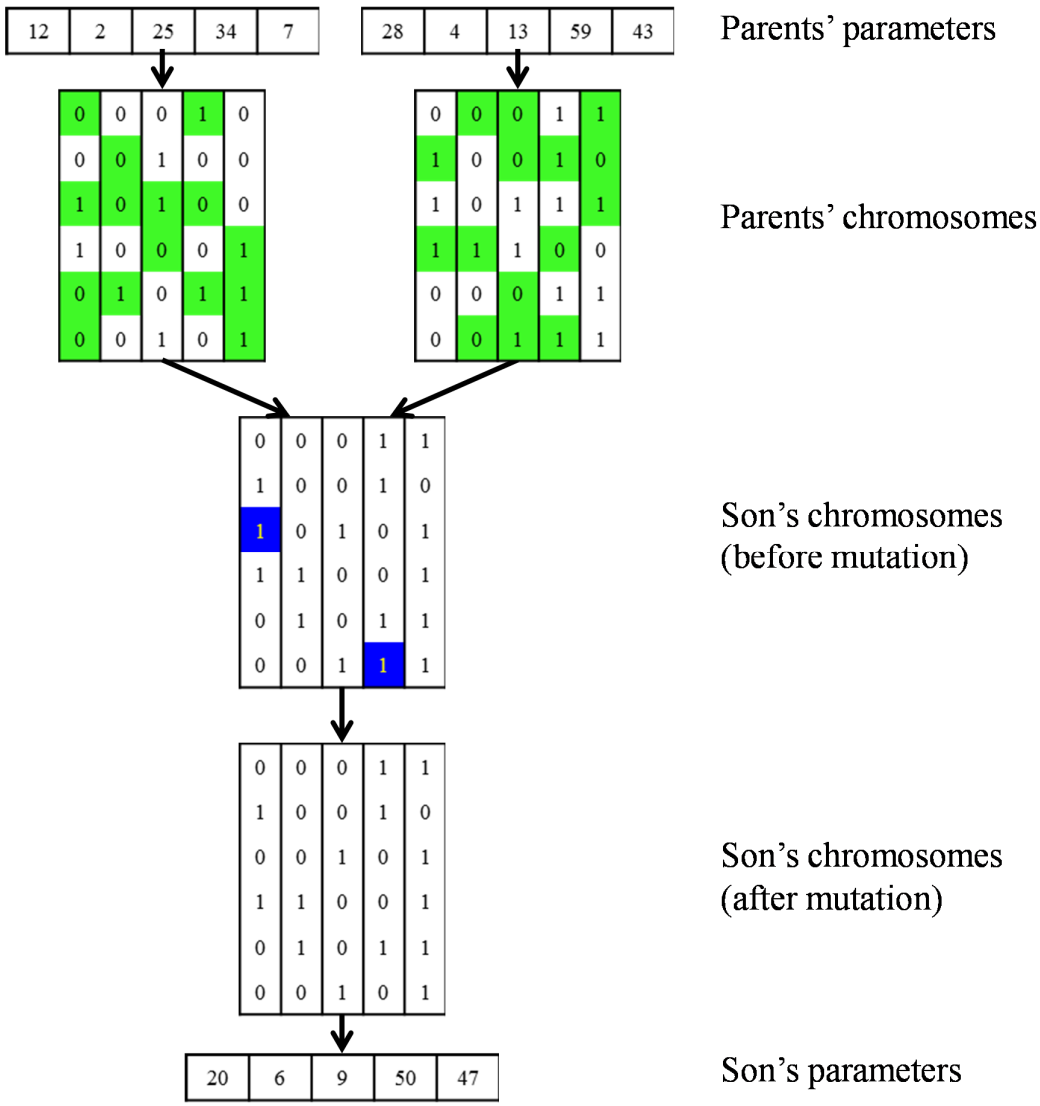

Figure III.2: An example of the mechanism for son generation implemented in the genetic algorithm.

Actually, analysis of the peak frequencies and amplitudes in the PSD allows evaluations of the rhythms characterizing the signal, their frequencies, and the relative power associated to each frequency band.

We introduced some changes to the original GA to improve its speed of convergence.

1. The global population was divided in 4 tribes. Each tribe has its own fitting function. The algorithm allows migration between tribes, so that each individual may choose the tribe

that consent its offspring to converge to the solution in the fastest way. In order to compute the FCs of each tribe, we first calculated three alternative cost functions. The first is the classic mean square error. The second aims at quantifying the similarity in the ratios between the local maxima and the local minima (i. e. it gives more emphasis to the maxima and minima of the PSD than to other values of the PSD). The third focuses the attention especially to the position of the peaks (i.e., the frequencies of the three rhythms). These three functions were then combined with different weights, in order to obtained four alternative FCs to be used in the four tribes. The fourth tribe (also named melting pot) is the one characterized by the strictest requirements.

2. The algorithm uses a dynamic mutation rate. The probability of a bit to switch is related to the similarity between the parents' chromosomes: the more similar the chromosomes, the higher the mutation rate. A high similarity between parents means that the population converged to a local maximum; in this condition, an increase in the mutation rate would favor the escape from the maximum attraction field.
3. An aging factor was introduced. This means that members of the previous generation can still generate sons and daughters, but starting with a decreased FC. Otherwise, the creation of new populations would erase all good old individuals, and if they had poor sons and daughters their legacy would be lost. On the other hand, if old individuals are not weakened, evolution may be too slow.
4. The order of bits inside chromosomes can be shuffled. Commonly each parameter is encoded in a single chromosome, but such a coding system is inefficient when combined with the dynamic mutation rate described above. When one of the parameters approaches its best value, it tends to be inherited by all the members of the population. This means that all the individuals have an almost identical chromosome, thus the mutation rate for the bits encoding this parameter grows rapidly and the partial information reached may be wasted in the successive generation. This problem can be avoided by spreading the information of each parameter among all the chromosomes. Figure III.2 illustrates a more standard coding system.

The algorithm stops either when individuals finish improving their FCs, or after 400 generations. At the end of the simulation the best individual belonging to the melting pot is taken as the best solution.

We noticed that the most beneficial changes are those which best resemble the natural selection.

3. RESULTS

Exempla of model fitting in four exemplary cases are shown in Figure III.3. The left panels refer to two healthy subjects, while the right panels refer to two tetraplegic patients. It is worth noting that the model is able to simulate the position and the relative amplitude of the three peaks in all three ROIs quite well. The other fitted PSDs are similar to those presented here, both for what concerns the shape and the quality of fitting.

The average values of estimated synaptic weights in the healthy population and in the tetraplegic patients are shown in the histogram of Figure III.4. Two main aspects of this figure deserve attention.

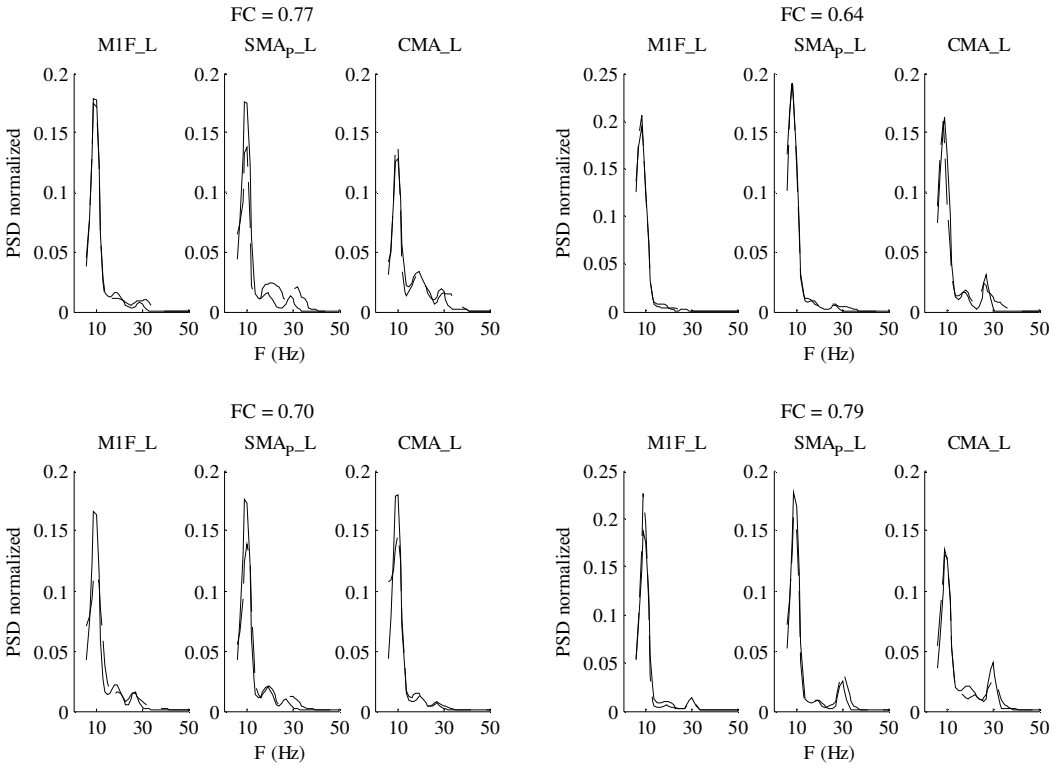

Figure III.3: Comparison between real (dashed line) and simulated (solid line) power spectral densities in the three regions M1F_L (primary motor cortex), SMA$_P$_L (supplementary motor cortex) and CMA_L (cingulate cortex) of the left hemisphere during execution of the foot imagery motor task. The left panels refer to two healthy subjects, while the right panels refer to two tetraplegic patients. All spectra are normalized to have unitary area in the range 6-50 Hz. The value of the fitting coefficient (ranging between 0 and 1) is shown above each panel.

First, by considering the overall fitting parameters, without distinguishing between healthy and tetraplegic subjects, one can observe that some weights are predominant compared with others. In particular, the stronger connections are those from the cyngulate cortex to the primary motor cortex, and from the cyngulate cortex to the supplementary motor cortex. A visual summary of the synaptic strengths, computed by using the average parameters in both populations, is shown in the bottom panel of Figure III.4.

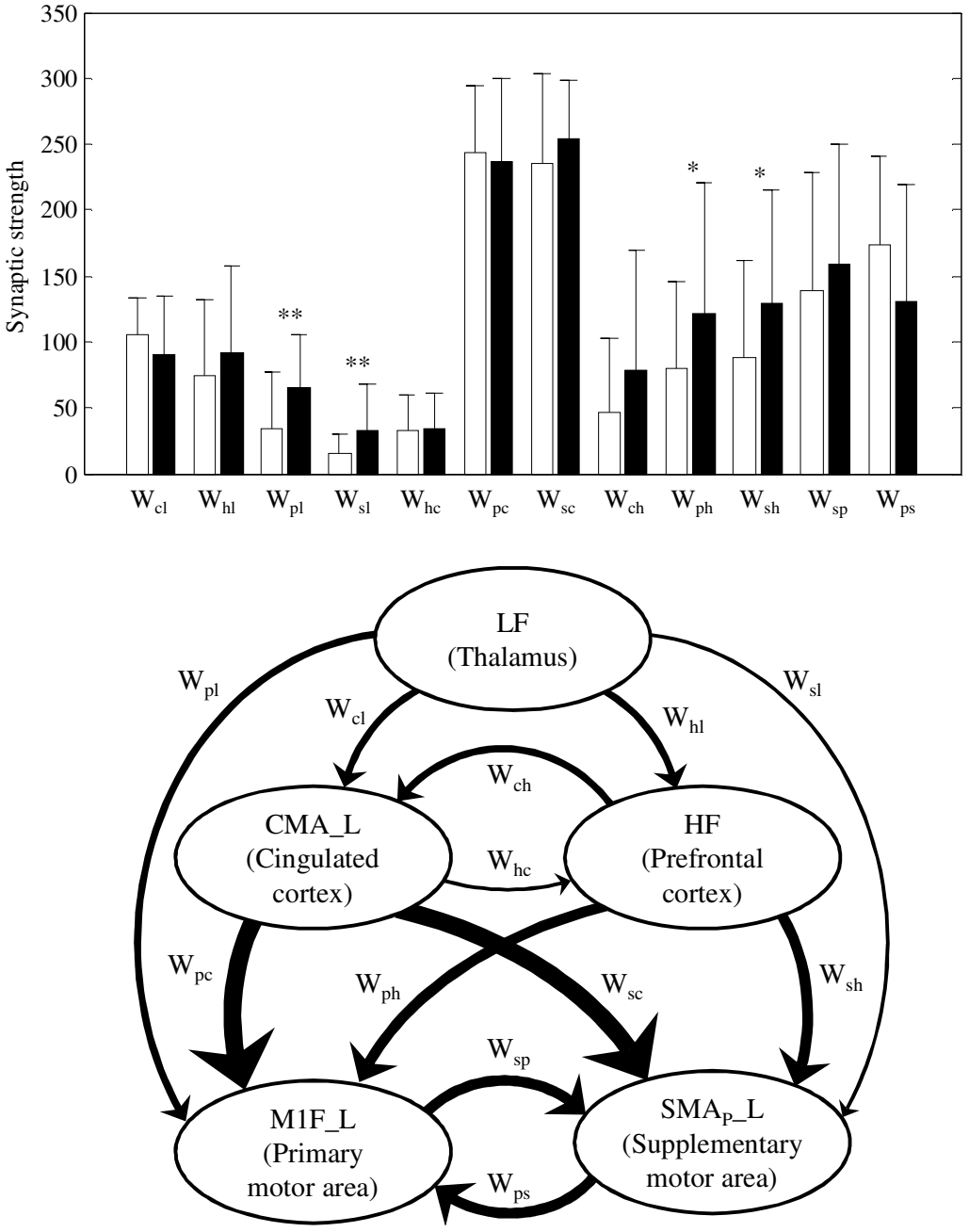

Figure III.4: Connectivity weights (mean value + SD) estimated on 5 healthy subjects and on 5 tetraplegic patients with the genetic algorithm described in the text. A qualitative example of the resulting connectivity, based on the average values on the entire population, is depicted in the bottom panel, where line thickness is proportional to the connectivity weight. It is worth noting in the upper panel the presence of very significant statistical differences ($p < 0.01$, columns with **) between healthy subjects and tetraplegic patients for what concerns the connections from the LF region to the primary motor and supplementary motor areas. Significant statistical differences ($p < 0.05$, columns with *) are also evident in the connections which link the HF region to the primary motor and supplementary motor areas.

Second, from a separate parameter estimates, one can detect statistically significant differences in the synaptic strength between healthy and tetraplegic subjects. In particular, connectivity in tetraplegic patients is about 12% higher (on average) compared with that of healthy volunteers. Differences in connection weights between the two classes are very significant ($p < 0.01$

evaluated with an untailed t-test) from the thalamus to the primary motor cortex and from the thalamus to the supplementary motor cortex. The differences in the connection weights are also significant ($p < 0.05$) from the high frequency region to some cortical ROIs.

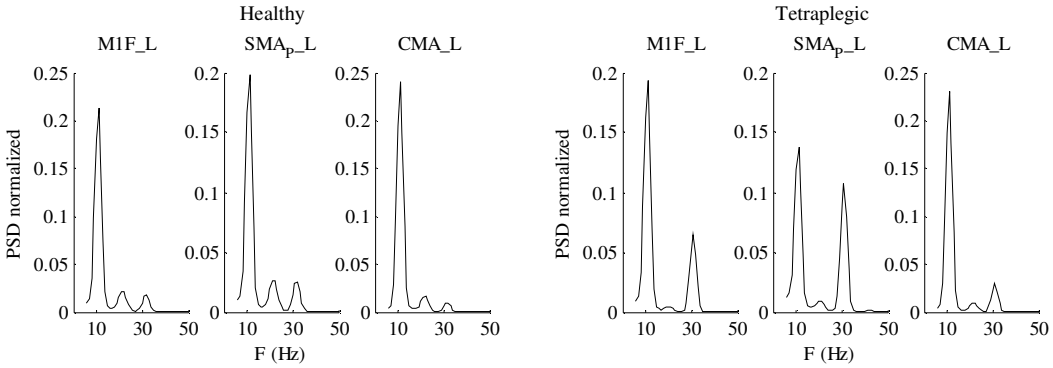

Figure III.5: Examples of paradigmatic power spectral densities simulated with the model using the average connection weights estimated on healthy volunteers (left panel) and on tetraplegic patients (right panel). All spectra are normalized to have unitary area in the range 6-50 Hz. It is worth noting the higher peak in the gamma range, and the lower peak in the beta range in tetraplegic patients compared with the healthy subjects.

Finally, we used the average values of the synaptic strengths in the two populations to compute paradigmatic PSDs (one for a typical healthy subject using the average parameters of that class, and the other for a typical tetraplegic subject). The results are illustrated in Figure III.5. As it is evident from this figure, the paradigmatic tetraplegic subject exhibits a stronger peak in the gamma band compared with that evident in the paradigmatic healthy volunteer and a smaller peak in the beta range. This difference is a consequence of the higher connectivity weights from the HF region and from the LF region.

4. DISCUSSION

The aim of this chapter was to derive patterns of connectivity among the main regions of interest (the cingulate cortex and the primary and supplementary motor areas) involved in simple motor tasks. To this end, we used neural mass models and electrophysiological data obtained with scalp EEG, propagated to the cortex. Moreover, we analyzed differences between normal and tetraplegic subjects. Although various attempts to derive connectivity from EEG, and to characterize EEG in pathological conditions are present in the literature, most works make use of empirical model (for instance based on coherence and correlation among time series). Just a few attempts to elucidate existing data via interpretative models can be found in the literature [David & Friston, 2003; Moran et al., 2008; Sotero et al., 2007].

In an interpretative model, parameters have a clear biophysical significance, and the model allows the formulation of hypotheses on the physiological mechanisms, the neural architecture and the parameter changes responsible for data generation. Promising models assume the presence of interacting neural masses, which are reciprocally connected and generate the neural signals responsible for the measured electrical activity. Similar models integrated with Bayesian inference (a framework named "Dynamic causal models" by the authors) were used by Friston and coauthors to estimate effective connectivity from neuroimaging data [David & Friston, 2003; Stephan et al., 2007], to analyze event related potentials [David et al., 2006] or to predict the spectral profile of local field potentials in the rat [Moran et al., 2008]. Neural mass models were used to study the transition to seizures and to model epileptic activity [Liley & Bojak, 2005; Wendling et al., 2002], to analyze the effect of drugs on EEG spectra [Rowe et al., 2005], or to simulate the effect of the overall brain connectivity on individual EEG rhythms measured on the scalp [Sotero et al., 2007].

This work goes in the same direction as previous papers from our group [Ursino et al., 2006; Zavaglia et al., 2006, 2008a, 2008b]. However, three main innovative methodological aspects deserve a critical discussion: the kind of information used to validate the model, the structure adopted for the model, and the fitting procedure for parameter estimation.

The first important issue concerns what kind of data the model is intended to reproduce, and so, which measurement is compared to model output. This is a crucial point, since the type and structure of a model is strictly dependent on the problem under study. In this work, we focused attention on the frequency content of cortical EEG, in particular on the peaks of power spectral density. Indeed, spectral measures are commonly used to summarize cortical dynamics and to assess changes in cortical activity during cognitive and/or motor tasks. It is generally believed that the alpha rhythm originates from the thalamus and is distinctive of a relaxed state. The beta rhythm is associated with normal waking activity, as it occurs during natural human motor behavior or after proprioceptive stimulation. A shift from alpha to beta rhythms is considered a marker of alerting. Gamma rhythms appear to be involved in higher mental activity, including perception and consciousness. Although these rhythms are currently described and analyzed in the neurophysiological literature [Buzsaki, 2006; Ward, 2003], the problem of how to link their changes to the underlying neural processes, the neural architecture and connectivity strength is still largely unsolved.

An important aspect is that we focused attention just on three ROIs, and we never tried a fitting to other ones. The ROIs were selected according to widely accepted considerations on their involvement in the preparation and execution of simple self-generated movements. In fact, there is

a general consensus that the M1F and the medial aspect of the SMA_p are amongst the main generator sources of the early and late components of the motor-related cortical potentials [Shibasaki & Hallett, 2006] which, in turn, reflect the physiological excitation of the cortical areas involved in preparing and producing movements. Anatomical and physiological studies on non-human primates have demonstrated that among the distinct cingulate motor areas buried in the cingulate sulcus, those roughly located at the same rostro-caudal level as the SMA_p proper (caudal CMA, dorsal and ventral parts) are primarily implicated in movement execution itself rather than in higher cognitive control of voluntary movements [Paus, 2001; Picard & Strick, 1996].

In order to simulate EEG spectral patterns in these areas, including both alpha and beta as well as gamma rhythms, we adopted a simple model structure based on a few a-priori assumptions. First we assumed that the cingulate cortex drives the primary motor area and the supplementary motor area during execution of the task, but it receives only negligible feedback from them. This assumption seemed justified by the attention that the cingulate cortex has received in the neuroscientific literature recently [Posner et al., 2007]. In these contributions the cingulate cortex is seen as a part of the cortex that is mainly involved in the promotion of action and movements of decisions. By contrast, the two motor areas may be connected by a reciprocal feedback. These areas are important in our model since the primary motor area is responsible for the execution of all voluntary movements, while the supplementary motor area implements internally generated or well-learned actions, i.e. actions which do not require monitoring the external environment.

A further assumption is that the three ROIs under analysis, if stimulated, can oscillate with an intrinsic beta rhythm. This assumption agrees with present knowledge. Indeed, as traditionally described in the literature, a motor related activity in the beta range is frequently located close to the sensory motor area following finger movements [Stancák Jr. & Pfurtscheller, 1996] and is reflected to the premotor area [Gómez et al., 2006]. As suggested by [Neuper & Pfurtscheller, 2001] beta oscillations may be “indicative of a resonant behavior of the connected networks in the sensorimotor areas”. This reflects our basic model assumption.

Beyond this fundamental aspect, the model incorporates two other important assumptions, which are used to generate alpha and gamma rhythms, but have a less evident physiological and neural counterpart.

First, model assumes that a low-frequency α rhythm originates from an external area (that we named “thalamic area”) and then propagates to the other regions of interest. Indeed, a classic idea on the genesis of alpha rhythms [Buzsaki, 2006] is that this rhythm arises from the endogenous activity of thalamic neurons, or from thalamo-cortical connections, especially involving the occipital region. Recent works on the cat, support the critical role of the thalamus for the generation of occipital oscillations [Lopes da Silva et al., 1980]. A recent study on the location of EEG rhythms in humans confirms that alpha rhythms are especially evident in the occipital or occipito-temporal regions, i.e., they mainly arise from posterior neural sources [Gómez et al., 2006]. Hence, although we cannot exclude that a source of alpha rhythms may also be present in the examined fronto-parietal regions, the most likely hypothesis is that this rhythm originates in thalamic and/or occipital regions, and is then transmitted toward the other regions of interest.

An important simplification, which deserves a brief comment, is that we neglected any feedback synapse from cortical regions to the “thalamic area”. Of course, cortico-thalamic feedbacks exist in the brain and may have a role in the modulation of the alpha spectral content. Our choice has been adopted just to reduce the number of parameters in the fitting procedure, in order to avoid

the problem of "overfitting". In fact, increasing the number of unknown parameters improves the quality of fitting, but worsens the reliability of parameter estimates.

A further important assumption is that also the gamma rhythm originates from an external area, that we supposed to be located in the frontal cortex. This hypothesis is corroborated by the observation that neurons in the frontal cortex shows the intrinsic capacity to oscillate at 40 Hz [Gutfreund et al., 1995; Llinás et al., 1991]. However, alternative hypotheses on the origin of gamma rhythms can be found in the literature [Jefferys et al., 1996] and we cannot exclude that this rhythm originates internally in the considered ROIs due to recurrent excitation and inhibition mechanisms (especially involving fast inhibitory interneurons). Hence, the gamma region in the model should be considered as a "latent source", that has not necessarily a physiological counterpart. This problem requires further theoretical and experimental work.

Once this model structure has been designed, a fundamental point concerns what aspects of the spectra should be used to perform a best fitting between model predictions and real data. In previous works we used a least-square criterion function of the difference between model and measured spectra [Ursino et al., 2006; Zavaglia et al., 2006, 2008a, 2008b]. Assuming a Gaussian distribution of the measurement error, a least square criterion corresponds to a maximal likelihood estimation, i.e., maximization of the a priori conditioned probability. A more complex Bayesian procedure has been adopted by Moran et al. recently [Moran et al., 2008] under the framework of dynamic causal models [Friston et al., 2003; Stephan et al., 2007]. A Bayesian procedure involves also the inclusion of some a priori knowledge on the probability distribution of the estimated parameters.

In the present work we tried an innovative strategy, based on the idea that not all aspects of the PSD are of equal interest. In particular, we focused attention especially on the position and relative amplitude of the main peaks in the power spectra, thinking that these summarize the underlying mechanisms generating EEG rhythms. Moreover we tried different complementary "cost functions" in the implementation of the genetic algorithm (GA). Although GA are time consuming compared with other minimization techniques, they offer the possibility to try different alternative solutions for the problem (implementing different tribes) and to overcome the problem of local minima (which often makes the result of fitting procedures untenable) by generating different sons through mutations in the parameter space.

Two main objectives have been pursued with this technique: to discover possible simple circuits, connecting the three aforementioned ROIs, able to explain the observed PSDs; and to detect possible differences in connectivity circuits between healthy subjects and tetraplegic patients. Results point out the existence of significant differences between the two classes, especially for what concerns the weights which link the LF (thalamic) and HF regions to the primary and the supplementary motor cortices. In particular, these weights are stronger in tetraplegic patients compared with healthy individuals and these differences are statistically significant. Differences in connectivity weights might reflect a higher awareness (related with the gamma component) and a greater attention (related with thalamic inputs) in the tetraplegic patient than in the normal individuals, i.e., greater concentration toward the task. The existence of larger and stronger connectivity weights in the cortical connectivity networks estimated in tetraplegic patients compared with those estimated in healthy volunteers has been previously observed by several authors [Mattia et al., 2009; De Vico Fallani et al., 2008].

A further interesting result of our work is that the greatest weights in the neural circuit are those which link the cingulate cortex to motor areas. This result underlines the importance of a feedforward signals from the frontal cortex in the initiation and planning of the voluntary movement.

In the present work we performed 12 statistical tests, hence a possible objection is that the significance level should be corrected to account for multiple hypotheses. The problem of whether correction is appropriate or not is quite complex and depends on the objective of the work. As clearly stated in recent publications [Roback & Askins, 2005] if the main goal is generation hypothesis or initial screening for potential solutions, it may be appropriate to use the standard significance level without corrections to avoid Type II errors (not detecting real differences or trends). Conversely, if the main goal is rigorous testing of a hypothesis, then an adjustment for multiple tests (like Bonferroni or Holm's methods) is needed. The objective of the present work is certainly "hypothesis generation", hence we preferred to use classical t test to avoid type II error. Of course, in order to "test the hypotheses" generated with our procedure, one needs to repeat the experiment with new "fresh" data, considering only the individual hypotheses to be verified, and using a correction. This may be the subject of future works.

Finally, it is important to discuss the main limitations of the present preliminary work, and possible lines for future changes.

A first aspect concerns the variability of parameter estimates within the same subject. Although this variability is less accentuate compared with that between the two classes, and between different subjects in the same class, it is still quite elevated. Analysis of how the connectivity pattern may vary in the same subject from one trial to the next still requires a deeper future analysis.

In the present model we assumed that connectivity originates from pyramidal neurons, and reaches the input of excitatory interneurons, i.e., we did not consider possible lateral connections from pyramidal neurons to inhibitory interneurons. Inhibitory inter-area connections, however, may be important to reduce neural activity, to avoid instability and to improve synchronization among rhythms. Lateral inhibitory synapses were considered by David et al. [David et al., 2006] and Stephan et al. [Stephan et al., 2007] in their DCM schema of neural populations for the analysis of event related responses. In particular, these authors assumed that lateral connections originating from pyramidal neurons target to all other populations (both excitatory and inhibitory) in the lateral ROIs, although they did not consider the presence of inhibitory interneurons with fast kinetics. Inclusion of lateral connections toward inhibitory interneurons may be of value in future works, to improve two aspects of results. First, it may help to maintain the activity of the motor and premotor ROIs far from saturation. Indeed, with the present values of parameters, these two populations are strongly activated and often work close to the upper saturation region of their sigmoid. Second, activation of fast inhibitory interneurons might help to explain the presence of gamma rhythms, even without introducing an ad hoc rhythm from an external population. The idea that gamma rhythms may originate from stimulation of fast inhibitory interneurons (or alternatively from gap junctions) has been proposed by various authors recently [Buzsaki, 2006; Traub et al., 2000]. Of course, a flaw of introducing lateral synapses to inhibitory interneurons is the increase in the number of free parameters, which may further complicate the convergence of the fitting procedure and the interpretation of results.

Another important limitation of the work presented in this chapter is that the model is able to simulate PSD spectra only if the rhythms in the three ROIs (in the alpha and gamma bands), have almost the same frequency. In view of that, we excluded all trials which present different frequencies in the spectra from the best fitting procedure. The reason for this limitation is that the three ROIs receive the alpha and gamma oscillations from the same external ROIs (i.e., the alpha rhythm from the LF region or thalamus; the gamma rhythms from the HF ROI, prefrontal, see Figure III.1). In order to generate rhythms with different frequencies in the alpha and gamma bands, one should hypothesize the presence of more LF and HF regions. However, this aspect would further complicate parameter estimation and would make the model less parsimonious. It is possible that introduction of lateral inter-region synapses directed to inhibitory interneurons may allow a more flexible positioning of rhythms in individual ROIs.

Finally, we are aware that use of the genetic algorithm, although very flexible in finding a good solution avoiding local minima, is time consuming. Alternative more efficient fitting methods (maybe introducing some prior probability for the estimate, according to a Bayesian approach [Friston et al., 2002]) may be attempted in future studies.

In conclusion, this work represents a first attempt to explain the presence of multiple rhythms in three ROIs involved in motor tasks, and their variability, using a simple model of interconnected populations. Encouraging results concern the capacity to obtain reliable PSD spectra, by acting on a few parameters representing the connection weights, and to detect significant differences between the two classes. However, important limitations are still evident: they are especially concerned with a lack of inhibitory interactions among ROIs, with the dispersion of individual parameter estimates, and with the difficulty to generate more flexible peaks in the spectra. Overcoming these limitations deserve much future work.

Nevertheless, despite their present limitations, we claim models of interacting neural mass may be of great value to gain a deeper insight into the mechanisms of rhythms generation in EEG, and to start the formulation of more quantitative hypotheses on the neural architecture and connectivity changes underlying motor/cognitive tasks.

IV. NEW NMM WITH FAST INHIBITORY SELF-LOOP[2]

1. INTRODUCTION

Analysis of brain activity at a mesoscopic scale (from a millimeter to several centimeters of the cortex) reveals the presence of synchronous oscillations, which cover a large spectrum of frequencies and can be detected using EEG, MEG or ECoG [Buzsaki, 2006]. It is generally assumed that these oscillations are not merely an epiphenomenon, but play a crucial role in many important processes of the cortex, especially involving association among different functions [Başar et al., 2000, 2001; Ward, 2003]. The study of brain rhythms, in turn, of their etiology and functional role is strictly connected with the estimation of effective connectivity among brain regions. Rhythms originating in one region, in fact, may be transmitted to other regions via long range excitatory connections, and this "system of rhythms" may serve important functions to associate information from one region to another, to detect the phase of events, or to drive synaptic plasticity, thus playing a pivotal role in learning and memory [Başar et al., 2000, 2001; Engel & Singer, 2001; Ward, 2003].

One way to improve our knowledge of this "system of rhythms", and to investigate the correlated problem of effective cortical connectivity, is through the use of dynamical mathematical models. In particular, a discipline named neurodynamics aims at analyzing the operations of the brain by investigating (via mathematical models and signal processing techniques) the dynamical aspects of electric or magnetic brain activity [Freeman, 1975; Nunez, 1995].

Mathematical models used to study brain dynamics can be roughly subdivided into two main classes, each with its virtues and drawbacks. In a first class of models, the activity of individual neurons is described in detail (generally using spiking neurons) and the properties of ionic channels, axons and dendrites often incorporated explicitly [Maex & De Schutter, 2007; Traub et al., 2005; Wang & Buzsáki, 1996]. Although these models are of the greatest value to understand the basic mechanisms of neural dynamics at a microscopic scale (for instance, to investigate mechanisms causing oscillations in a network of neurons) they are too cumbersome and computationally onerous to analyze the behavior of entire cortical regions at a mesoscopic level.

Much attention in recent years has been devoted to the so-called "neural mass models" (NMMs), first introduced by Wilson and Cowan [Wilson & Cowan, 1972], Freeman [Freeman, 1978], and Lopes da Silva et al. [Lopes da Silva et al., 1974] in the mid-seventies. In these models, the dynamics of entire neural populations and of their synapses are described using just a few state variables (i.e., a few differential equations) under the assumption that neurons in the same population share similar inputs and synchronize their activity. Besides a smaller computational complexity, these models offer a more parsimonious description of neural dynamics in terms of parameters and mechanisms involved, generally ascribing rhythm generation to feedback loops

[2] The contents of this chapter are published in Neuroimage (Ursino et al., 2010).

between excitatory and inhibitory neural populations. One of the first models of this type is the Wilson-Cowan oscillator, which is still largely used today to study synchronization among neural oscillations [Wilson & Cowan, 1972]. Lopes da Silva et al. [Lopes da Silva et al., 1974], proposed a simple model of two populations in feedback (one excitatory and the other inhibitory) to simulate the generation of the α rhythm in the thalamus. Freeman proposed a similar model to study dynamics in the olfactory cortex [Freeman, 1978]. These models have been subsequently improved by Jansen et al. [Jansen & Rit, 1995; Jansen et al., 1993]: their model encompasses the interaction between three neural populations with different synaptic kinetics (pyramidal neurons, excitatory interneurons, inhibitory interneurons), as it occurs in a single cortical column. The Jansen equations are frequently used today to build models of interconnected cortical areas devoted to the analysis of EEG dynamics in large regions of the brain [David & Friston, 2003], to study effective connectivity from EEG or fMRI data [Babajani & Soltanian-Zadeh, 2006] or to investigate how event related potentials (ERPs) depend on intrinsic connectivity [David et al., 2005]. Friston et al. [Friston, 2005; Kiebel et al., 2008] developed a mathematical formalism, named Dynamic Causal Modeling (DCM), to provide a theoretical framework for the study of brain dynamics: it uses some variations of the Jansen model to characterize dynamics in cortical regions, together with a Bayesian approach for parameter estimation from data. Others [Babajani & Soltanian-Zadeh, 2006] used neural mass models to link data obtained from metabolic imaging (PET or fMRI) and electromagnetic signals (EEG or MEG). Sotero et al. [Sotero et al., 2007] developed a model of the overall cortical dynamics (still based on a variation of the Jansen model) to investigate how the distribution of brain rhythms on the cortex may depend on effective connectivity among the ROIs (regions of interest). Their model includes 71 brain areas with anatomical connectivity matrices among these areas. Models for the analysis of EEG at a mesoscopic scale were formulated by Wright, Robinson, Rowe et al. in a series of papers from the mid-nineties [Rennie et al., 2002; Robinson et al., 2001; Wright et al., 2003]. Although these models use a continuum in space instead of discrete neural populations, they share many aspects with neural mass models; in particular they exploit a few equations to summarize neural dynamics.

An important advancement in the use of neural mass models was provided by Wendling et al. [Wendling et al., 2002]. Studying hippocampal dynamics during epilepsy, they proposed the addition of a fourth population to the Jansen model to account for the presence of $GABA_A$ interneurons with fast synaptic kinetics [White et al., 2000]. With this model they were able to simulate the dynamics of real EEG signals measured with intracerebral electrodes in the hippocampus during the transition from interictal to fast ictal activity. Recently, the Wendling model was used by Ursino, Zavaglia et al. to simulate the multimodal power spectral density in cortical regions [Zavaglia et al., 2006, 2008a] and to assess cortical connectivity via parameter estimation techniques [Cona et al., 2009; Ursino et al., 2006] during simple motor tasks. In particular, these studies stress the importance of fast inhibitory interneurons in the genesis of power in the γ band.

Neural mass models were used by Moran et al. in a series of recent papers to simulate spectral densities of EEG and MEG recordings [Moran et al., 2007, 2009]. In these last models, the authors introduced recurrent connections among inhibitory interneurons and spike rate adaptation. Using linearity and stationarity assumptions, they investigated how the model's biophysical parameters (e.g., post-synaptic receptor density and time constants) influence the cross-spectral density of responses measured directly.

This short summary underlines the rising importance that neural mass models are acquiring for the study of brain dynamics. Analysis of the literature, however, and previous simulations of our group [Ursino et al., 2006; Zavaglia et al., 2006] also reveal some important limitations of these models. First, a single neural mass model (consisting of three (Jansen) or four (Wendling) neural populations connected via multiple feedbacks) when stimulated with input white noise produces just a single rhythm, with a narrow band, or, in some cases, a wide band spectrum. This "intrinsic rhythm" may originate either from instability of the feedback loops or, more frequently, from noise amplification caused by a resonance in a given frequency band [Grimbert & Faugeras, 2006]. Moreover, to produce rhythms in different bands, these models necessitate a change in the synaptic time constants. In particular, simulating γ rhythms in these models requires the use of very small values for the time constant of fast interneurons (i.e. a few ms) [Wendling et al., 2002; Zavaglia et al., 2008a]. Conversely, real spectra measured during motor or cognitive tasks often reveal the presence of multiple rhythms in the same ROI [Rowe et al., 2004; Ursino et al., 2006; Zavaglia et al., 2006]. The simultaneous coexistence of several rhythms appears as an important characteristic of brain dynamics, which may have important computational functions.

Hence, the following problems are "on the table". How can we simulate different rhythms in a single ROI within the framework of NMMs? Are these models adequate to simulate γ oscillations, which play an essential role in many high-level cognitive tasks?

David and Friston [David & Friston, 2003] suggested that a multi-modal spectrum can be obtained via NMMs by assuming the presence of different sub-populations in the same cortical region with different synaptic kinetics (i.e., different sub-populations of pyramidal neurons, excitatory interneurons, etc…). A similar approach was followed by Zavaglia et al. [Ursino et al., 2006; Zavaglia et al., 2006] to simulate α, β and γ rhythms in some ROIs during simple motor tasks. It is worth noting that the same idea was implicitly followed also by Sotero et al. [Sotero et al., 2007]; in fact, these authors simulated the distribution of δ, α, β and γ rhythms separately, which is the same as to consider four separate systems of rhythms with distinct sub-populations of neurons. Although this approach may be consistent with the physiological reality, it appears not parsimonious: you need one specific population of neurons for each rhythm you want to generate. A more parsimonious approach was proposed by our group recently: we hypothesized that each region can produce just one intrinsic rhythm due to its internal dynamics, but it can receive additional rhythms from other regions via long-range excitatory connections [Cona et al., 2009; Zavaglia et al., 2008a]. With this model one does not need to replicate too many populations of neurons, but still needs to modify synaptic kinetics from one region to another. However, with this model it is still difficult to obtain more than two simultaneous rhythms in the same ROI.

In the present work, we suggest a variation in NMMs which can help to overcome the previous limitations, and can be of value to build a system of interconnected rhythms among ROIs. Our variation is based on some recent experimental and modeling results, suggesting that γ rhythms can be generated by a network of fast inhibitory interneurons without the participation of the other populations.

Whittington, Traub and Jefferys [Jefferys et al., 1996; Whittington et al., 1995] numerically simulated a network of isolated inhibitory neurons tonically excited by an external input, and showed that the neurons tend to entrain their activity into rhythmic firing at about 40 Hz thanks to reciprocal inhibition. Subsequent studies which investigated the oscillatory behavior of large inhibitory interneuron networks assuming slow and weak synapses [Tiesinga & José, 2000; Wang & Buzsáki, 1996; White et al., 1998], confirmed that these networks can produce coherent

oscillations when subject to external excitation. Oscillations, however, appeared scarcely robust to variations in the excitatory drive. To improve robustness one needs to incorporate fast and strong inhibitory synapses into the network, but in this case a stronger external excitatory drive is required to overcome inhibition [Neltner et al., 2000]. These results suggest that fast-spiking inhibitory interneurons play a pivotal role in the generation of γ-band oscillations [Bartos et al., 2007].

The previous modeling results are supported by experimental data. First, oscillations of inhibitory post-synaptic potentials at frequencies in the γ-band occur in the hippocampal and neocortical slices even after blockade of glutamate receptors [Jefferys et al., 1996; Whittington et al., 1995]. Basket cells are highly interconnected in the hippocampus and in the neocortex [Bartos et al., 2007] where they can form an extensive mutually interconnected interneuron network [Kisvárday et al., 1993; Sik et al., 1995] with a large divergent synaptic output to other neurons [Cobb et al., 1995].

Despite the large number of theoretical and experimental data that stress the role of a fast inhibitory network in the genesis of γ-rhythms, we are not aware that this mechanism is solidly incorporated into neural mass models. Moran et al. incorporated recurrent self-connections between inhibitory interneurons in their recent model [Moran et al., 2007, 2008] motivating this choice with the necessity to generate high-frequency oscillations in the γ band. However, they used only one populations of inhibitory interneurons, without a distinction between $GABA_{A,fast}$ and $GABA_{A,slow}$ synaptic kinetics.

According to the previous discussion, three main objectives have been pursued in this chapter: i) to enrich the NMM of a single region by adding a new feedback loop, through which fast inhibitory interneurons can produce a γ rhythm per se (i.e., without the participation of the other neural populations); ii) to demonstrate that the modified model can easily produce EEG PSD of a single region characterized by two peaks (i.e., two activities in different bands), using a very parsimonious description of connectivity weights and without altering model time constants. iii) to demonstrate that a model of interconnected ROIs can produce complex multimodal spectra and that a long-range connection between two ROIs is much more efficient to transmit rhythms if it targets fast inhibitory interneurons, rather than pyramidal neurons.

The model is first presented in a synthetic form and the mechanism of γ-rhythm generation analyzed ("reduced model"). Then, the role of connectivity between populations of excitatory and inhibitory interneurons internal to the cortical region is studied, laying particular attention to the role of $GABA_{A,fast}$ interneurons ("complete model"). Subsequently, the effect of connectivity between two or three cortical regions is shown ("coupled complete model"). The discussion underlines the main innovative aspects of the proposed model.

2. METHOD

2.1. A single region model: a brief summary

As described in the previous chapter, the model of a cortical region consists of four neural populations, which represent pyramidal neurons, excitatory interneurons, and inhibitory interneurons with slow and fast synaptic kinetics, respectively. Each population represents a group of neurons of the same type, which approximately share the same membrane potential and so can be lumped together. All populations are described with a similar mathematical formalism, as in Figure IV.1.

Briefly, each population receives an average postsynaptic membrane potential (v) from other neural populations, and converts this membrane potential into an average density of spikes fired by the neurons. In order to account for the presence of inhibition (when potential is below a given threshold) and saturation (when potential is high) this conversion is simulated with a static sigmoidal relationship. Moreover, each population sends synapses to other populations (or, in case of pyramidal neurons, to other regions too). Each synaptic kinetics is described with a second order system, but with different parameter values.

However, differently from chapter III, throughout the present chapter we will assume a variational model, i.e., all quantities are considered as variations with respect to a hypothetical basal value. Moreover, this basal value is taken at the central point of the sigmoidal relationship. As a consequence, all quantities have zero mean value and are centered at the basal value, assumed equal to zero. A similar assumption has been done also by others when developing recent neural mass models [David et al., 2005].

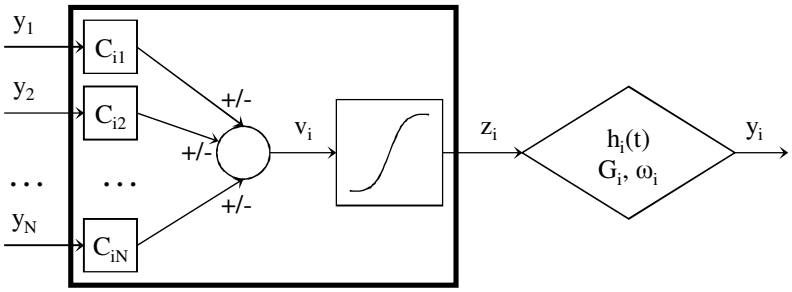

Figure IV.1: Layout of the general model of a single population.

Of course, the use of a variational model also exhibits some important limitations: in particular, neither the position of the working point nor the slope of the sigmoid at the equilibrium value vary with the connectivity parameters. This simplification has been adopted to maintain the model in the linear region: this choice helps the analysis of rhythm transmission, avoiding that the equilibrium point in some population shifts to the sub-threshold or to the saturation region due to an excessive connectivity [Ursino et al., 2006]. This limitation can be overcome in future works, for instance by using a non-zero mean value for model inputs (thus making the equilibrium values to depend on connectivity parameters too).

In the following, a quantity which belongs to a neural population will be denoted with the subscript p (pyramidal), e (excitatory interneuron), s (slow inhibitory interneuron) and f (fast inhibitory interneuron).

Hence, the previous concepts are summarized by the following equations

$$v_i = \sum_j C_{ij} y_j \qquad \text{IV.1}$$

$$z_i = S(v_i) = \frac{2e_0}{1 + e^{-rv_i}} - e_0 \qquad \text{IV.2}$$

$$\frac{d^2 y_i}{dt^2} = G_i \omega_i z_i - 2\omega_i \frac{dy_i}{dt} - \omega_i^2 y_i \qquad \text{IV.3}$$

where the subscript j refers to a presynaptic neural population, y_j is the post-synaptic potential change induced by a unitary synapse, C_{ij} represent the connectivity constant from the j-th population to the i-th one, and the sum in the right hand member of Eq. IV.1 extends to all populations which make synapses to the i-th population. Parameters e_0 and r in Eq. IV.2, assumed equal for all populations, set the maximal saturation and the slope of the sigmoidal relationship, while G_i and ω_i in Eq. V.20 represent the strength and the reciprocal of the time constant of the individual synapses. It is worth noting that, by giving different values to G_i and ω_i (i = p, e, s, f) one can mimic the impulse responses of the different synapses (excitatory, $GABA_{A,slow}$ and $GABA_{A,fast}$). In the following, these impulse responses will be denoted with symbols $h_e(t)$, $h_s(t)$ and $h_f(t)$, assuming that excitatory interneurons have the same kinetics as pyramidal cells (i.e., $h_p(t) = h_e(t)$).

2.2. A network of fast inhibitory interneurons: the "reduced model"

Previous versions of neural mass models [Freeman, 1975; Jansen & Rit, 1995; Wendling et al., 2002] assumed that each neural population (p, e, s, f) receives its synaptic inputs from other populations in the same region or from pyramidal neurons in other regions. As a consequence, a neural population isolated from the others and stimulated by white noise cannot exhibit an intrinsic rhythm. Only connections with other populations can induce the presence of rhythms, due to a balance between excitation and inhibition.

Conversely, experimental and computational results (summarized in the Introduction) underscore that a network composed of fast inhibitory interneurons can induce γ rhythms, even without the presence of other neural populations. Since this mechanism may play a significant role in the brain, providing a clock for pyramidal cells [Jefferys et al., 1996], we modified the description of the fast inhibitory interneurons taking into account the possible effect of their re-entrant connections. Indeed, basket cells (GABAergic interneurons) are highly interconnected and there is a high probability to find a chemical synapse between two closely placed fast-spiking basket cells [Bartos et al., 2007].

It is worth noting that the Jansen model was already modified in previous works with the introduction of a recurrent self-loop: for instance, Sotero et al. [Sotero et al., 2007] introduced a self-excitatory loop for the pyramidal population to account for the majority of intracortical fibers within a voxel; Moran et al. [Moran et al., 2007] introduced a self-loop among inhibitory interneurons to generate γ rhythms. However, none of these models used $GABA_{A,fast}$ synapses.

The simple model of isolated fast inhibitory interneurons (named the "reduced model") is described in Figure IV.2. Here, to have realistic dynamics, we assumed that these interneurons synapse with themselves (hence, we included a self-loop with impulse response $h_f(t)$) and that are tonically excited by an external input (which may come from populations in the same area or from other cortical areas). The excitation is simulated with white noise (say $u_f(t)$) with zero mean value and variance $\sigma^2 = 5s^{-2}$, which acts through excitatory synapses (impulse response $h_e(t)$). The mean value of the input noise is taken as zero, since we are working with a variational model.

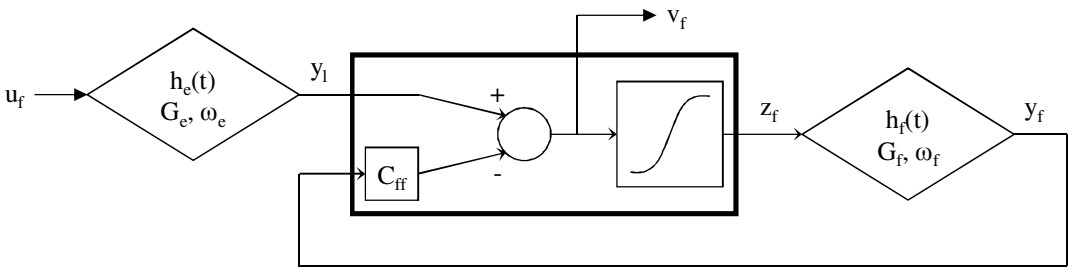

Figure IV.2: Layout of the model of $GABA_{A,fast}$ inhibitory interneurons.

A deeper comprehension of the mechanisms through which this fast interneuron model generates a γ rhythm can be achieved via an analytical approach, by studying the linearized model around its critical points. The critical points are those for which the derivative of the state vector $Y_f = (y_f, \dot{y}_f)$ are zero, at the mean value of the input ($u_f = 0$). We can write:

$$\begin{cases} v_f = -C_{ff} y_f \\ z_f = S(v_f) = \dfrac{2e_0}{1 + e^{-r v_f}} - e_0 \\ \dfrac{dy_f}{dt} = 0 \\ \dfrac{d^2 y_f}{dt^2} = G_f \omega_f z_f - 2\omega_f \dfrac{dy_f}{dt} - \omega_f^2 y_f = 0 \end{cases} \quad \text{IV.4}$$

where C_{ff} represents the strength of connections among inhibitory interneurons.

The only solution is the origin of the phase space $Y_f = (0,0)$, so $v_f = 0$. The sigmoid is the only block that has to be linearized. By replacing its expression with the first order Taylor expansion in the critical point:

$$z_f = \left.\frac{\partial S(v_f)}{\partial v_f}\right|_{v_f=0} v_f = \frac{e_0 r}{2} v_f \quad \text{IV.5}$$

one can obtain the transfer function of the linearized model in the frequency domain:

$$H(j\omega) = \frac{G_e \omega_e (\omega_e + j\omega)^2}{(\omega_e + j\omega)^2 [\omega_f (K + \omega_f) + 2\omega_f j\omega + (j\omega)^2]} \quad \text{IV.6}$$

where $K = \frac{e_0 r}{2} C_{ff} G_f$ is the loop gain. It can be easily verified that if the parameters are all positive the model is asymptotically stable. H can be seen as the product of two transfer functions H_1 and H_2 such that

$$H_1(j\omega) = G_e\omega_e\frac{(\omega_f + j\omega)^2}{(\omega_e + j\omega)^2} \quad \text{IV.7}$$

$$H_2(j\omega) = \frac{1}{\omega_f(K + \omega_f) + 2\omega_f j\omega + (j\omega)^2} \quad \text{IV.8}$$

Since $\omega_e < \omega_f$, H_1 represents a low-pass filter which attenuates high-frequencies compared with the low frequencies (the attenuation ratio is ω_e/ω_f) and so it cannot be responsible for γ frequency amplification. H_2 is a second order low-pass filter, so its behaviour is totally described by its natural frequency ω_n and its damping factor δ.

$$\omega_n = \sqrt{\omega_f(K + \omega_f)} \quad \text{IV.9}$$

$$\delta = \sqrt{\frac{\omega_f}{K + \omega_f}} \quad \text{IV.10}$$

If the parameters are chosen to have physiologically plausible values (see section 3.) then $\delta < \frac{1}{\sqrt{2}}$. In this case, a resonance occurs at ω_{peak}, where

$$\omega_{peak} = \sqrt{\omega_f(K - \omega_f)} \quad \text{IV.11}$$

ω_{peak} is typically located in the γ band. The latter point will be examined in section 3. via a parameters sensitivity analysis on K and ω_f.

2.3. Model of a single cortical area: the "complete model"

In sub-section 2.2. we considered only a single population, and so Eq. IV.11 holds only for the "reduced model". Of course, the activity of this gamma rhythm (and thus its frequency) changes when interneurons are connected to other populations. To model a whole cortical area (the "complete model", either an overall ROI as in Zavaglia et al. [Zavaglia et al., 2008a], or a voxel as in Sotero et al. [Sotero et al., 2007]) we need to connect the four populations via excitatory and inhibitory synapses, with impulse response $h_e(t)$, $h_s(t)$ or $h_f(t)$. The average numbers of synaptic contacts among neural populations are represented by eight parameters, C_{ij} (see Figure IV.3), where the first subscript represents the target (post-synaptic) population and the second subscript is the pre-synaptic population. These connections agree with those proposed by Wendling et al. [Wendling et al., 2002] but with the addition of the new self-loop C_{ff}.

An important aspect of the model is the external inputs. Since inputs originate from pyramidal neurons in other cortical areas, in the following we will assume that they always act via excitatory synapses (hence, with impulse response $h_e(t)$). In previous works [Ursino et al., 2006; Zavaglia et al., 2008a], we assumed that inputs target pyramidal cells. However, lateral connections in the cortex target all layers [Felleman & Van Essen, 1991], hence inputs can actually reach both pyramidal cells and excitatory interneurons as well as inhibitory interneurons [David et al., 2005]. For brevity, in the following, we will consider only inputs to pyramidal neurons and to fast inhibitory interneurons. A parameters sensitivity analysis has been performed also on inputs to slow inhibitory and excitatory interneurons, but is not reported since it did not produce appreciable changes in model dynamics. This aspect will be further analyzed in section 4. .

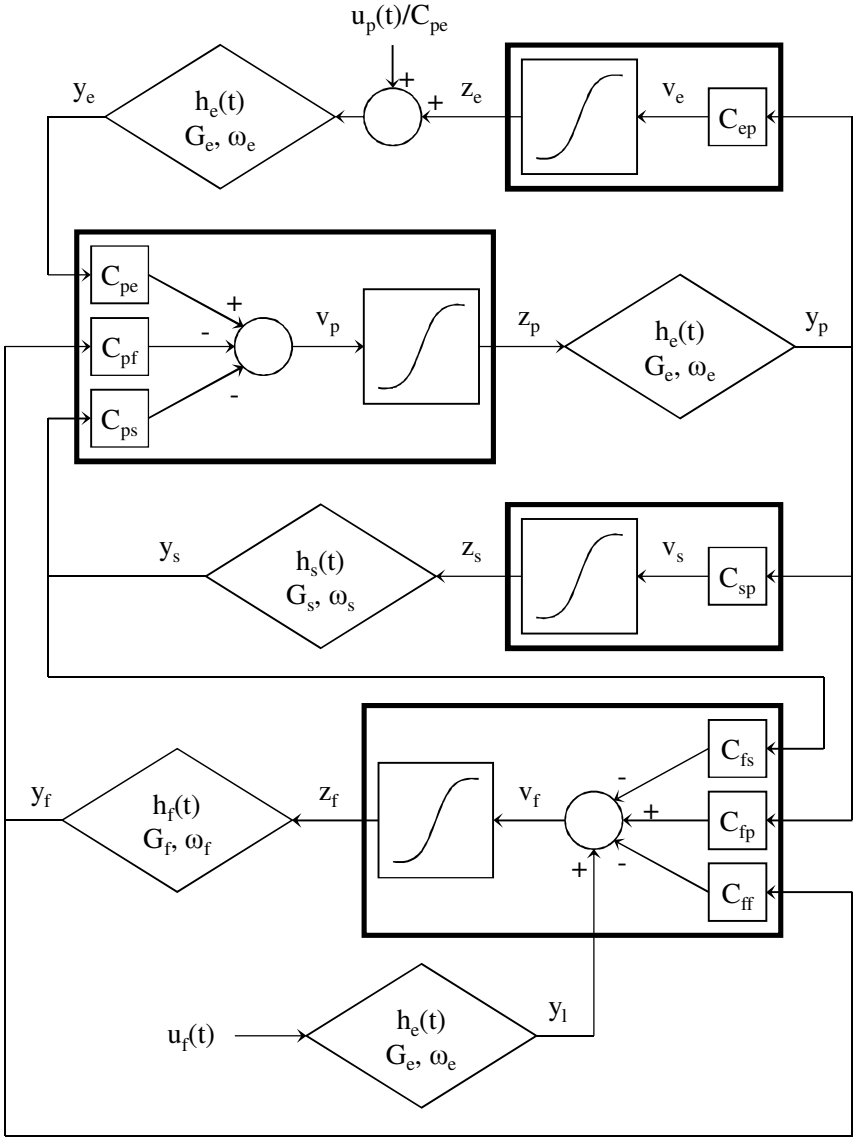

Figure IV.3: Layout of the model of a single region: four neural populations (pyramidal cells, excitatory interneurons, $GABA_{A,slow}$ inhibitory interneurons and $GABA_{A,fast}$ inhibitory interneurons) which communicate via excitatory and inhibitory synapses. Worth noting is the presence of a new feedback loop with gain C_{ff}.

In conclusion, compared with the model described in our previous work [Zavaglia et al., 2008a], the new "complete model" has two changes: i) fast inhibitory interneurons may receive an external input (say $u_f(t)$) from pyramidal neurons of other populations. ii) Fast inhibitory interneurons exhibit a negative self-loop, i.e., they not only inhibit pyramidal neurons (as in Wendling model), but also inhibit themselves. The final model is displayed in Figure IV.3. It corresponds to the following set of differential equations:

Pyramidal neurons

$$\frac{dy_p(t)}{dt} = x_p(t) \quad \text{IV.12}$$

$$\frac{dx_p(t)}{dt} = G_e\omega_e z_p(t) - 2\omega_e x_p(t) - \omega_e^2 y_p(t) \quad \text{IV.13}$$

$$z_p(t) = \frac{2e_0}{1 + e^{-rv_p}} - e_0 \quad \text{IV.14}$$

$$v_p(t) = C_{pe}y_e(t) - C_{ps}y_s(t) - C_{pf}y_f(t) \quad \text{IV.15}$$

Excitatory interneurons

$$\frac{dy_e(t)}{dt} = x_e(t) \quad \text{IV.16}$$

$$\frac{dx_e(t)}{dt} = G_e\omega_e\left(z_e(t) + \frac{u_p(t)}{C_{pe}}\right) - 2\omega_e x_e(t) - \omega_e^2 y_e(t) \quad \text{IV.17}$$

$$z_e(t) = \frac{2e_0}{1 + e^{-rv_e}} - e_0 \quad \text{IV.18}$$

$$v_e(t) = C_{ep}y_p(t) \quad \text{IV.19}$$

Slow inhibitory interneurons

$$\frac{dy_s(t)}{dt} = x_s(t) \quad \text{IV.20}$$

$$\frac{dx_s(t)}{dt} = G_s\omega_s z_s(t) - 2\omega_s x_s(t) - \omega_s^2 y_s(t) \quad \text{IV.21}$$

$$z_s(t) = \frac{2e_0}{1 + e^{-rv_s}} - e_0 \quad \text{IV.22}$$

$$v_s(t) = C_{sp}y_p(t) \quad \text{IV.23}$$

Fast inhibitory interneurons

$$\frac{dy_f(t)}{dt} = x_f(t) \quad \text{IV.24}$$

$$\frac{dx_f(t)}{dt} = G_f\omega_f z_f(t) - 2\omega_f x_f(t) - \omega_f^2 y_f(t) \quad \text{IV.25}$$

$$\frac{dy_l(t)}{dt} = x_l(t) \quad \text{IV.26}$$

$$\frac{dx_l(t)}{dt} = G_e\omega_e u_f(t) - 2\omega_e x_l(t) - \omega_e^2 y_l(t) \quad \text{IV.27}$$

$$z_f(t) = \frac{2e_0}{1 + e^{-rv_f}} - e_0 \qquad \text{IV.28}$$

$$v_f(t) = C_{fp}y_p(t) - C_{fs}y_s(t) - C_{ff}y_f(t) + y_l(t) \qquad \text{IV.29}$$

It is worth noting that we used a sigmoidal function centered at zero, which corresponds to the use of a variational model.

2.4. Model of connectivity among areas: the "coupled complete model"

In order to study long-range connectivity let us consider two cortical areas (each described via Eqs. IV.12-V.20), which are interconnected through long-range excitatory connections with a time delay. The presynaptic and postsynaptic regions will be denoted with the superscript k and h, respectively. The generalization to more than two regions is trivial. To simulate connectivity, we assumed that the average spike density of pyramidal neurons of the presynaptic area (z_p^k) affects the target region via a weight factor, W_j^{hk} (where j = p or f, depending on whether the synapse target to pyramidal neurons or fast inhibitory interneurons) and a time delay of 10 ms, T. This is achieved by modifying the input quantities u_p^k and/or u_f^h of the target region.

Hence, we can write

$$u_j^h(t) = n_j^h(t) + W_j^{hk} z_p^k(t - T) \qquad \text{IV.30}$$

$n_j(t)$ represents Gaussian white noise (mean value $m_j = 0$ and variance $\sigma_j^2 = 5s^{-2}$) which account for all other external inputs not included in the model.

3. RESULTS

3.1. Parameters sensitivity analysis on the population of $GABA_{A,fast}$ interneurons: the "reduced model"

Figure IV.4 shows the results of a parameters sensitivity analysis performed on C_{ff} and ω_f in Eq. IV.8. The analysis has been performed both with the linearized model described in sub-section 2.1. (linearized solution) and the nonlinear model (Eq. IV.4, numerical solution). The left panels (a, c and e) show the square amplitude of the transfer function of the linearized model; the right panels (b, d and f) show a comparison between the linearized model (dashed line) and the output of the nonlinear model (solid line); the latter has been computed, after numerical integration of the differential equations, as the PSD of the output divided by the PSD of the input u_f. The curves have been computed using three different values of parameters ω_f and C_{ff} (see Eq. IV.10).

Table IV.1: Model basal parameters

Parameter		Symbol	Value
Average gains	(mV)	G_e	5.17
		G_s	4.45
		G_f	57.1
Poles	(s^{-1})	ω_e	75
		ω_s	30
		ω_f	75
Number of synaptic contacts		C_{ep}	54
		C_{pe}	54
		C_{sp}	54
		C_{ps}	67.5
		C_{fp}	54
		C_{fs}	27
		C_{pf}	540
		C_{ff}	27
Sigmoid saturation	(s^{-1})	e_0	2.5
Sigmoid steepness	(mV^{-1})	r	0.56
Time delay	(ms)	T	10

As suggested by the theoretical study on the linearized model, the parameters sensitivity analysis confirms that the system has a resonance peak whose position can be changed within the frequency range of the γ-band (30-50 Hz) by acting on the two parameters. As a consequence, the input noise is amplified in correspondence of this peak and $GABA_{A,fast}$ interneurons exhibit an oscillatory activity in the γ band. Hence, $GABA_{A,fast}$ neurons can generate γ activity even if isolated from the other populations, thanks to the self-loop included in the model.

3.2. Parameters sensitivity analysis on a cortical area: the "complete model"

Simulations performed in a previous paper [Zavaglia et al., 2006] demonstrate that the model of Wendling et al. [Wendling et al., 2002], stimulated with input white noise to pyramidal cells (u_p (t)), produces just a unimodal spectrum (i.e., a spectrum with a single well defined peak) whose position primarily depends on the synaptic kinetics (i.e., ω_e, ω_s, ω_f) parameters. Conversely, the model presented here (Figure IV.3), including a self-loop between fast inhibitory interneurons, can generate more than one oscillatory rhythm within a single ROI.

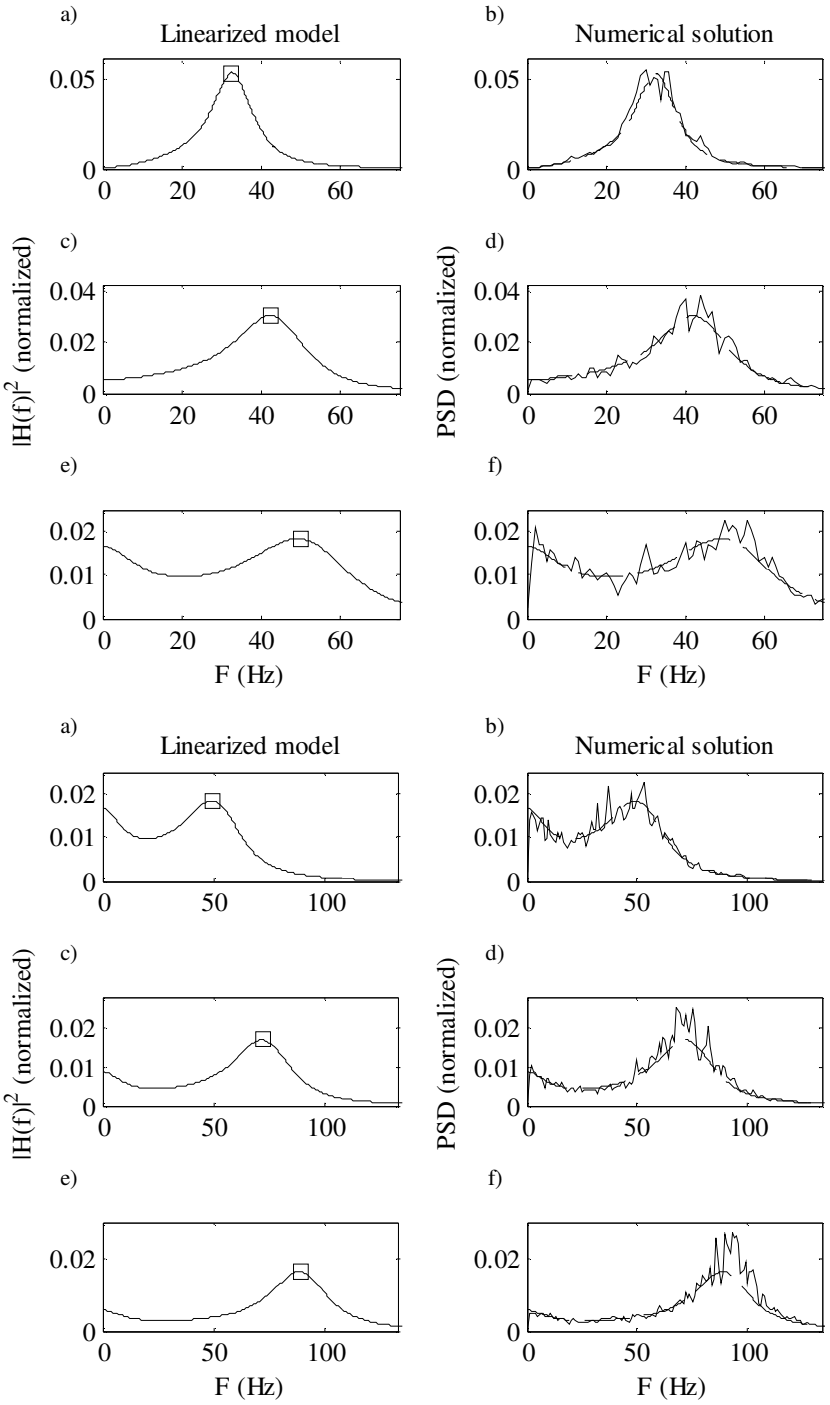

Figure IV.4: Comparison between the analytical and numerical solutions obtained with the model of a single loop of $GABA_{A,fast}$ interneurons. For each row, different values of ω_f (respectively 40 s^{-1}, 70 s^{-1} and 100 s^{-1}, upper panels) and C_{ff} (respectively 27, 54 and 81, lower panels) have been used.

An example is shown in Figure IV.5 (panel a). Two rhythms are evident in the PSD, one in the β range and the other in the γ range. The parameters values used in the simulations are reported in Table IV.1 [Jansen & Rit, 1995]. We used a value for the time constants of $GABA_{A,fast}$ interneurons of 13 ms, which is in accordance with in-vivo studies [White et al., 2000].

3.2.1. Generation of γ-band power

In order to identify the loops that are essential to obtain a rhythm in the γ band, we performed a parameters sensitivity analysis on the six gains which describe the strength of the connections among the four neural populations. In particular, the PSD was computed by assigning a value zero to each gain, while the other five gains are maintained at the basal value. The results show that,

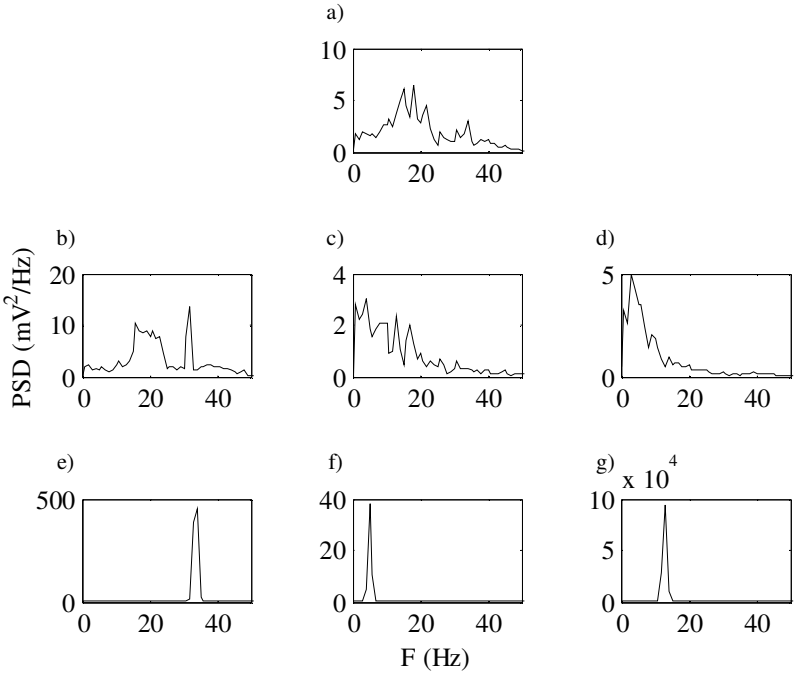

Figure IV.5: PSD of a single region setting off some connections among neural populations. The first panel represents the output of the whole model with parameters as in Table IV.1. The other six panels represent the power spectra respectively when $C_{ep} = 0$, $C_{ps} = 0$, $C_{fp} = 0$, $C_{fs} = 0$, $C_{pf} = 0$, $C_{ff} = 0$.

when connections from pyramidal cells toward excitatory interneurons (C_{ep}) or from $GABA_{A,slow}$ interneurons toward pyramidal cells (C_{ps}) are set to 0 (Figure IV.5 b and c) the two rhythms persist. When the connection from pyramidal cells toward $GABA_{A,fast}$ interneurons (C_{fp}) is set to 0, the two rhythms are not clearly distinguishable, but the power band is still fairly broad (0-40 Hz) (Figure IV.5 d). Conversely, when the connection from $GABA_{A,slow}$ interneurons toward $GABA_{A,fast}$ interneurons (C_{fs}) is cut (Figure IV.5 e), the two rhythms collapse in a single one oscillating in the γ band. Instead, when the connections from $GABA_{A,fast}$ interneurons to pyramidal cells (C_{pf}) or from $GABA_{A,fast}$ interneurons toward themselves (C_{ff}) are cut (Figure IV.5 f and g), the two rhythms collapse in a single one located at low frequencies, suggesting a crucial role for these connections in the generation of γ rhythm.

The previous simulations show that the presence of fast inhibitory interneurons with a self-loop is essential to generate a γ rhythm within a single region. However, these simulations were just performed according to an ON/OFF criterion, i.e. by individually eliminating the contribution of single connectivity weights.

Hence, we performed a more exhaustive analysis on the whole connectivity parameter space. Here, simulations have been performed by systematically varying the seven parameters which represent the internal connectivity (except C_{ff}). For each parameter, we used six different values within a physiological range (0, 27, 54, 81, 108, 135), while the other parameters (ω_e, ω_s, ω_f, G_e,

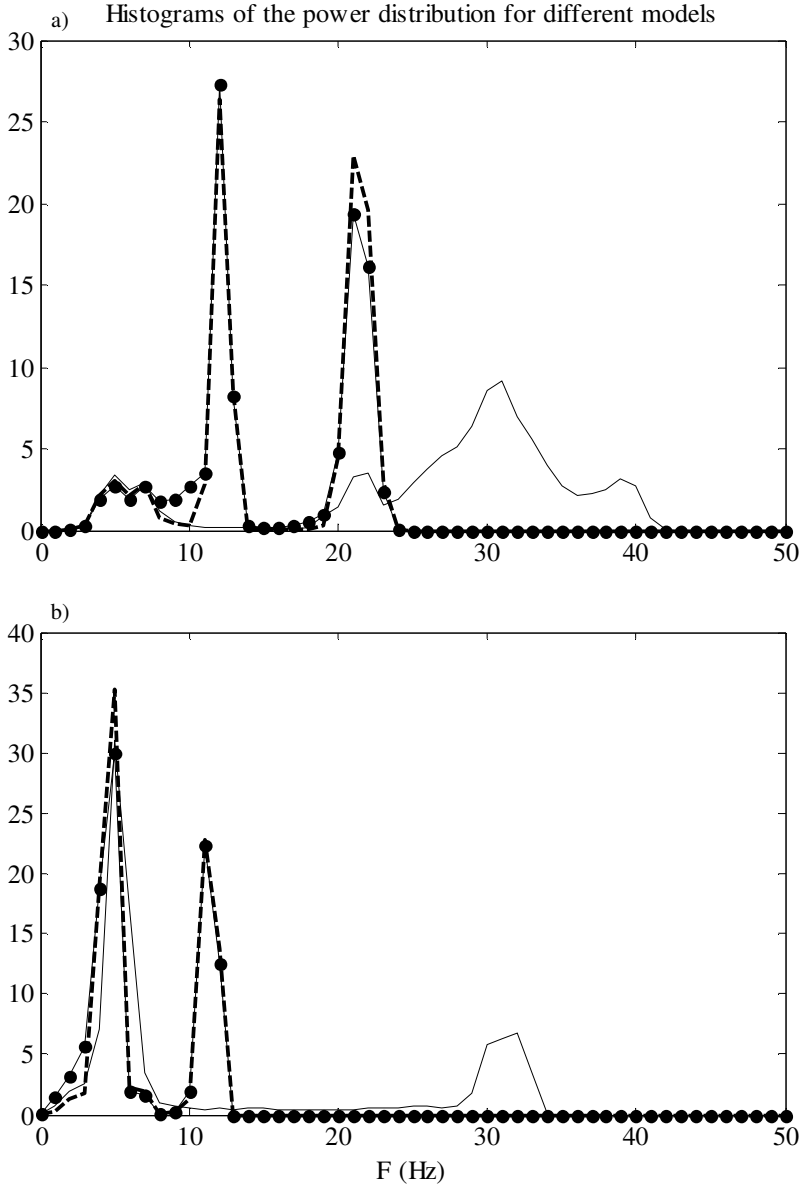

Figure IV.6: Panel a shows a histogram of the power distribution obtained with the model by Wendling (dashed line), with the new model (solid line) and with the control model (marked line). For each frequency f, the figure indicates the percentage of simulations in the parameters space D for which 95% of the power is below f. Similarly, panel b indicates the percentage of simulations in the parameters space D for which 50% of the power is below f. See text for details.

G_s, G_f) were maintained at the values reported in Table IV.1. Hence, the total number of points probed in the parameter space (D) was $6^7 = 279936$.

For each parameter set, three simulations have been performed: one for the Wendling model, another for the new model, and the last for a control model, that is, a model equal to Wendling model plus the white noise input for the $GABA_{A,fast}$ interneurons. The control model has been analyzed to verify that the differences between the model by Wendling and the new one are actually due to the $GABA_{A,fast}$ loop. For each model and for each parameter set, we computed the PSDs.

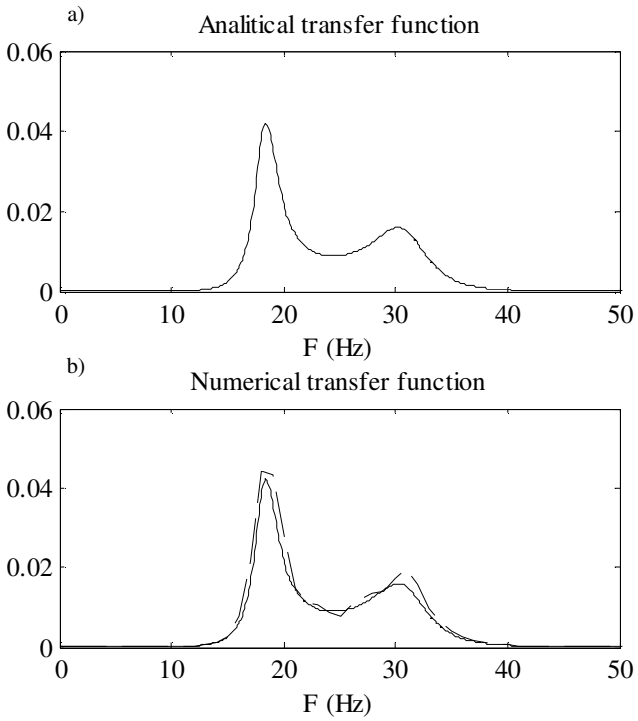

Figure IV.7: Example of a bimodal spectrum generated with the new model. Panel a shows the squared modulus of the transfer function (solid line) of the associated linearized system around a stable equilibrium point. Panel b shows the squared modulus of the transfer function computed as the PSD of the numerical solution of the model divided by the PSD of the input noise (dashed line). In panel b the solid line represents the same plot as in panel a.

The first analysis was devoted to ascertain the possibility to generate a significant power in the γ band by each model. To this end, for each parameter value, and for each model, we computed: i) an upper frequency for the spectrum, defined as the frequency below which 95% of power is contained; ii) an average frequency for the spectrum, defined as the frequency below which the spectrum contains 50% of its power. Results are presented in Figure IV.6, in the form of an histogram showing the percentage of results for each frequency range. Results show that 95% of the power for Wendling's model and for the control model is always located between 0 and 25 Hz, whereas for a high percentage of simulations the new model shows significant power activation also in the γ band (Figure IV.6 panel a). Moreover for about 1/4 of the simulations the new model generates half of the power at frequencies higher than 25 Hz (panel b). This means that the new model not only can generate γ activity, but it is also suitable for the generation of power spectral peaks in the γ band.

These results clearly demonstrate that only if $C_{ff} \neq 0$, we can produce an evident γ rhythm using physiological values for time constants, further supporting the importance of the new loop.

A further set of simulations has been performed by systematically varying parameter C_{ff} (i.e., strength of the inhibitory interneurons fast loop) from 0 to 236.25, while all other parameters are set at the same value as in Table IV.1. Results, not shown for briefness, demonstrate that the frequency of the second peak in the spectrum progressively increases from 30-40 Hz to 100-120 Hz by increasing C_{ff}, although at high values of this parameter the amplitude of the γ peak significantly decreases.

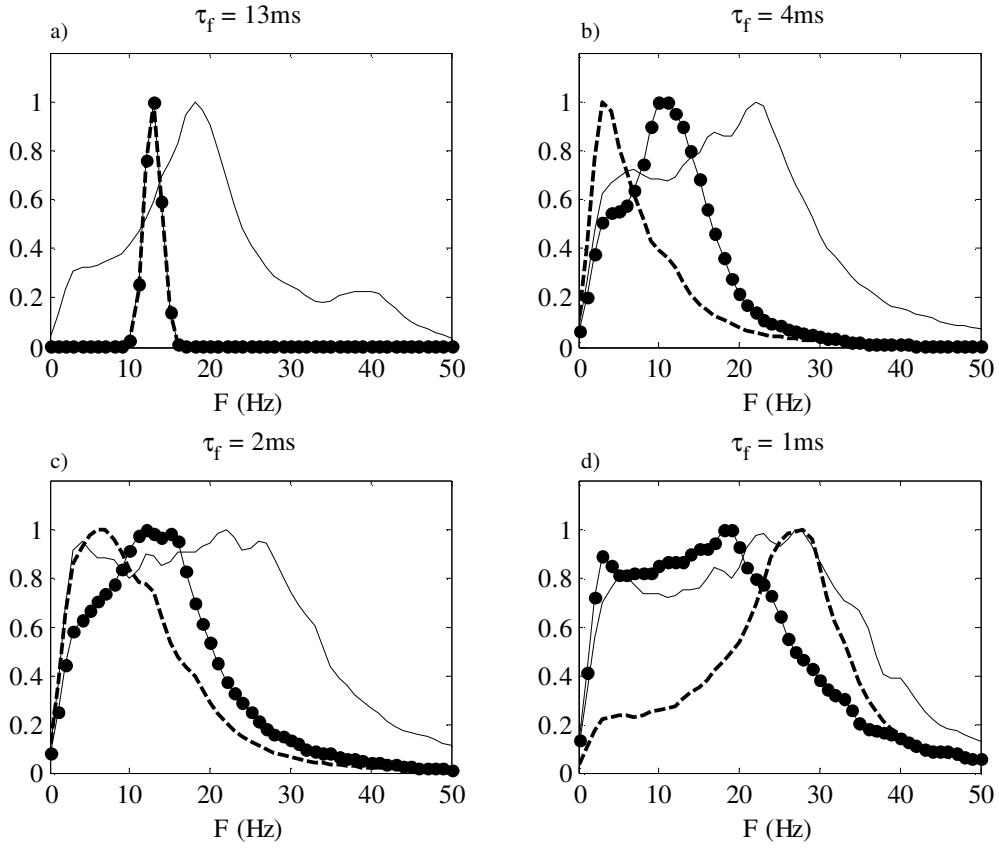

Figure IV.8: Power spectra of the model by Wendling (dashed line), of the new model (solid line) and of the control model (marked line), when the time constant of $GABA_{A,fast}$ interneurons is changing. The values of the other parameters are from Table IV.1.

3.2.2. Bimodal spectra

A subsequent analysis was devoted to ascertain the possibility of generating two distinct peaks in PSD. This point has been handled by studying the transfer function of the linearized system (LS) around its equilibrium points. For each set of parameters the equilibrium points have been calculated and the stability evaluated (Hartman-Grobman theorem) looking at the real part of eigenvalues. About 25% of the parameter sets gives at least one stable LS for the model by Wendling, while this percentage rises to about 54% for the new model. Among the stable LSs we looked for those that could generate at least two distinct resonance peaks. To this end, the 8th

degree polynomial at the denominator of the transfer function has been factorized in four 2nd degree polynomials $DEN_i(s) = (s-p_{i,1})(s-p_{i,2})$. Every $DEN_i(s)$ block can generate a resonance if it

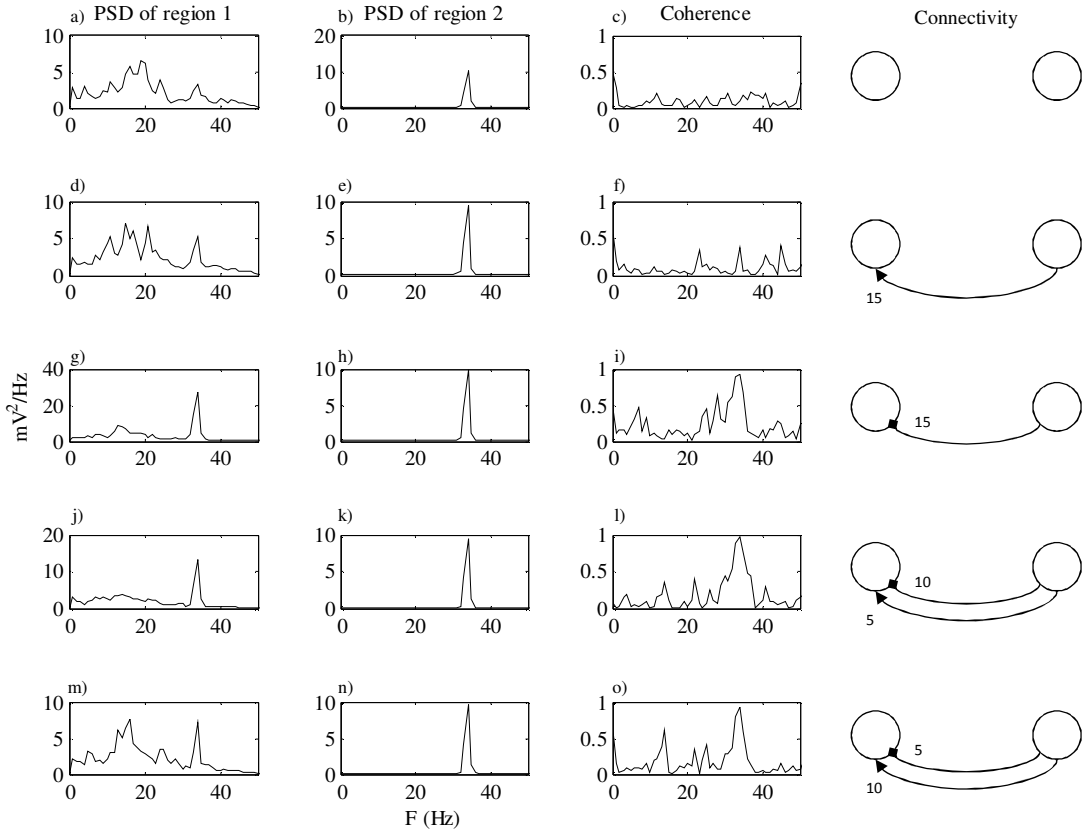

Figure IV.9: PSD of two regions (first region in the first column (panels a, d, g, j, m) and second region in the second column (panels b, e, h, k, n)) communicating by different connectivity patterns. The coherence between the two regions is represented in the third column (panels c, f, i, l, o); the connectivity patterns are represented in the fourth column. The arrow indicates connectivity toward pyramidal cells, the square indicates connectivity toward $GABA_{A,fast}$ interneurons. See the text for other parameters values.

has two complex conjugate poles that verify the following constraints: $Re(p_i) < 0$, $Re(p_i) > -|Im(p_i)|$ (damping factor less than $1/\sqrt{2}$). Results show that these constraints are verified in about 12% of the simulations in the new model, but just in 0.04% (118 sets of parameters) in the model by Wendling. Hence, the new model is much more suitable to produce two distinct resonance peaks than the former one. Finally, we further looked for those resonance peaks which are at least 10 Hz apart from one another, and which exhibit a damping factor $\delta < 0.1$: these last stricter constraints ensure the presence of two well evident peaks in the spectra. An example for the new model when the latter constraints are satisfied is shown in Figure IV.7. However, these conditions are limited (less than 1% of the simulations) even in the new model. Most conditions characterized by two well defined peaks in the spectra are associated with unstable equilibrium points, i.e., the development of limit cycle dynamics. The latter analysis may be the subject of future work.

3.2.3. Role of time constants

A last set of simulations has been performed to show the role of the time constant of fast synaptic kinetics. To this end, PSD has been computed in the three models using the values of connectivity strength reported in Table IV.1, and progressively reducing the time constant τ_f from 13 ms to 1 ms. Results, shown in Figure IV.8, confirm that the present model can produce a significant power in the γ band for all values of τ_f. If τ_f is reduced down to 1 ms, a broadband spectrum can be observed. Conversely, Wendling model and the control model can produce significant power in the γ band only if the time constant used for fast synaptic kinetics is as low as 1-2 ms.

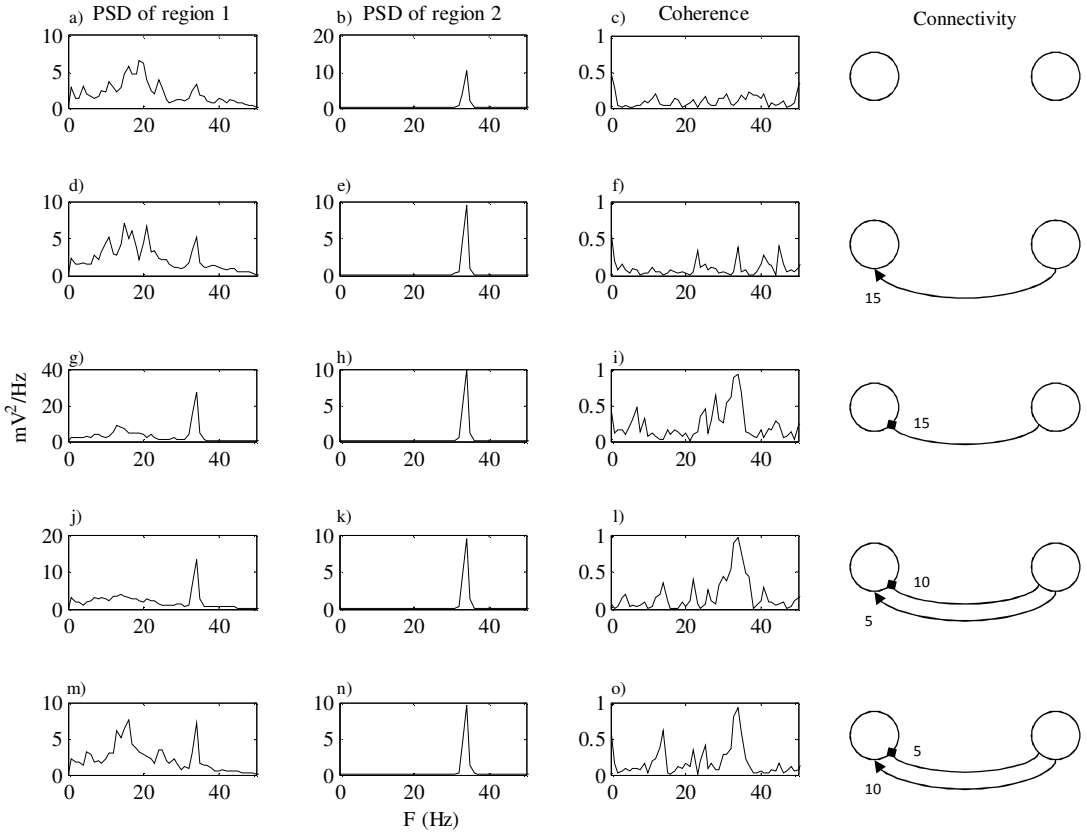

Figure IV.10: PSD of two regions communicating by different connectivity patterns. In this simulation the values of the parameters are the same as in Figure IV.9 except for the parameter C_{pf} of the second region, which has been changed ($C_{pf} = 0$) in order to obtain a rhythm around 5 Hz. All the panels represent the same quantities as in Figure IV.9.

3.3. Connectivity between two cortical areas: the "coupled complete model"

Further simulations were performed to study the transmission of rhythms from one region to another as a consequence of connectivity with time delay between the two regions. In these simulations, parameters were given so that populations exhibit limit-cycle behaviour (i.e., oscillations arise as the consequence of internal instability), to emphasize rhythm generation and transmission (see also the analysis in sub-section 3.2.).

Figure IV.9 shows the behaviour of a model composed of two interconnected regions. In each panel the first two columns represent the PSD of the two regions; the third is the coherence

function while the fourth column represents the connectivity diagram. In all simulations parameter C_{pf} is set to 540 in the first region, whereas it is set to 108 in the second one. All other parameters have the same values as in Table IV.1. As a consequence of these choice, the first region exhibits two rhythms (the first in the β and the second in the high γ range) while the second region exhibits only one narrow rhythm in the low γ range. The results of different simulations are shown, with the connectivity strength from the second to the first region progressively increased. Moreover, the connectivity was directed either to fast inhibitory interneurons, to pyramidal neurons, or to both. The most interesting result is that if the connectivity is sent towards pyramidal cells the rhythm is not induced in the target region and also the coherence function is low (panels d-f and m-o), whereas if the connectivity is sent to $GABA_{A,fast}$ interneurons, the presence of a new induced peak is evident (panels g-l) and the first region exhibits three simultaneous rhythms.

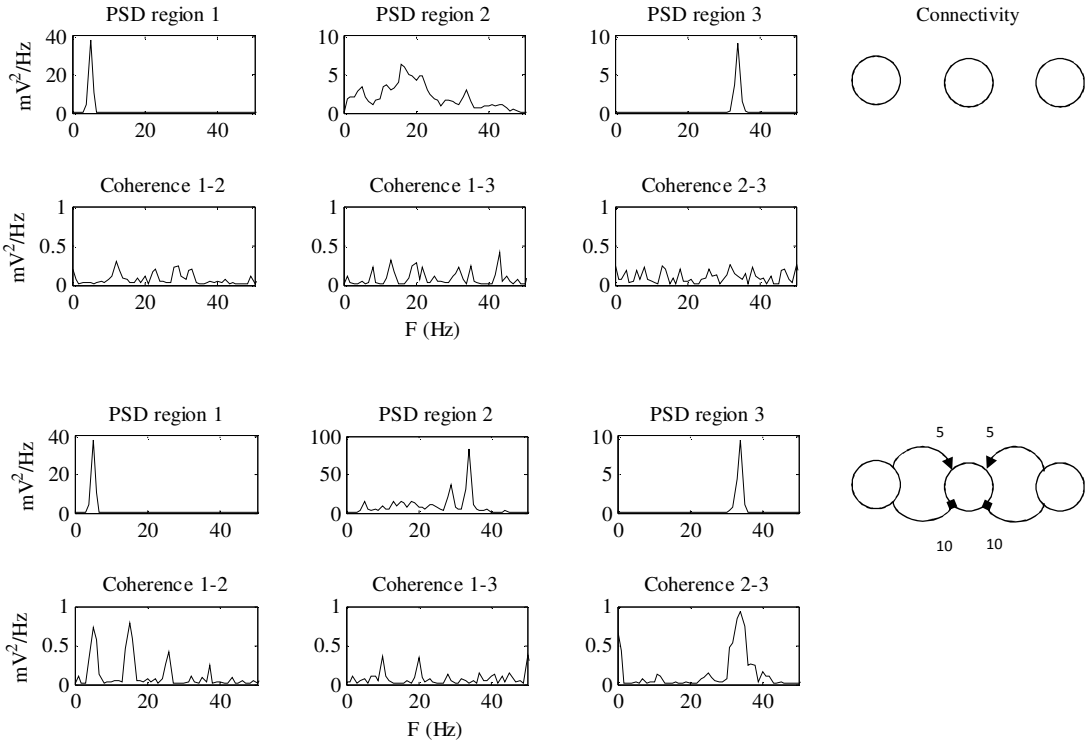

Figure IV.11: PSD of three regions communicating by different connectivity patterns. The first region (panels a, d, g, l) is simulated with a value of C_{pf} = 0, the second region (panels b, e, h, k) with a value of C_{pf} = 540 and the third region (panels c, f, i, l) with a value of C_{pf} = 108. The other panels represent the connectivity patterns and the coherences between the regions.

Figure IV.10 shows another example of connection between two regions. In these simulations the parameter C_{pf} of the second region has been set to 0 in order to obtain a rhythm around 5 Hz. This region could simulate an area which oscillates at low frequency, for example the thalamus. It is worth noting that, if the connections are sent to $GABA_{A,fast}$ interneurons, the first region exhibits three rhythms, with one in the θ band (5 Hz) induced by the second region. This behaviour is reflected in the coherence function.

Figure IV.11 shows the effect of connectivity among three regions. All the regions are simulated with the parameters reported in Table IV.1, but the first region has C_{pf} = 0 to reproduce the activity of an area with a rhythm in the θ band and the third region has C_{pf} = 108 to reproduce the activity of an area which oscillates in the γ range. It is worth noting that in this case the PSD of the second region exhibits a multiple spectrum (with intrinsic and induced rhythms), comprehensive of the contributions from all the regions. The coherence is high in correspondence of the induced rhythms.

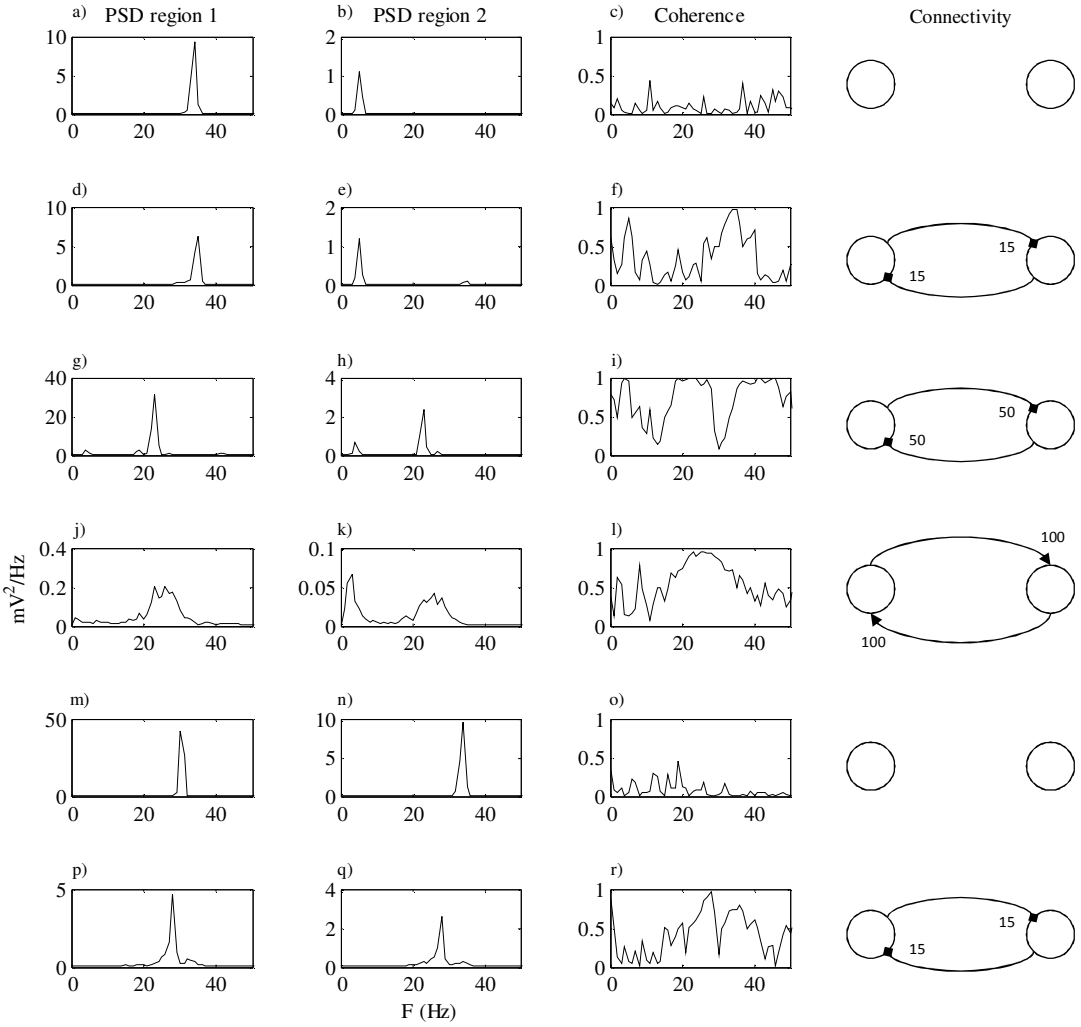

Figure IV.12: PSD of two regions communicating by different connectivity patterns. In the first 4 rows (panels a-l) the first region is simulated with a value of C_{pf} = 108 while the second region with a value of C_{pf} = 27. In the last two rows (panels m-r) the first region is simulated with a value of ω_f = 55 s^{-1} and with a value of C_{pf} = 108 while the second region with a value of ω_f = 75 s^{-1} and a value of C_{pf} = 108 All the panels represent the same quantities as in Figure IV.9.

Of course, real connections in the cortex often exhibit feedback loops. A comprehensive study of all the possible combinations of connectivity patterns among two, three or even more regions, would require a combinatorial explosion of possibilities. For the sake of brevity we just investigated an example of two regions with feedback connections to show that this kind of

connectivity does not change the results dramatically in comparison to unidirectional connectivity, while an extensive study could be addressed in future works.

In Figure IV.12 the upper panels (panels a-l) analyze the case in which one region oscillates in the θ band and the other in the γ band. The bottom panels (panels m-r) analyze a case in which one region oscillates in the low γ band and the other in the high γ band. In both cases, multimodal spectra can be produced in both regions if connections have a sufficient strength. In this case too, connections to fast inhibitory interneurons are more efficient to cause rhythm propagation. Worth noting is that feedback connections may also induce a shift in one peak (by way of example, let us see the third row, where a peak in the β band appears, which was not originally present in either of the two regions).

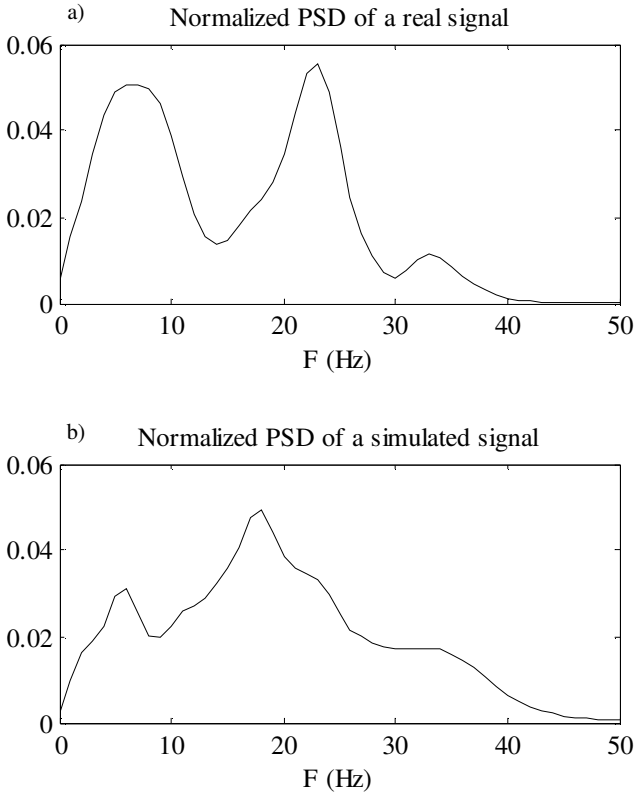

Figure IV.13: Panel a shows the power spectrum of a real cortical signal. Panel b shows the spectrum of a signal simulated with a model of two interconnected regions: the first region has an intrinsic α rhythm, while the second one oscillates in β and γ ranges. The parameters which have different values from those reported in Table IV.1 are: for the first region $\omega_e = 120\ s^{-1}$, $\omega_f = 55\ s^{-1}$, $C_{fp} = 121.5$, $C_{fs} = 40.5$, $C_{pf} = 27$, $C_{ff} = 135$; for the second region $\omega_f = 55\ s^{-1}$. The weight factors are: $W_p^{21} = 200$, $W_p^{12} = 90$, $W_f^{21} = 0$, $W_f^{12} = 0$. When the two regions are connected to each other the second one shows a power spectrum similar to the real one.

Finally, Figure IV.13 shows a comparison between a real PSD obtained on an healthy volunteer during a simple movement task [Zavaglia et al., 2008a] and a spectrum simulated with a model of two interconnected regions. In this case we did not try a best fitting, but we simply looked for a manual adjustment of connectivity parameters to show the similarity between real spectra and simulated ones. This result emphasizes that spectra similar to those found in vivo can be obtained with a parsimonious model, and just adjusting a few connectivity weights.

4. DISCUSSION

The work presented in this chapter extends the possibilities offered by neural mass models to simulate real power density spectra, and to investigate effective connectivity patterns. The main new issues are concerned with: The possibility to generate γ-rhythms using just a chain of fast-inhibitory interneurons, without the presence of the other neural populations; of course, in real physiological conditions the frequency of this rhythm is not fixed, but is modulated by the other populations (sub-section 4.1.); The possibility to engender multiple rhythms in the same model, without the need to include multiple synaptic kinetics (sub-section 4.2.); The role played by inputs converging into fast inhibitory interneurons to propagate rhythms from one region to another (sub-section 4.3.).

In the following, each of these items is discussed separately.

4.1. γ-rhythm generation

Our theoretical analysis stresses the possibility to generate a peak in PSD within the γ-band in a simple way, by just introducing an inhibitory loop among fast interneurons. This loop is physiologically motivated by the presence of significant interconnections between fast basket cells, as observed in the hippocampus [Cobb et al., 1997] and in the neo-cortex [Kisvárday et al., 1993]. The idea that a self-loop of one population to itself (frequently used in competitive neural networks) can enrich the dynamics of neural mass models was already exploited by Sotero et al. in their recent model of overall brain dynamics [Sotero et al., 2007]. However, these authors included a loop between pyramidal cells only, assuming that, at a large scale, "pyramidal-to-pyramidal connections become increasingly important, accounting for the majority of intracortical fibers". A similar loop among inhibitory interneurons has been used by Moran et al. [Moran et al., 2007] to simulate γ rhythms: however, these authors did not use two distinct populations of interneurons; in particular, they did not simulate interneurons with $GABA_{A,fast}$ kinetics. A large amount of modeling and experimental work suggest that fast inhibitory networks play a significant role in the genesis of γ rhythms [Bartos et al., 2007; Jefferys et al., 1996; White et al., 1998; Whittington et al., 1995].

Our analysis underscores that γ oscillations can be obtained using physiological values for the time constant of fast inhibitory synapses (range 10-20 ms), contrarily to previous works [Wendling et al., 2002; Zavaglia et al., 2006, 2008a] where one needed to use very small values (a few ms) for the time constant of $GABA_{A,fast}$ interneurons. Furthermore, the lower the time constant, the higher the oscillation frequency. This result agrees with data reported by Whittington et al. [Whittington et al., 1995] (see also Figure 4 in Jefferys et al. [Jefferys et al., 1996]). These authors, both via computer simulations in integrate and fire neural networks and in experimental trials during pentobarbital infusion, observed that the frequency of γ rhythms is inversely related with the time constant of the inhibitory post-synaptic current. Moreover, the value of the time constants in their work is close to that used in our model.

A further interesting result of our analysis is that the frequency of γ-rhythms is directly related with the connectivity strength among fast interneurons (i.e., parameter C_{ff} in Figure IV.2). If this parameter is increased by twofold or threefold with respect to its basal value, model predicts oscillations in the ultra γ range (about 70 Hz). For even greater values of parameter C_{ff}, oscillation frequency may increase up to 80-100 Hz, although the amplitude of the PSD peak significantly decreases. This dependence of frequency on connectivity requires further experimental validation.

It is worth noting that Rennie et al. [Rennie et al., 2000], using a continuum model of electrical activity in the cortex, also ascribed the emergence of γ rhythm to a resonance near 40 Hz. However, in their model the resonance depends on a modulation of synaptic strength, hence to a different mechanism compared with that exploited in the present work.

In conclusion, the model ascribes the occurrence of a γ rhythm to the presence of a resonance occurring within the network of fast inhibitory interneurons, here described by means of a simple feedback loop. In the linearized model, the frequency and amplitude of the resonance peak depend on the time constant of the $GABA_{A,fast}$ synapses and on the strength on reentrant connections between these interneurons. In the non-linear model, these quantities can also be modulated by the excitatory input to the fast interneurons: the latter may affect the working point in the sigmoidal characteristic, thus altering the loop gain.

Of course, the mechanism exploited in the present model to generate γ rhythms may not be the unique one; alternative mechanisms may be effective to generate γ rhythms in different conditions, as reviewed by Jefferys et al. [Jefferys et al., 1996]. These may include a recurrent inhibition between an excitatory and an inhibitory population, or the presence of intrinsic pacemaker cells. The first mechanism is widely exploited in classic models of neural oscillators (such as the Wilson-Cowan oscillator [Wilson & Cowan, 1972]) and is commonly adopted in more traditional neural mass models [Freeman, 1978; Lopes da Silva et al., 1974]. However, to produce γ rhythms, this mechanism must assume the presence of very small time constants for the synapses. Particularly, results in Figure IV.8 show that γ rhythms in power spectral density can be generated using the Wendling model [Wendling et al., 2002], but one needs a time constant for fast inhibitory interneurons as low as 1-2 ms. For what concerns the second mechanism, examples of intrinsic pacemaker cells in the cortex are well documented [Gutfreund et al., 1995; Llinás et al., 1991], although we are not aware of their use within neural mass models.

Finally, it is remarkable that not only fast interneurons, but also gap junctions can be important for some forms of γ oscillations [Wang & Buzsáki, 1996]. Probably gap junctions increase the oscillation power, although are not necessary for their generation [Bartos et al., 2007]. Their effect may be that of increasing coupling between interneurons populations, i.e., an increase in the coupling terms C_{ij} of our model.

4.2. Multiple rhythms in the same ROI

If the four populations (pyramidal neurons, excitatory interneurons, slow and fast interneurons) which constitute a cortical column are connected with realistic connectivity loops (Figure IV.3) the model can produce two simultaneous rhythms: the first, in the γ band, can be ascribed to a resonance of fast inhibitory interneurons; a second, at lower frequencies (in the α band or β band) emerges from the other feedback loops (i.e., loops engaging pyramidal neurons, excitatory interneurons and slow inhibitory interneurons). It is worth noting that this "intrinsic rhythm" is that obtainable from the traditional Jansen and Rit model [Jansen & Rit, 1995] and represents the core of most recent studies using neural mass models [Babajani & Soltanian-Zadeh, 2006; David & Friston, 2003; David et al., 2005; Sotero et al., 2007; Zavaglia et al., 2006].

Jefferys et al., in their review paper on mechanisms generating γ rhythms [Jefferys et al., 1996], suggested that "the fact that inhibitory networks can sustain a rhythm in the γ frequency range… separates the synchronizing control or clock from the specific neural processing of information". This idea substantially agrees with the results emerging from our model: a higher frequency

rhythm originating in the fast-inhibitory loop modulates (and is modulated by) a slower rhythm within the same region, originating from slower synapse time constant.

The parameter sensitivity analysis shown in Figure IV.5 and Figure IV.6 supports this viewpoint. If parameter C_{ff} is set at zero, the model cannot generate a significant power in the γ-band (using physiological values of time constants) but all power is concentrated below 25 Hz. Conversely, a significant power above 30 Hz can be obtained with many combinations of parameters if C_{ff} is significantly different from zero. In the latter condition, if connectivity between pyramidal, excitatory and slow-inhibitory interneurons are changed, one can observe evident changes in PSD within the α and β bands, whereas the PSD still exhibits a significant contribution in the γ band (panels b and c in Figure IV.5).

Analysis of the poles in the linearized model also supports a pivotal role for parameter C_{ff}. Only the present model (with $C_{ff} \neq 0$) can frequently produce two resonant peaks if linearized around a stable equilibrium point (Figure IV.7) whereas with $C_{ff} = 0$ the presence of distinct resonant peaks in the transfer function becomes very rare. Nevertheless, our analysis also suggests that, in most conditions, the present model (as well as the Wendling model) does not exhibit stable equilibrium points, but its behavior arises from limit-cycle oscillations. We did not explored these aspects in this work, but they might be the subject of future more refined theoretical analyses.

Definitely, the previous analysis suggests that the model can generate a variety of PSDs, with two simultaneous rhythms (α + γ, or β + γ) or even a wide-band spectrum, by simply altering internal connectivity parameters, without the need of any ad hoc changes in the synaptic time constants. These bimodal oscillations may arise from the presence of two resonant peaks in the linearized model or from a more complex non-linear limit cycle dynamics.

4.3. The role of fast interneurons on rhythm transmission between ROIs

A remarkable result of our simulations is the pivotal role played by long-range excitatory connections which terminate into fast inhibitory interneurons. Indeed, the present work introduces a new testable hypothesis that we cannot find in previous studies: i.e., that excitatory input to fast inhibitory interneurons plays a fundamental role to transmit rhythms from one region to another. Our results clearly show that a moderate synapse from pyramidal neurons in the pre-synaptic ROI to fast inhibitory interneurons in the post-synaptic ROI is able to transmit rhythms very efficaciously, as observable in the spectrum of the target region and in the coherence between EEGs in the two regions. Conversely, excitatory synapses from pyramidal to pyramidal neurons are less effective in rhythms transmission, as revealed by the low value of coherence between the two ROIs. Only if the strength of synapses is increased by one order of magnitude, pyramidal to pyramidal connections become really efficacious and one can observe a high coherence (above 0.5) in the frequency band interested by the rhythm.

According to the literature [Felleman & Van Essen, 1991], long-range connectivity originates exclusively from pyramidal neurons, but may target to different populations of neurons depending on the type of connection. In the present study we focused attention just on two of these connections (from pyramidal to pyramidal and from pyramidal to fast inhibitory) to study two target populations with different time constants. Time constants, in fact, are the main determinants of population dynamics. However, we repeated the simulations in Figure IV.9, Figure IV.10, Figure IV.11 and Figure IV.12 assuming that connectivity reaches also the slow inhibitory and the

excitatory interneurons (these are not presented for briefness). The presence of these further inputs does not appreciably modify the previous results.

We claim that the reason why a population of fast interneurons may be so efficacious to receive an external rhythm, and transmit it to other populations in the same area (especially to pyramidal cells), can be found in its fast dynamics, which allow the preservation of the overall spectral content of the external rhythms. Moreover, the inhibitory loop of $GABA_{A,fast}$ interneurons with themselves is faster compared to the loop composed of $GABA_{A,fast}$ interneurons and pyramidal cells; for this reason the perturbations that reach fast inhibitory interneurons have a stronger effect on the entire dynamics of the system.

It is worth noting that the term "efficient connection" has been used here just to denote the capacity to propagate a rhythm from one population to another. Of course, it is does not necessarily implies efficiency in a wider computational meaning, i.e. the capacity to maximize information transmission with a reduced wiring cost (such as evaluated in "small world network", see [Achard & Bullmore, 2007]).

The observation that rhythm transmission is particularly efficient when connections target fast inhibitory interneurons may have a cognitive significance. In fact, according to the classic distinction developed by Felleman and van Essen [Felleman & Van Essen, 1991],connectivity may vary depending on the hierarchical level along the processing stream. In particular, in the visual cortex lateral connections target all layers, while top-down (backward) connections target supra-granular and infra-granular layers. In both cases, inhibitory interneurons can be among the target cells. Conversely, bottom-up (forward) connections terminate in layer 4, making synapses only to excitatory interneurons. Hence, according to Felleman and van Essen schema, model predicts a stronger capacity to transmit rhythm via lateral and top-down connections, but poorer capacity via forward connections. This distinction may have a cognitive role, suggesting that rhythm transmission (especially in the beta and gamma ranges) may be especially important in high level cognitive processes, which involve lateral connections among regions at the same hierarchical levels, and top-down influences from higher hierarchical centers.

An important aspect, which deserves attention, is whether multi-modal spectra, as those obtained in the present study, are actually found during real measurements in vivo. Indeed, several recent studies show real spectra in cortical regions similar to those reported in Figure IV.9, Figure IV.10, Figure IV.11 and Figure IV.12. Spectra with two distinct peaks are presented in Rowe et al. [Rowe et al., 2004] (see Figure 4 in that work). In previous papers of our group we tried to fit real spectra obtained after localization of the cortical sources, starting from high-density scalp EEG during simple movement tasks [Ursino et al., 2006; Zavaglia et al., 2008a]. Frequently these spectra exhibited multiple peaks, in the α, β and γ bands (the reader can look at Figure 4 in [Zavaglia et al., 2008a], for various exempla). An exemplum of a real spectrum (taken from [Zavaglia et al., 2008a]) is shown in Figure IV.13 and compared with a PSD obtained with a model of two interconnected regions. In this figure we did not try an automatic best fitting, but we simply adjusted connectivity parameters manually to arrive at an acceptable qualitative agreement. Best fitting of the present model to real spectra will be the subject of future model applications, maybe through the use of Bayesian estimation techniques [Moran et al., 2008].

A recent work by Rosanova et al. [Rosanova et al., 2009], using TMS stimulation in human volunteers, further supports the existence of different rhythms (α, β and γ) in different cortical regions, and the possibility that rhythms are propagated from one region to another via effective

connectivity pathways. In particular, TMS evoked an α-band oscillation in the occipital cortex, a β-band oscillation in the parietal cortex and a β/γ-band oscillation in the frontal cortex, but each region could also receive a different rhythm (thus showing multimodal spectra) from other regions via brain connections.

In the present work we studied both uni-directional (Figure IV.10 and Figure IV.11) and bi-directional (Figure IV.12) connections. In the first case, the target population may receive a further rhythm (besides its intrinsic rhythm) from the other population, with the appearance of a more complex spectrum. This should be easily observable in vivo [Rosanova et al., 2009]. The case of bi-directional connection is more complex, since the spectra of both populations are simultaneously affected (let us consider, for instance, the exemplum in the bottom panel in Figure IV.12). In this condition, it may be difficult to assess the mechanisms leading to multimodal spectra from in vivo data, without the use of mathematical models and algorithms for effective connectivity estimation. This work wishes to represent a new step in that direction.

4.4. Limitations and possible improvements

Finally, at the end of this discussion we wish to point out some limitations of our work and lines for future improvements.

The present model is basically derived from the model by Wendling et al. [Wendling et al., 2002], and differs from the recent model by Moran et al. [Moran et al., 2007, 2008, 2009] due to the presence of inhibitory interneurons with $GABA_{A,fast}$ synaptic kinetics. We are aware that the model by Wendling et al. was originally proposed with reference to the hippocampus, and that some differences may exist between the hippocampus and the cortex. Nevertheless, there are several reasons which justify the use of the Wendling model for the cortex too, and the extension and improvement we propose in the present work.

First, fast inhibitory interneurons not only represent a significant portion of GABAergic interneurons in the hippocampus [Freund & Buzsáki, 1996] but they are also present in the cerebral cortex [González-Burgos et al., 2005; Thomson et al., 1996]. Second, several experimental studies used receptor antagonists to analyze individual mechanisms involved in neural oscillations; their results suggest that similar cellular and network mechanisms, as those seen in the hippocampus, generate γ oscillations in the cortex too [Bartos et al., 2007; Cunningham et al., 2003; Whittington et al., 1995]. The previous two points support the idea that fast $GABA_A$ mechanisms operate in the cortex (as in Wendling model of the hippocampus) and that they have a role in generating γ rhythms both in the hippocampus and in the cortex via similar mechanisms.

Of course, other types of neurons exist in the cortex and in the hippocampus, besides the four populations included in the Wendling model. At the present stage of our knowledge, a four population model may represent a good compromise between simplicity and completeness, since it encompasses all main dynamical aspects (i.e., the main types of time constants). However, inclusion of a larger number of neuron populations, each with its own synaptic dynamics, might improve the physiological reliability of neural mass models in future years and might represent a subject of interesting future activity.

Finally, it is remarkable that other authors in the past decades developed significant models to describe EEG spectra based on a "neural field approximation". The basic idea of these models is that the number of neurons in the cortex is large and the density of synaptic connections is high.

Hence, these models consider the cortex as a continuum and use a set of nonlinear partial differential equations in space and time to describe the spatiotemporal evolution of neural activity. These models, with inclusion of fast inhibitory kinetics to simulate γ-band oscillations, might allow a further more complete analysis of brain rhythms, illustrating conditions in which rhythms may propagate, amalgamate or dissipate in a continuum space. This aspect may also represent an important subject of future work.

In conclusion, the present study proposes a new and simple method to generate γ rhythms within neural mass models, without the need to modify synaptic kinetics. In particular, three different conditions have been analyzed with the model: in the first (named "reduced model") we just considered connectivity among fast interneurons taken alone, and demonstrated that this model can produce a gamma rhythm per se. In a second condition (named the "complete model") we simulated the behavior of a single ROI (mimicked through the interaction among four populations) and showed that this model can produce a spectrum with two distinct peaks (in the beta and gamma ranges, or in the alpha and gamma ranges). In particular, a γ rhythm emerging from a fast interneuron loop modulates (and is modulated by) the internal slower rhythm emerging from the other loops. Finally, the last model (named the "coupled complete model") was obtained by considering the interaction between two or three interconnected ROIs; it can simulate more complex multimodal spectra, with a variety of rhythms (some intrinsic and some received from other ROIs) similar to those observed in vivo. In particular, the results stress that long-range excitatory synapses with time delay, directed to fast interneurons are particularly effective in transmitting rhythms from one region to another. These results, which may be tested by ad hoc experiments, can help the construction of more adequate models to fit in vivo data, and can be exploited to attain a deeper comprehension of the effect of connectivity patterns among ROIs.

V. ANALYSIS OF THE RHYTHMIC ACTIVITY EVOKED BY TMS[3]

1. INTRODUCTION

The study of brain rhythms represents an important aspect of modern neuroscience. The electrical activity of the brain is very complex, including different oscillatory patterns at different frequencies, which may change depending on a particular task. It is generally assumed that these rhythms are not merely epiphenomena, but play a relevant role in many perceptive, motor and cognitive functions.

Different hypotheses on the role of brain rhythms have been proposed in the recent literature. Oscillatory fluctuations in the theta and gamma bands are assumed to play a pivotal role in several aspects of memory, including storage and retrieval of individual events or sequences of events, short-term plasticity, novelty detection [Düzel et al., 2010]. According to a popular hypothesis [Singer & Gray, 1995] a role of gamma-band oscillations may be that of binding attributes of the same events to form a coherent percept, still maintaining these attributes separate from those of other events simultaneously present. Beta oscillations are assumed to play a role in motor tasks, since induced oscillations in the beta-band have been observed in sensory motor areas after voluntary body movements (or even after a movement imagination) or after sensory stimulation [Neuper et al., 2006]. A further hypothesis is that beta activity is related to increased alertness in thalamo-cortical systems [Steriade et al., 1993]. Alpha oscillations changes are also observed during motor tasks [Neuper et al., 2006]; moreover, they have been interpreted (together with other low-frequency oscillations) as processes which coordinate top-down control both in working memory and in long-term semantic memory [Klimesch et al., 2010]. In any case, the main function of rhythm propagation seems to be that of realizing an "assembly code", in which information participating to a given task is distributed over different regions; rhythms would allow "long distance" communication among ROIs, still maintaining this communication selective, i.e., engendering parallel processing. A stimulating hypothesis is that different rhythms constitute separate networks for parallel processing in the brain, which emerge transiently during certain stages of information processing mediated by synchrony over multiple frequency bands [Varela et al., 2001]. Of course, validation of these hypotheses on a more careful quantitative basis may benefit from the use of computational models, which are sophisticate enough to encompass the main aspects of rhythm generation and transmission, but simple enough to allow easy simulation on a computer.

An estimation of the intrinsic rhythms of brain regions, and of how these rhythms can be transmitted and modified as a consequence of brain connectivity, can be achieved using the TMS combined with the EEG. TMS/EEG, indeed, allows to perturb regions of the human cortex directly with an impulsive disturb, and measure the dominant frequencies generated by the underlying cortical areas [Van Der Werf et al., 2006; Paus et al., 2001; Rosanova et al., 2009]. In

[3] The contents of this chapter are published in Neuroimage (Cona et al., 2011).

particular, Rosanova et al. [Rosanova et al., 2009] observed the dominant oscillation rate (natural frequency) in three brain regions (BA 19 in the occipital lobe, BA 7 in the parietal lobe, and BA 6 in the frontal lobe) following TMS stimulation of different intensities in a group of healthy volunteers. Results show that the natural frequency can be directly measured in virtually any area of the cerebral cortex. Moreover, the authors hypothesized that these natural rhythms can be transmitted from one region to another (or that the intrinsic rhythms can be modified) as a consequence of connectivity among them.

The previous results are suitable to be analyzed using neurologically inspired computational models. Actually, the impulse response is a classical instrument in modeling literature to estimate parameters and validate model structure in a straightforward way. Computational models, in turn, are essential to reach a deeper understanding of the neural mechanisms involved in rhythms generation and in their propagation.

In the last decade Esser et al. [Esser et al., 2005, 2009] developed a cortico-thalamic model to simulate the effect of a TMS impulse. The authors modeled the single neural cells as spiking neurons in different layers of the cortex and successfully reproduced some experimental aspects such as frequency, timing, dose response, and pharmacological modulation of epidurally recorded responses to TMS.

This kind of model allows brain dynamics to be analyzed at a microscopic level (ion channels currents and action potentials), but it is computationally very expensive and time demanding. A complementary approach is given by neural mass models, which simulate large ensembles of neurons just considering their average state variables (voltages and spiking rates), thus reducing greatly the time and the variables required. Despite their reduced degree of detail, neural mass models can reproduce many phenomena observed in experimental EEG recordings (rhythms generation and propagation, epileptic seizures, etc.) and have been widely exploited to infer the neural dynamics underlying these phenomena [Cona et al., 2009; Wendling et al., 2002].

As stated in the previous chapter, we developed a neural mass model to study rhythm generation and rhythm transmission among connected cortical regions. The model was built starting from equations proposed by Jansen and Rit [Jansen & Rit, 1995] and Wendling et al. [Wendling et al., 2002], with inclusion of a new loop to simulate the role of fast GABA-ergic interneurons in the genesis of gamma oscillations [Ursino et al., 2010]. The model is able to simulate multiple rhythms within the same ROI and the transmission of rhythms from one region to another, by simply modulating a few parameters which represent short-range connections within a region and inter-area long-range connectivity.

Our model is particularly suitable to analyze the experimental results by Rosanova et al. [Rosanova et al., 2009]. In particular, some model predictions (the presence of intrinsic rhythms in individual ROIs and the possibility to transmit rhythms via a few effective connections among ROIs) agree at least qualitatively with these experimental data.

Hence, the present study was designed with the following two main purposes:

1. to analyze whether the response of individual ROIs to direct TMS stimulation can be simulated with sufficient accuracy with the model by modifying just a few internal parameters of that region. This aspect is the same as to fit the natural rhythm of a ROI with a biologically inspired model;

2. to analyze whether a model of interconnected ROIs can at least approximately explain how natural rhythms can be transmitted or modified as a consequence of inter-region connections.

In this work, we simulated the behavior of BA 19, BA 7 and BA 6 with a network of three interconnected regions. Parameters are given to reproduce the effect of TMS stimulation with three different intensities in five subjects.

2. METHOD

2.1. Experimental data recording: EEG and TMS

Five right-handed subjects (SUBJ1, SUBJ2, SUBJ3, SUBJ4, SUBJ5) participated in this study. During the experiment, subjects were lying on an ergonomic chair, relaxed, and with eyes open looking at a fixation point on a screen. A focal bipulse, figure-of-eight coil with 60mm wing diameter driven by a biphasic stimulator (eXimia TMS Stimulator; Nexstim) was used to stimulate the subjects' cortex. Three cortical sites (middle or superior occipital gyrus, superior parietal gyrus, and middle or caudal portion of the superior frontal gyrus) were selected based on an atlas of brain regional anatomy [Tamraz & Comair, 2005], anatomically identified on a T1-weighted individual MRI (resolution 1 mm) acquired with a 1 T Philips scanner and were targeted by means of a Navigated Brain Stimulation (NBS) system (Nexstim). We recorded high-density EEG using a TMS-compatible 60-channel amplifier (Nexstim) which gates the TMS artifact and prevents saturation by means of a proprietary sample-and-hold circuit [Virtanen et al., 1999]. The EEG signals, referenced to an additional electrode on the forehead, were filtered (0.1–500 Hz) and sampled at 1450 Hz with 16-bit resolution. Two extra sensors were used to record the electrooculogram. In most cases, no TMS-induced magnetic artefacts were detected, and in all cases, the EEG signals were artefact-free after the stimulus. TMS trials containing noise, muscle activity, or eye movements were automatically detected and rejected. The event related potentials were obtained by averaging across all the trials of each session (100-200 per session). More technical details on the procedure can be found in Rosanova et al. [Rosanova et al., 2009]. For each subject, we stimulated each cortical area at eight different TMS intensities (range, 20–160 V/m). Firstly we defined the EEG-threshold for each subject, then we used the three intensities above this threshold (medium, medium/strong and strong) for the analysis with the model. The TEPs under the threshold were not significant with respect to the baseline activity and so they could not be used to attempt a reliable parameter fitting.

2.2. Cortical sources reconstruction

In order to reconstruct the cortical sources of EEG responses to TMS, we first created, for each subject, an individual cortical mesh (7204 vertices) by adapting an average Montreal Neurological Institute (MNI) cortex to the subject's MRI data (this step was performed by employing the free license package SPM at http://www.fil.ion.bpmf.ac.uk/spm). Then, we co-registered the meshes of the cortex, the skull (2000 vertices) and scalp (2000 vertices) together with the EEG sensors positions into the subject's MRI space. The cortex, skull and scalp meshes were aligned with a 3-spheres head model (conductive head volume) that was used to compute the forward solution according to the Berg method [Berg & Scherg, 1994] as implemented in the Brainstorm software package (freely available at http://neuroimage.usc.edu/brainstorm). Finally, the inverse solution was computed on a single trial basis by applying an empirical Bayesian approach with estimation of covariance components using Restricted Maximum Likelihood [Friston et al., 2006]. In order to compute the overall current evoked by TMS in different cortical areas, cortical sources were attributed to different Brodmann areas using an automatic tool of anatomical classification (http://www.ansir.wfubmc.edu). Currents recorded within each area were cumulated in order to produce a new time series.

2.3. Model of a single cortical area

First, a brief model justification is provided on the basis of the neurophysiological literature. Then, the model is qualitatively described. Finally all model equations and details are given.

2.3.1. Justification for the model structure

The neocortex is a 6-layer structure, which contains several types of neurons, excitatory and inhibitory [DeFelipe et al., 2002]. Neurons characterized by excitatory (glutamatergic) synapses include pyramidal neurons, which represent the majority of cells and are especially present in layers 2 and 6, and spiny stellate cells, mainly located in the middle cortical layer (i.e., the granular layer or layer 4). Most inhibitory interneurons form GABAergic synapses (although different types of neurons are also present) and are distributed in all layers.

The complete microstructure of the cortical column is certainly complex, and its simulation may require inclusion of a large number of neural populations, depending on the objectives of the model (for instance, Sotero et al. [Sotero et al., 2010], used up to eight populations in a recent work, see Discussion). Usually, however, authors tried to use a "minimal" model, which incorporates the smallest number of populations and of intrinsic synapses necessary to reach their objectives.

As suggested by DeFelipe et al. [DeFelipe et al., 2002], the basic microcircuit of the cortical column is formed by the pyramidal cells and by its input-output connections. Indeed, pyramidal cells are the only ones which send long-range (extrinsic) synapses; moreover, they represent the main source of the EEG signal (hence, this population represents the "output" of any neural mass model). According to this point of view, traditional "minimal" neural mass models embody three neural populations, which account for excitatory interneurons in the granular layer (layer 4) and for pyramidal neurons and inhibitory interneurons in the agranular layers. This minimal circuit considers just two feedback loops: pyramidal cells send their excitation to the two other populations via intrinsic connections, and receive inputs (respectively excitatory and inhibitory) from them.

It is worth noting that this model represents the simpler structure able to generate realistic EEG patterns. In fact, the negative feedback loop between pyramidal and inhibitory populations is mostly responsible for the rhythm generation (a simpler model for rhythm generation, the Wilson Cowan oscillator [Wilson & Cowan, 1972], includes two populations only, without excitatory interneurons, but provides quite schematic oscillatory waveforms). The positive loop between pyramidal neurons and excitatory interneurons has two basic functions: it amplifies the activity and modulates the rhythms to ensure a richer variety of behaviors [Jansen & Rit, 1995].

The previous "minimal" three-population model has been used by several authors in recent years to simulate various aspects of the EEG, such as power spectral density and ERP [David et al., 2005; Moran et al., 2007], and to study the role of intrinsic and extrinsic connectivity among ROIs [David et al., 2004; Sotero et al., 2010].

A significant extension of the previous model was suggested by Wendling et al. [Wendling et al., 2002]; these authors proposed addition of a fourth population of inhibitory GABAergic interneurons with faster synaptic kinetics. This modification was based on a series of studies in the hippocampus [Miles et al., 1996], which demonstrate that there are two types of $GABA_A$ synaptic responses in CA1 pyramidal neurons: a faster near the soma and a slower in the dendrites. The presence of fast kinetics is essential to generate rapid neural phenomena (evident

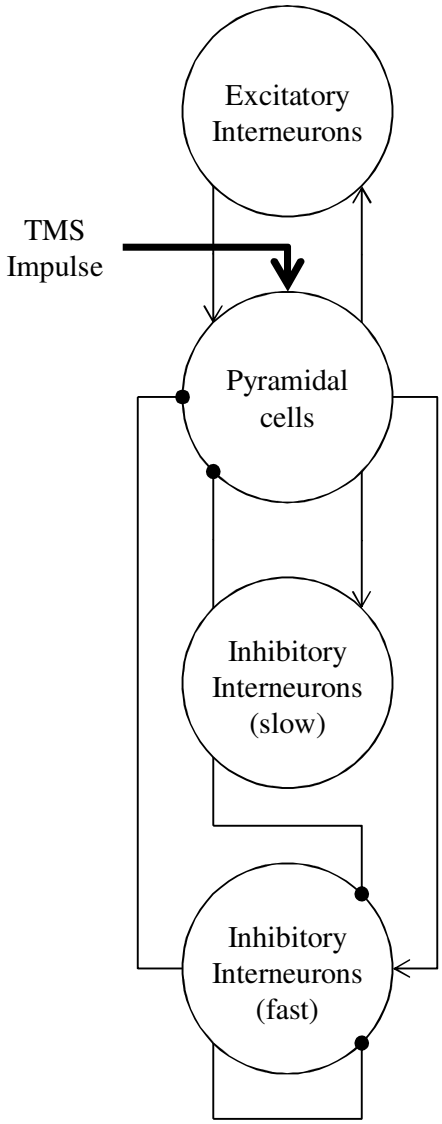

Figure V.1: Model of a cortical area.

not only in the hippocampus but in other ROIs too), such as gamma and ultra-gamma oscillations and epileptic spikes. A further aspect that should be taken into account is that GABAergic interneurons are richly interconnected [DeFelipe et al., 2002]. Banks et al. [Banks et al., 2000] showed that the two populations of interneurons interact, i.e., slow GABA interneurons do not only inhibit pyramidal neurons, but also send their inhibition to the fast GABAergic interneurons. Furthermore, experimental works in vitro [Bartos et al., 2007; Kisvárday et al., 1993; Sik et al., 1995], and theoretical computational studies [Tiesinga & José, 2000; Wang & Buzsáki, 1996;

White et al., 1998] suggest that a population of strongly interconnected fast GABAergic interneurons can produce a gamma rhythm per se, i.e., without the participation of the other populations. Accordingly, in recent works we suggested to incorporate a negative self-loop of the fast inhibitory population to itself [Ursino et al., 2010]; with this loop, the cortical column can generate robust gamma oscillations which coexist with a slower oscillation produced by the other internal loops [Moran et al., 2007, 2009].

Table V.1: Description of model parameters and variables

Symbol	Description	Subscript/Superscript
$h_i(t)$	Impulse response of synapse of type i	i = e for excitatory
G_i	Gain of synapse of type i	s for $GABA_{A,slow}$ inhibitory
ω_i	Pole of synapse of type i	f for $GABA_{A,fast}$ inhibitory
v_i	Membrane potential of neural population i	i,j = p for pyramidal cells
z_i	Spiking rate of neural population i	e for excitatory interneurons
x_i, y_i	State variables of neural population i	s for $GABA_{A,slow}$ interneurons
u_i	External input to neural population i	f for $GABA_{A,fast}$ interneurons
C_{ij}	Number of synaptic contacts from neural population j to neural population i	l for state variables of the external input to $GABA_{A,fast}$ interneurons
e_0	Maximum neural activation rate	-
r	Steepness of neural activation rate	
W_i^{hk}	Connection strength from region k to neural population i of region h	i = p for pyramidal cells
		f for $GABA_{A,fast}$ interneurons
D^{hk}	Connection delay between region k and region h	h, k = 6, 7, 19 for BA 6, 7, 19 respectively

2.3.2. Qualitative model description

Following the previous considerations, the general schema of the model used in this chapter to simulate a single ROI is shown in Figure V.1. Alternative, more complex models and possible changes will be critically commented in section 4. .

The model of a cortical region consists of four neural populations (Figure V.1), which represent pyramidal neurons (subscript p), excitatory interneurons (subscript e), and inhibitory interneurons with slow and fast synaptic kinetics ($GABA_{A,slow}$ and $GABA_{A,fast}$, subscripts s and f, respectively). Each population represents a group of neurons of the same type, which approximately share the same membrane potential and so can be lumped together. All populations are described with a similar mathematical formalism. Briefly, each population receives an average postsynaptic membrane potential, v, from other neural populations, and converts this membrane potential into an average density of spikes fired by the neurons. In order to account for the presence of inhibition (when potential is below a given threshold) and saturation (when potential is high) this conversion is simulated with a static sigmoidal relationship. Moreover, each population sends synapses to other populations (or, in case of pyramidal neurons, to other regions too). Each synaptic kinetics is described with a second order system, but with different parameter values.

To model a whole cortical region, the four populations are connected via excitatory and inhibitory synapses, with impulse response $h_e(t)$, $h_s(t)$ or $h_f(t)$, assuming that pyramidal neurons and excitatory interneurons synapses have similar dynamics. The average numbers of synaptic contacts among neural populations are represented by eight parameters, C_{ij} (see Table V.1), where

the first subscript represents the target (post-synaptic) population and the second subscript refers to the pre-synaptic population. These connections agree with those proposed by Wendling et al. [Wendling et al., 2002] but with the addition of the new self-loop C_{ff}. Table V.1 shows a list of model parameters with their meaning.

2.3.3. Model equations

Pyramidal neurons

$$\frac{dy_p(t)}{dt} = x_p(t) \quad \text{V.1}$$

$$\frac{dx_p(t)}{dt} = G_e\omega_e z_p(t) - 2\omega_e x_p(t) - \omega_e^2 y_p(t) \quad \text{V.2}$$

$$z_p(t) = \frac{2e_0}{1 + e^{-rv_p}} - e_0 \quad \text{V.3}$$

$$v_p(t) = C_{pe}y_e(t) - C_{ps}y_s(t) - C_{pf}y_f(t) \quad \text{V.4}$$

Excitatory interneurons

$$\frac{dy_e(t)}{dt} = x_e(t) \quad \text{V.5}$$

$$\frac{dx_e(t)}{dt} = G_e\omega_e\left(z_e(t) + \frac{u_p(t)}{C_{pe}}\right) - 2\omega_e x_e(t) - \omega_e^2 y_e(t) \quad \text{V.6}$$

$$z_e(t) = \frac{2e_0}{1 + e^{-rv_e}} - e_0 \quad \text{V.7}$$

$$v_e(t) = C_{ep}y_p(t) \quad \text{V.8}$$

Slow inhibitory interneurons

$$\frac{dy_s(t)}{dt} = x_s(t) \quad \text{V.9}$$

$$\frac{dx_s(t)}{dt} = G_s\omega_s z_s(t) - 2\omega_s x_s(t) - \omega_s^2 y_s(t) \quad \text{V.10}$$

$$z_s(t) = \frac{2e_0}{1 + e^{-rv_s}} - e_0 \quad \text{V.11}$$

$$v_s(t) = C_{sp}y_p(t) \quad \text{V.12}$$

Fast inhibitory interneurons

$$\frac{dy_f(t)}{dt} = x_f(t) \quad \text{V.13}$$

$$\frac{dx_f(t)}{dt} = G_f\omega_f z_f(t) - 2\omega_f x_f(t) - \omega_f^2 y_f(t) \quad \text{V.14}$$

$$\frac{dy_l(t)}{dt} = x_l(t) \quad \text{V.15}$$

$$\frac{dx_l(t)}{dt} = G_e\omega_e u_f(t) - 2\omega_e x_l(t) - \omega_e^2 y_l(t) \quad \text{V.16}$$

$$z_f(t) = \frac{2e_0}{1 + e^{-rv_f}} - e_0 \quad \text{V.17}$$

$$v_f(t) = C_{fp}y_p(t) - C_{fs}y_s(t) - C_{ff}y_f(t) + y_l(t) \quad \text{V.18}$$

Numerical values of parameters that are not found by the algorithm are reported in Table V.2.

2.4. Model of connectivity among areas

Neurophysiological and neuroanatomical studies [Felleman & Van Essen, 1991] show that long range connections from pyramidal neurons to distal cortical regions can reach all populations, depending on the type of connection. In particular, bottom-up connections especially reach excitatory interneurons in the granular layer; top-down connections reach both pyramidal cells and inhibitory interneurons; lateral connections reach all types of neurons [Felleman & Van Essen, 1991]. In the work described in the previous chapter [Ursino et al., 2010], we performed a sensitivity analysis on the role of these connections for rhythm propagation and found that the most influential connections are "from pyramidal to pyramidal" and "from pyramidal to fast inhibitory". The other two connections play a less important role for rhythm transmission. Hence, thinking to the necessity of a limitation in the number of estimated parameters, long-range synapses which target slow inhibitory interneurons or excitatory interneurons have not been considered.

Table V.2: Numerical values of constant parameters

Parameter		Value
ω_e	(rad/s)	75
ω_s	(rad/s)	30
ω_f	(rad/s)	75
G_e	(mV)	5.17
G_s	(mV)	4.45
G_f	(mV)	57.1
C_{ep}		5
C_{pe}		25
C_{sp}		60
e_0	(Hz)	2.5
r	(mV^{-1})	0.56

Accordingly, to simulate cortical connectivity between two regions (the pre-synaptic and post-synaptic regions will be denoted with the superscript k and h, respectively), we assumed that the average spike density of pyramidal neurons of the pre-synaptic area (z^k) affects the target region via a weight factor, W_j^{hk} (with j = p or f, depending on whether the synapse targets pyramidal neurons or $GABA_{A,fast}$ interneurons) and a time delay D^{hk}. This is achieved by modifying the membrane potential v_p^h and/or v_f^h of the target region, with the time dynamics of an excitatory synapse.

2.5. Simulation of TMS experiments and fitting procedure

In order to simulate the TMS experiment described above, we implemented a model of connectivity among three cortical regions, simulating BA 19, BA 7 and BA 6 (Figure V.2).

An automatic fitting between simulated EEG and real data has been achieved in the time domain. In particular, we focused attention on the 200 ms following the TMS impulse. Experimental time series were compared with membrane potentials of pyramidal neurons simulated with the model. Since the two quantities have a different scale, all experimental time series were multiplied by a constant gain to have the same scale as the simulated signals. It is worth noting that, in the present model, we used the sum of postsynaptic potentials of pyramidal neurons to calculate the source of the EEG signal. Although this assumption is usually adopted in neural mass models [Jansen & Rit, 1995; Wendling et al., 2002] recent studies suggest that EEG waves are generated by synaptic currents [Avitan et al., 2009; Nunez & Srinivasan, 2006]. We think that the use of potentials instead of currents may be acceptable in the present study, since we are especially interested in the frequency content of activity evoked by the TMS pulse. Moreover, the model works in the linear region of the sigmoidal function, where current and potential are almost proportional.

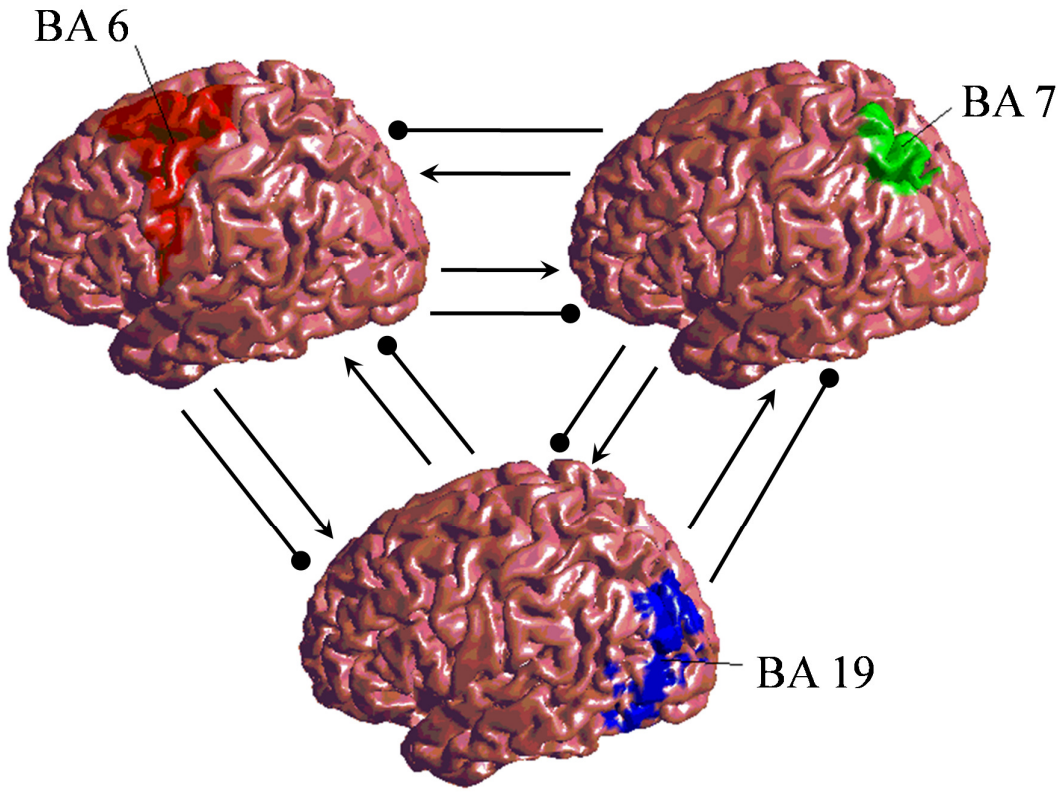

Figure V.2: Connectivity pattern. Arrows indicate connections toward pyramidal cells, circles indicate connections toward $GABA_{A,fast}$ interneurons.

In the present work fitting has been attempted only in a frequency range above 8 Hz (i.e., theta and delta rhythms have been excluded, since they probably require a more complex model including thalamic regions, see section 4.). As a consequence, the real TMS-evoked potentials (TEPs) were preprocessed with a high-pass filter (Chebyshev 2^{nd} type with cutoff frequency f_t =

8Hz). Furthermore, oscillations in the experimental signals occurring in the first 10 ms after the perturbation were also neglected, because they are mostly artefactual [Rosanova et al., 2009]. After fitting, model and real signals were also compared in the time frequency domain. To this end, time frequency maps were obtained using the continuous wavelet transform with Morlet wavelets [Tallon-Baudry et al., 1996].

The aim of the fitting procedure was to find for each subject and each stimulation intensity a set of model parameters able to reproduce the experimental data (5 subjects x 3 intensities = 15 fittings). Considering one subject, for each stimulation intensity we have 9 experimental signals to be fitted, representing the responses of the 3 BA to the stimulation of each of them.

First, we applied the whole fitting procedure described below to subject SUBJ5 with medium TMS intensity. The fitting procedure has been subdivided into two steps.

In the first step, we fitted the impulse response of a single region when the same region receives the TMS stimulus (this step was repeated three times, once for each BA). The effect of the TMS stimulus in the single cortical area was simulated as a step change, Δy_p, in the membrane potential of pyramidal cells, in accordance with other TMS implementations in neural models [Esser et al., 2005]. The estimated parameters were the synaptic contacts among the neural populations (C_{ij}) and the intensity of the stimulus Δy_p. To reduce the number of variables for the fitting, we used as free variables only those internal connection strengths (C_{ps}, C_{fp}, C_{pf}, C_{ff}, C_{fs}, see also Table V.1 for the meaning of symbols) that most influenced the frequency content of the model output, according to our previous study [Ursino et al., 2010], for a total of 6 parameters per ROI. The complete list of parameters is shown in Table V.1. The optimization procedure was a combination of a Genetic Algorithm (GA) (for a similar application of GA to neural mass models see Cona et al. [Cona et al., 2009]) and the simplex method (Matlab's fminsearch). We used a GA in order to arrive at an optimal solution, independently of the initial guess [Holland, 1975]. To facilitate the convergence of the GA we used Dynamic Time Warping (DTW) [Sakoe & Chiba, 1978] to compare the simulated TEPs with the experimental ones. DTW has been used as a generalization of the Mean Square Error (MSE) because it is less influenced by time shifts and by limited deformations when comparing waveforms. The simplex method was applied once every 50 generations of the GA, in order to explore various local minima of the variable space, and as the final step of the fitting procedure. A more detailed description of the GA is given in sub-section 2.6. .

In the second step we used the same fitting algorithm (GA and simplex method) to find a unique cortical connectivity pattern that could describe the experimental TEPs of all regions both directly and indirectly stimulated by TMS (i.e., all 9 signals simultaneously). This time, the algorithm acted not only on the number of synaptic contacts within each region, but also on the inter-regional connectivity strengths (directed to pyramidal cells, W_p, and to $GABA_{A,fast}$ interneurons, W_f, for a total of 12 free parameters) and on their time delays, D. The delays between any pair of regions were forced to be equal, thus reducing their number from 6 to 3, resulting in 15 more free parameters (33 parameters in total). The results from the first step were used here as the starting points for the internal parameters in order to boost the convergence. In this second step we used MSE as the error function instead of DTW, which is more computationally expensive, since the initial guess was sufficiently accurate. To handle the multi-objective optimization with the GA (we had to find a unique set of parameters for 9 different signals) we followed a particular strategy that makes use of more than a cost function. More precisely, we calculated 9 MSEs, one

for each signal, and evaluated the individuals of the GA with 10 different cost functions that depends on these MSEs:

1. The first cost function (mixing function, MF) is given by a weighted sum of the 9 MSEs, where we gave more importance to the fitting of the directly stimulated regions:

$$MF = \frac{1}{6}\sum_{i} E_{i,i} + \frac{1}{12}\sum_{i\neq j} E_{i,j} \qquad \text{V.19}$$

   where $E_{s,r}$ represents the MSE between the real and the simulated TMS evoked potential on the Brodmann area BA r when BA s is stimulated with TMS;

2. The other cost functions (specific functions) are also weighted sums of the 9 MSEs, but each one gives the most importance to a single different MSE:

$$SF_{s,r} = \frac{1}{2}E_{s,r} + \frac{1}{16}\sum_{(i,j)\neq(s,r)} E_{i,j} \qquad \text{V.20}$$

In this way we obtained 10 votes for each individual, where the first (mixing function) rewards the individuals that best fit the 9 signals altogether (with particular attention to the 3 TEPs of the directly stimulated regions), while the other 9 (specific functions) reward the individuals that best fit one single signal. The probabilities for each individual to enter the mating pool (individuals who will produce children) are equally distributed between the 10 votes, so an individual that fits one of the 9 signals very well has nearly the same probability to reproduce itself as an individual that fits all signals quite well. In this way the 9 signals are fitted in parallel with the goal of reaching a global minimization. The output of the GA is the set of parameters given by the individual with the lowest value for the first cost function. For the simplex method we used a single cost function which is the mixing function of the GA.

Since activities evoked by TMS in all the subjects and with all the stimulation intensities were quite repeatable in the frequency domain (i.e., TMS evoked similar natural rhythms), we used the same architecture for the three regions and varied only the inter-region connectivity. Hence, we set the internal parameters within each region (parameters C_{ij} in Table V.1) to the same values estimated above, and we re-estimate only the inter-region connection strengths (W_i^{hk}) and the TMS intensities (Δy_p) for all the other trials (i.e., to simulate subject SUBJ5 with medium-strong and strong intensity, and subjects SUBJ1, SUBJ2, SUBJ3, SUBJ4 with all intensities). In this way, each fitting differs from the others for 15 parameters (12 inter-regional connections and 3 TMS intensities).

We assumed that inter-region connectivity is less stable than connectivity within the regions, since it reflects the integrative behavior of the brain, which may be highly plastic. Conversely, our idea is that internal connectivity within a cortical column is less variable among subjects, reflecting the particular specialization of that region. Indeed, we observed that the natural rhythms of the three ROIs exhibit just moderate changes from one subject to another, which further justifies our idea to maintain the same ROIs for all subjects.

We are aware that this is a simplification of the reality, which corresponds to a “parsimony principle”: it is probable that differences among internal parameters of the ROIs exist between individuals, but these are less important for the study of rhythms transmission, which is the main goal of the present work.

2.6. The genetic algorithm

For the GA we used a population of 500 chromosomes (individuals) which evolves for 1000 generations. Each chromosome Ch_i (i = 1,…,500) consists of N_g genes $G_{i,j}$ (j = 1,…,N_g) encoded with real numbers that represent the values of the parameters to be estimated. Each gene $G_{i,j}$ can vary in a limited range $[m_j, M_j]$ that depends on the parameter it represents. The offspring is generated as follows:

1. 200 individuals are generated through crossover: iteratively, two individuals Ch_m and Ch_f (parents) are selected with a probability inversely proportional to their cost function, and the genes of the new individual Ch_s (son) are randomly selected from the ones of the parents and modified with an additive noise

$$G_{s,j} \in \{X + R_N | X \in \{G_{m,j}, G_{f,j}\}, R_N \sim N(0, \sigma_j)\}, \forall j = 1, \dots, N_{gene} \quad \text{V.21}$$

   where $R \sim N(\mu, \sigma)$ means that R is a value extracted from a normal distribution with mean μ and standard deviation σ, and σ_j depends on the parameter represented by the j-th gene of each chromosome;

2. 250 individuals are generated through mutation: iteratively, one individual Ch_p (parent) is selected with a probability inversely proportional to its cost function, and the genes of the new individual Ch_s (son) are copied from the ones of the parent with an additive noise and a small probability p_{mut} to be mutated

$$G_{s,j} = \begin{cases} R_U \sim U(m_j, M_j) & \text{if } R_{mut}(s,j) < p_{mut} \\ G_{p,j} + R_N, R_N \sim N(0, \sigma_j) & \text{otherwise} \end{cases}, \quad \forall j = 1, \dots, N_{gene} \quad \text{V.22}$$

   where $R \sim U(m, M)$ means that R is a value extracted from a uniform distribution between m and M, and $R_{mut}(s,j) \sim U(0,1)$;

3. 50 individuals are randomly generated in order to continuously add new genetic material.

The new individuals are compared with the old ones (for a total of 1000 individuals) and only the best 500 are chosen to form the new generation. The cost functions of old individuals are increased each generation by a 10% factor (aging) to avoid stagnation.

The parameters σ_j and p_{mut} vary as a sinusoidal function of the current generation. In this way the algorithm goes through alternating epochs in which the new individuals are generated in more or less deterministic ways: when σ_j and p_{mut} have small values ($0.001 \cdot (M_j - m_j)$ for σ_j and 0.01 for p_{mut}), the new generations are scarcely affected by random mutations and the population tends to converge to a local minimum, while when σ_j and p_{mut} have high values ($0.01 \cdot (M_j - m_j)$ for σ_j and 0.1 for p_{mut}), the new generations are heavily influenced by random mutations and the population tends to spread in the variable space in order to explore it.

3. RESULTS

3.1. Preliminary parameter fitting on a single subject

As described in section 2. , the first fitting procedure was performed on a single subject (SUBJ5) using a stimulus of medium intensity (120 V/m). The impulse intensity and 33 parameters (describing internal and extrinsic connectivity patterns) were fitted. Parameter values are shown in Table V.3. Results are summarized in Figure V.3, Figure V.4, Figure V.5 and Figure V.6.

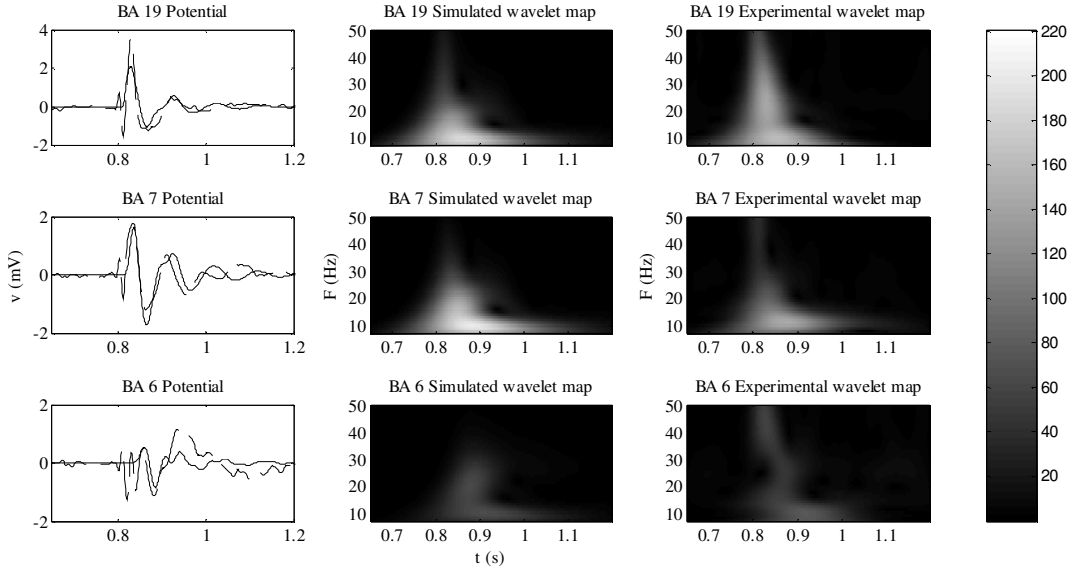

Figure V.3: Stimulation of BA 19. Simulated (solid line) and experimental time responses (dashed line) are shown in the first column. The second and third columns show the simulated and the experimental time-frequency maps, respectively.

Table V.3: Parameters found by the fitting algorithm on SUBJ5 with TMS of medium intensity

Parameters		BA 19	BA 7	BA 6
Δy_p		-0.05	-0.035	-0.0065
C_{ps}		54.5	57	31
C_{fp}		81	97.5	136.5
C_{fs}		0.1	39	21
C_{pf}		4.7	10.5	11.5
C_{ff}		16	16	18
W_p to BA 19		-	0	16.5
W_p to BA 7		94.5	-	0
W_p to BA 6		0.57	25.5	-
W_f to BA 19		-	81	24.5
W_f to BA 7		75.5	-	11.5
W_f to BA 6		0	0	-
D to BA 19	(ms)	-	1	8.3
D to BA 7	(ms)	1	-	16.6
D to BA 6	(ms)	8.3	16.6	-

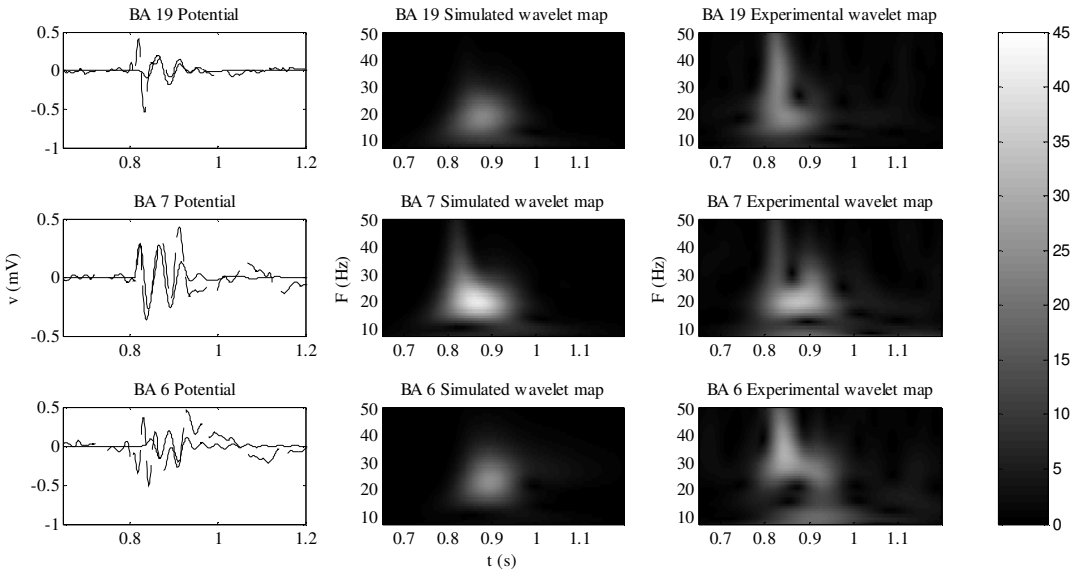

Figure V.4: Stimulation of BA 7. The panels represent the same quantities as in Figure V.3.

Figure V.3, Figure V.4 and Figure V.5 display the time patterns and the time-frequency maps of the simulated and real signals in response to TMS stimulation on BA19 (Figure V.3), on BA7 (Figure V.4) and on BA 6 (Figure V.5), compared both in time and frequency domains. Results show that the model can reproduce the main experimental patterns of cortical activity quite satisfactorily. The main result is that each region displays a different intrinsic rhythm when directly stimulated, and this rhythm exhibits evident changes as a consequence of the stimulation of another region. The model can explain both aspects, ascribing the first to the internal parameters of the region, and the second to the mutual long-range connections among regions. Focusing on BA 19, one can observe that this region exhibits an activity mainly in the alpha range

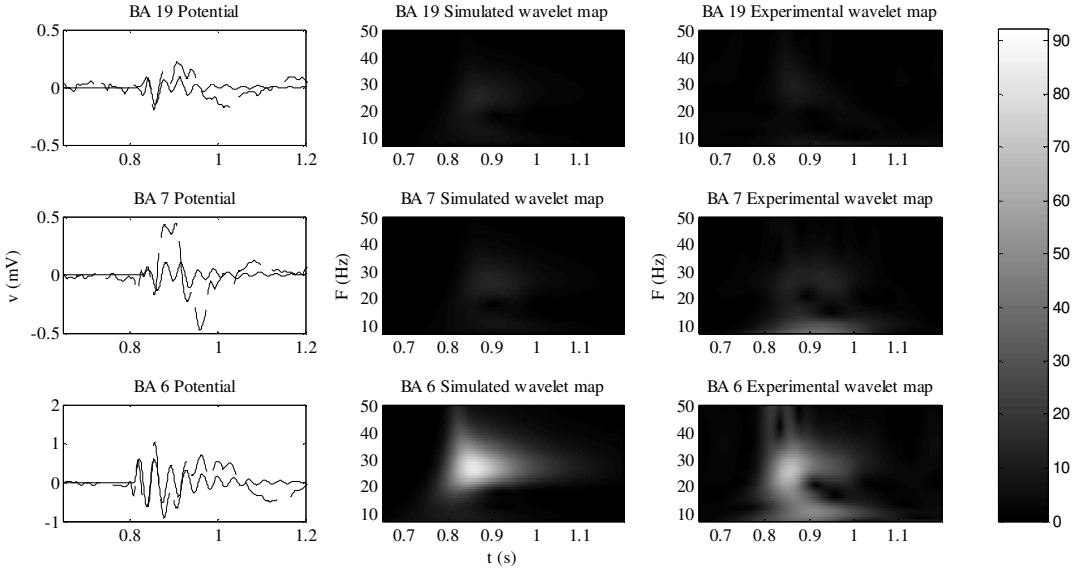

Figure V.5: Stimulation of BA 6. The panels represent the same quantities as in Figure V.3.

when it is directly stimulated by TMS, although with components also in the beta and gamma ranges (Figure V.3), while it oscillates in the beta and gamma range respectively when BA 7 (Figure V.4) and BA 6 (Figure V.5) are stimulated. BA 7 exhibits an activity in beta range when directed stimulated (Figure V.4), while it oscillates mostly in alpha and gamma range respectively when the BA 19 (Figure V.3) and BA 6 (Figure V.5) are stimulated. BA 6 oscillates mostly in gamma range when it is stimulated by the TMS (Figure V.5), and it oscillates in beta and in alpha range respectively when BA 7 (Figure V.4) and BA 19 (Figure V.3) are stimulated.

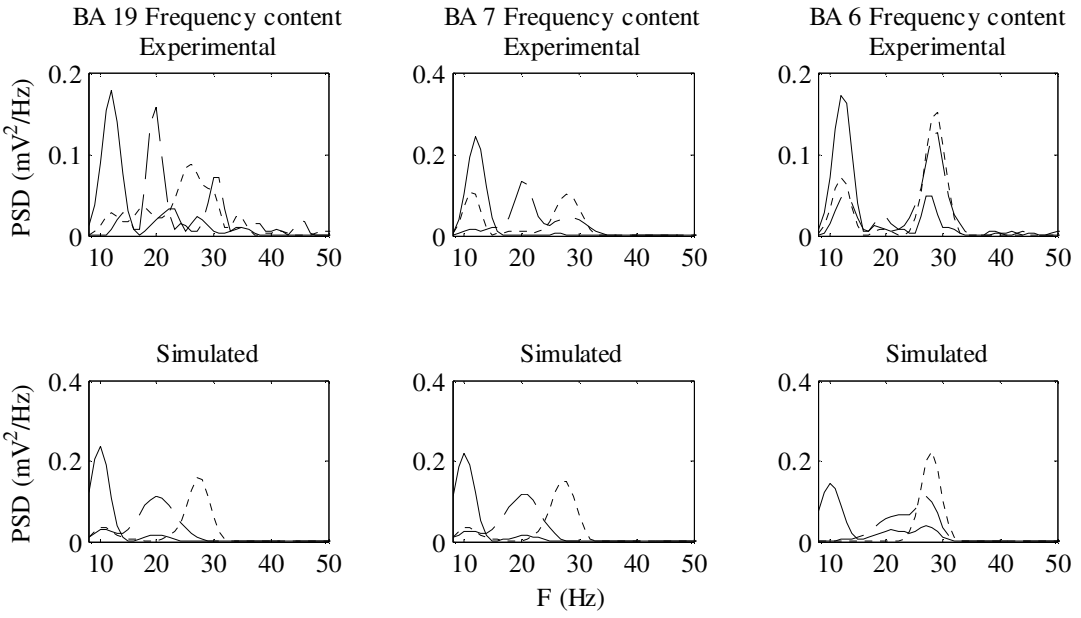

Figure V.6: Power spectral densities evoked in each region by different TMS stimulations. Panels show how the frequency content of a ROI changes depending on the position of the TMS stimulus (solid lines: stimulus on BA 19; dashed lines: stimulus on BA7; dotted lines: stimulus on BA 6). The upper panels show experimental spectra, while the lower panels show the spectra of the signals simulated with the model.

When estimating the intrinsic connectivity, we focused on those internal parameters involving $GABA_{A,fast}$ interneurons (C_{fp}, C_{pf}, C_{ff}, C_{fs}), since this neural group plays a crucial role in the generation of different rhythms [Ursino et al., 2010]. In particular, the loop gain between pyramidal cells and $GABA_{A,fast}$ interneurons (C_{fp} and C_{pf} in Table V.3) for BA 19 has a small value (81×4.7) compared to BA 7 (97.5×10.5). As discussed in Ursino et al. [Ursino et al., 2010; Zavaglia et al., 2010] when these two parameters are small the model oscillates at low frequencies. This explains why BA 19 natural frequency is located in alpha range. As discussed before BA 7 oscillates in beta range and BA 6 in gamma range. This could be ascribed to a further increase in the loop gain between pyramidal cells and $GABA_{A,fast}$ interneurons from 97.5×10.5 for BA 7 to 136.5×11.5 for BA 6 and to parameter C_{ff} which is greater for BA 6 than for BA 7. Even if the difference for C_{ff} is small (16 for BA 7 and 18 for BA 6), this parameter has a great impact on the dynamic of the region [Ursino et al., 2010; Zavaglia et al., 2010].

Figure V.6 summarizes the changes in PSD within each region, simulated by changing the position of TMS stimulation (bottom panels) compared with real spectra (upper panels). It is well evident that the frequency content of each ROI changes depending on the stimulation site. In

detail, BA 19 and BA 7 have a similar behavior in the model. They exhibit a peak in the alpha band with a residual activity in the beta band when BA 19 is stimulated, a peak in beta band with a smaller alpha activity when BA 7 is stimulated, and a peak in gamma band with some alpha activity when BA 6 is stimulated. BA 6 exhibits a wide spectrum, with a peak mainly focused on alpha band when BA 19 is stimulated, two peaks in beta and gamma bands when BA 7 is

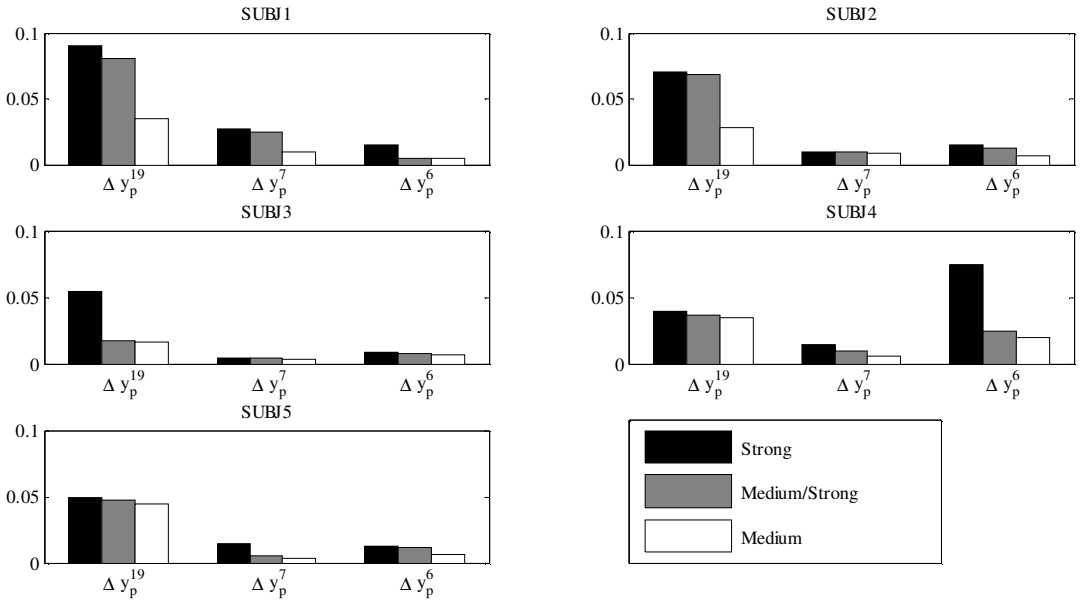

Figure V.7: Comparison of TMS intensities estimated with the fitting algorithm in the 15 trials. Each panel refers to a different subject and shows the step inputs Δy_p used at input to the model, to simulate the TMS impulse in BA 19, BA 7 and BA 6. Different values have been estimated for each intensity of the TMS (strong, medium/strong and medium). It is worth noting that the estimated intensities actually decrease as the real TMS intensities are reduced.

stimulated, and finally, a peak in gamma band when it is stimulated.

It is worth noting that similar peaks are evident in the real spectra: the main difference is the presence of additional peaks in real spectra not present in the simulated ones (in particular, a gamma peak evident in BA19 after stimulation of BA7, and some alpha peaks evident in BA6 when the other two regions are stimulated). These differences, already evident in Figure V.3, Figure V.4 and Figure V.5, are related to the difficulty to simulate some slow oscillation patterns, or some gamma oscillations in the initial period after stimulation.

3.2. Generalization of model results

The previous results suggest that each single region exhibits a different natural frequency when stimulated with TMS. This intrinsic rhythm can be ascribed to the internal parameters of the region. Moreover, these rhythms can be propagated from one region to another thanks to the extrinsic connectivity.

In order to generalize these results, we repeated the estimation procedure on all available trials (i.e., using medium-strong and strong intensities on subject SUBJ5, and all the three intensities in the other four subjects). During these fittings, the intrinsic connectivity parameters within each

region were set to the same values estimated before (see Table V.3), assuming that they exhibit smaller inter-subject variability. Hence, parameter estimation was performed only on the impulse

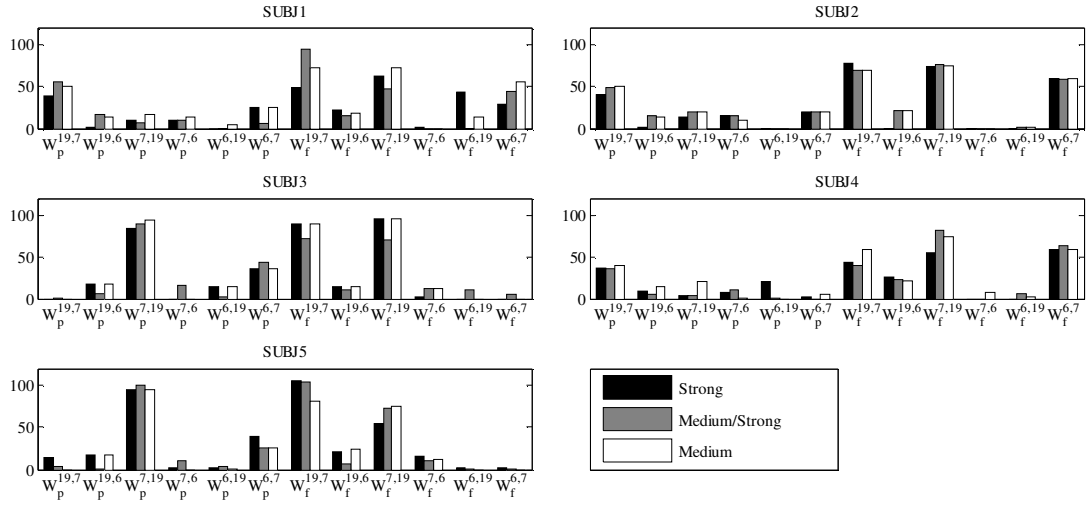

Figure V.8: Comparison of inter-region connection strengths estimated with the fitting algorithm. Each panel refers to a different subject and shows how the inter-regional connection strengths among BA 19, 7 and 6, change as the real TMS intensities decrease (for the meaning of parameters see Table V.1).

intensity, and on 12 parameters describing extrinsic inter-region connectivity.

Table V.4 summarizes the correlation coefficients between model and empirical waves for all trials, as an index of fitting accuracy. Results are in general satisfactory. Just in a few cases, a poor correlation coefficient is obtained. Results can be summarized as follows:

1. in most cases, a good fitting (i.e., a high correlation) is obtained for what concerns the ROI directly stimulated;

Table V.4: Correlation coefficients between model and empirical TEPs

	Strong intensity			Medium/strong intensity			Medium intensity		
SUBJ1	0.95	0.89	0.93	0.93	0.97	0.59	0.98	0.72	0.78
	0.62	0.98	0.89	0.95	0.96	0.63	0.69	0.96	0.79
	0.86	0.86	0.96	0.84	0.72	0.94	0.97	0.72	0.98
SUBJ2	0.99	0.73	0.87	0.97	0.28	0.82	0.99	0.89	0.77
	0.49	0.88	0.88	0.61	0.87	0.98	0.59	0.96	0.85
	0.94	0.80	0.37	0.97	0.83	0.40	0.89	0.88	0.43
SUBJ3	0.72	0.60	0.65	0.83	0.46	0.94	0.84	0.92	0.81
	0.91	0.68	0.79	0.98	0.95	0.89	0.94	0.91	0.55
	0.96	0.80	0.85	0.83	0.73	0.92	0.61	0.51	0.98
SUBJ4	0.81	0.80	0.90	0.53	0.38	0.63	0.92	0.92	0.76
	0.98	0.98	0.29	0.70	0.91	0.88	0.54	0.98	0.74
	0.82	0.61	0.91	0.53	0.52	0.92	0.81	0.86	0.50
SUBJ5	0.85	0.94	0.63	0.58	0.76	0.75	0.89	0.97	0.96
	0.51	0.90	0.38	0.79	0.99	0.95	0.82	0.99	0.78
	0.84	0.98	0.82	0.85	0.60	0.71	0.96	0.76	0.84

2. in most cases, the waveforms in the other two ROIs (not directly stimulated) can be simulated pretty well. This aspect of fitting reflects the inter-region connectivity among ROIs;

3. just in a few cases, a single waveform is poorly reproduced. However, these poor fitting results are often associated with waves having a poor statistical significance (i.e., the impulse response exhibit a weak difference compared with the basal pre-impulse activity) or unpredictable alpha or gamma waves.

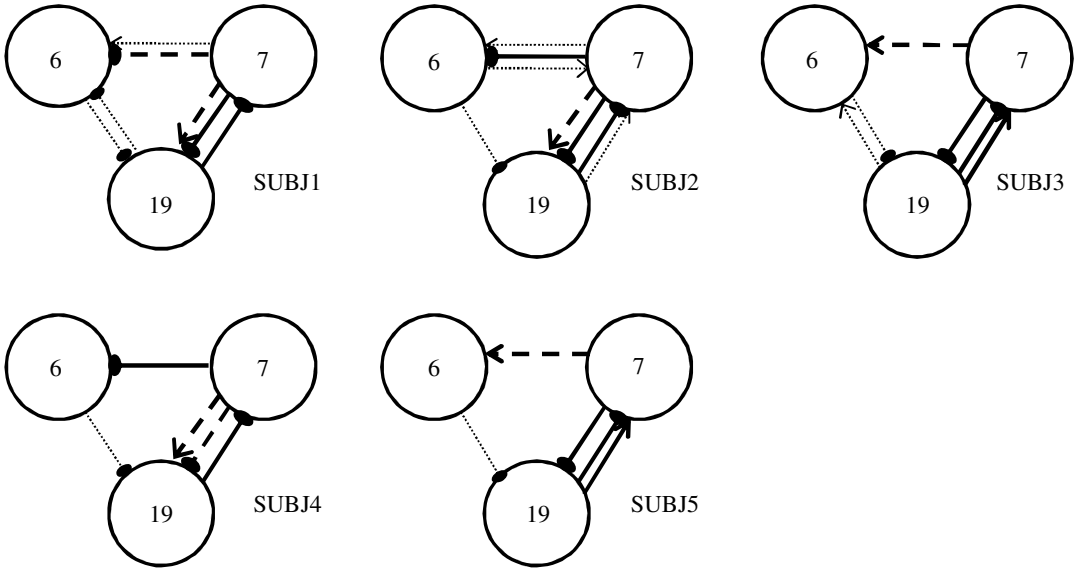

Figure V.9: Schematic summary of the inter-region connectivity patterns estimated in 5 subjects with the fitting algorithm. Each weight has been first mediated over three trials (with strong, medium/strong and medium intensity). Weights have then been subdivided into four classes: $W > 50$: continuous thick line; $40 < W \leq 50$: dashed thick line; $13 < W \leq 40$: dotted thin line; $W \leq 13$: no connection shown. Synapses directed to pyramidal neurons are indicated with arrows, while synapses directed to $GABA_{A,fast}$ interneurons are indicated with closed circles.

Results on estimated parameters are summarized in Figure V.7 and Figure V.8.

Figure V.7 shows that the estimated impulse intensity actually increases with the strength of the TMS stimulation, although with a large variability among subjects. Figure V.8 shows that inter-region connectivity remains quite stable within the same subject, i.e., it is not easy to detect a clear dependence of connectivity on the impulse strength. However, connectivity exhibits a greater variability from one-subject to another.

Figure V.9 summarizes the main connectivity patterns in the five subjects, mediated over the three different trials. Briefly, all subjects exhibit a strong connectivity between BA 7 and BA 19, and this especially occurs by targeting fast interneurons. Subjects SUBJ3 and SUBJ5 also exhibit a strong connectivity towards pyramidal neurons from BA 19 to BA 7, whereas SUBJ1, SUBJ2 and SUBJ4 exhibit medium-strong connectivity towards pyramidal neurons from BA 7 to BA 19. Hence, the occipital and parietal regions are strongly interconnected, but generally in a non-symmetrical way. Furthermore, all subjects exhibit a strong or medium-strong connection from BA 7 to BA 6, some with a prevalent target to fast interneurons (SUBJ1, SUBJ2, SUBJ4) other with a prevalent target to pyramidal neurons (SUBJ3, SUBJ5). On this general pattern, some

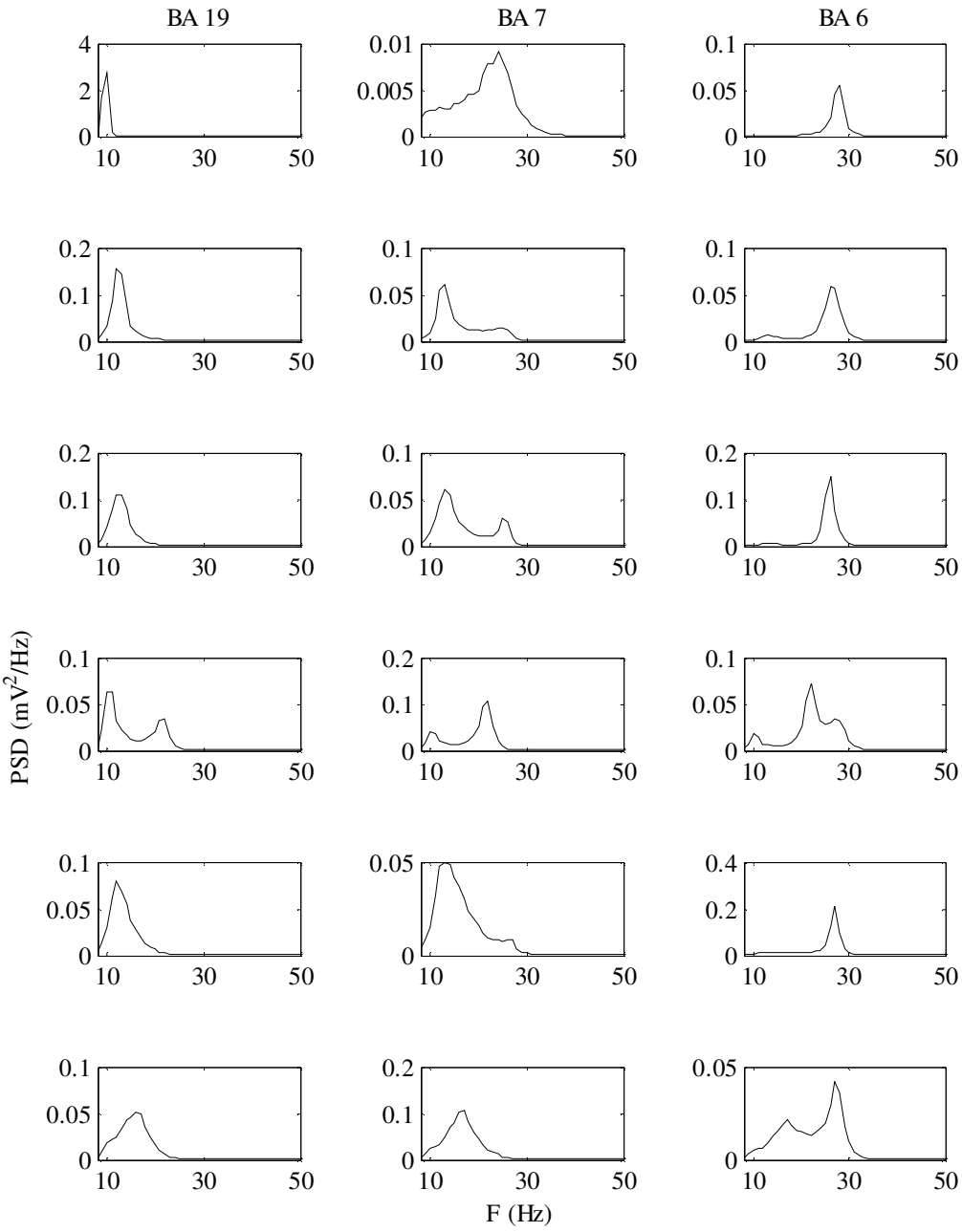

Figure V.10: Power spectral densities computed in all ROIs (BA 19, BA 7 and BA 6) from model simulation tracings, when all ROIs are independently stimulated with white Gaussian noise (mean value 0; variance $1Hz^2$; duration 100s). The upper row considers the case of no connectivity among ROIs. The other rows represent results obtained using the connectivity patterns estimated on each subject (SUBJ1-SUBJ5) mediated over three trials.

variants are evident among subjects, especially concerning feedback connections from BA 6 to the other ROIs. All subjects exhibit a clear although small feedback connection from BA 6 to BA 19 targeting fast interneurons and, in some cases, a feedforward connection from BA 19 to BA 6. In a single case, a feedback connection from BA 6 to BA 7 is also evident. Other connections of weaker strength (not reported in Figure V.9 for simplicity) sometimes connect regions 6-19 and 6-6 (see Figure V.8 for a more complete presentation).

The interregional connectivity estimated above determines the propagation of rhythms from one region to another, which may cause the emergence of multimodal rhythms. In order to further investigate this aspect, we simulated the behavior of the ROIs when they are stimulated with Gaussian white noise (indeed, Gaussian white noise is commonly used to simulate a complex input coming from many independent sources [David & Friston, 2003; Jansen & Rit, 1995; Wendling et al., 2002]).

Results show that all ROIs exhibit power in the frequency band evoked by TMS when they are directly stimulated by white noise, and are not interconnected (Figure V.10, first row). In particular, in these conditions BA19 exhibits power density in the alpha range, BA7 in beta range, and BA6 in gamma range.

The other rows in Figure V.10 illustrate the cases in which the three ROIs are interconnected and are all stimulated with independent white noise. Here, we used the same connectivity patterns estimated in the five subjects mediated over three trials (with medium, medium-strong and strong stimulation). The figure shows that multimodal spectra can be obtained in the different regions, but they can vary significantly among subjects, depending on the estimated connectivity. Even small changes in connectivity can evoke evident changes in the spectral morphology. These relationships between connectivity estimated by TMS, and spectral patterns in presence of enduring activity may represent possible testable predictions for future studies.

4. DISCUSSION

4.1. Objective of the study

The study of brain rhythms is assuming an increasing importance in modern cognitive neuroscience. Many works, appeared in the last decade, provide increasing evidence that brain activity in different frequency bands plays a peculiar role in perception, motion and cognition [Başar et al., 2000, 2001; Jensen et al., 2007]. Furthermore, a correlation between different cortical rhythms and brain topography has also been explored by means of source localization algorithms and combined EEG-fMRI: these studies underline a correlation between alpha rhythms and occipital cortical activity [Gómez et al., 2006; Gómez-Herrero et al., 2008; Laufs et al., 2003; Michel et al., 1992; Tinguely et al., 2006], beta rhythms and parietal activity [Feige et al., 2005; Gómez et al., 2006; Laufs et al., 2003; Mantini et al., 2007; Michel et al., 1992; Tinguely et al., 2006] and between frontal cortex activity and gamma rhythms [Mantini et al., 2007], although large variations in this topography can be found depending on the particular task. Up to our knowledge, despite this large amount of data, simple models able to simulate rhythm generation, their propagation between different regions, and their dependence on brain connectivity parameters are still at the pioneering stage. Of course, brain activity is too much complex, contains many non-linear effects, and depends on too many parameters, to try a unique modeling synthesis. Hence, individual ad hoc experiments are needed, able to reveal specific aspects of brain dynamics, for their subsequent synthesis within neurophysiologically inspired models which focus on limited goals.

TMS-EEG, joined with mathematical modeling techniques, may constitute an innovative engineering approach to the study of brain dynamics. Mathematical models, in fact, require an input signal with wide-spectrum (such as white noise or an impulsive perturbation) for inner parameter identification and subsequent validation. TMS-EEG may provide an adequate non-invasive input perturbation for model testing. On the other hand, a model allows data obtained through TMS-EEG to be summarized into a coherent theoretical structure and hypotheses to be tested in rigorous quantitative terms. Hence, there is a potential symbiosis between neural dynamical models and the TMS-EEG technique. Stressing this aspect is one of the main objectives of the present work.

Recent data obtained with single-pulse TMS [Van Der Werf & Paus, 2006; Van Der Werf et al., 2006; Paus et al., 2001; Rosanova et al., 2009] show that different brain regions may exhibit different natural frequencies, that can propagate among regions, and can be at least in part detected looking at the transient (200 ms) response induced by a TMS pulse.

The concept of natural frequency is extremely important in systems engineering, in that it can help the identification of the internal structure of complex dynamical systems. The natural frequency signifies that a system, receiving a wide-band input (i.e., an input whose power is distributed over a large band) exhibits the tendency to amplify only the power contained within a specific frequency band. This kind of behavior can be evoked by a single impulse with short-duration. Furthermore, if a non-linear system becomes unstable, self-sustained oscillations may arise with a frequency close to the natural one.

The recent finding that different natural frequencies in BA 19, BA 7 and BA 6 can be evoked by single-impulse TMS, and that these frequencies show a typical propagation behavior, together with the lack of simple neurocomputational models of brain rhythms, motivated the present study

with two main purposes: to analyze whether the impulse response evoked in a ROI can be at least partly simulated using a simple neural mass model; to study whether the system of rhythms observed in multiple ROIs can be reproduced using simple connectivity patterns. In the present work, we assumed that rhythms are generated as a consequence of feedback loops within the cortical columns. A different possibility, not considered here but which cannot be excluded, is that rhythms can be produced by neurons with intrinsic-oscillatory properties, which impose their own oscillation on the network in which they are embedded [Jefferys et al., 1996; Steriade et al., 1993].

We claim that both objectives have been achieved, although several critical points needing discussion and further work are also evident.

4.2. Comments on results

A first important result is that most time-frequency properties of the impulse response, evoked within 200 ms by a short TMS stimulus, can be simulated fairly well acting only on a few internal parameters of the ROI, representing the number and the strength of the connections between neural populations. Moreover, these internal parameters may be maintained at the same values in different subjects, still achieving rather accurate simulation of brain rhythms. This result suggests that it may be possible to characterize the dynamic properties of occipital, parietal and frontal regions separately, ascribing them to the internal loops between populations, especially involving fast inhibitory interneurons. Differences in the internal parameters may represent testable predictions, which may be the subject of further experimental work.

The second important aspect of this work consists in the possibility to simulate how natural rhythms can propagate from one region to another, as a consequence of reciprocal connectivity. Results by Rosanova et al. [Rosanova et al., 2009] have clearly shown that a TMS short pulse not only affects activity in the underlying cerebral region, but can also induce statistically significant changes in other regions. Rosanova and colleagues suggested that these changes can be ascribed to connectivity among regions, but this hypothesis can be hardly tested in vivo. Hence, we tested the hypothesis “in silico” using a neural mass model developed previously [Ursino et al., 2010]. Our results suggest that changes in brain rhythms observed by varying the position of the TMS stimulus over the scalp can actually be explained by simple connectivity patterns among ROIs and that a rhythm, generated in one region, can propagate toward other regions inducing a complex wide-band spectrum. Furthermore, results show that these connectivity patterns are quite constant within the same subject, although they exhibit evident inter-subject variations. In particular, our results suggest the presence of strong (although asymmetric) feedback connections between BA 19 and BA 7, of a strong feedforward connection from BA 7 to BA 6, and of some weaker and variable feedback connection between BA 6 and BA 19 (or, less frequently, between BA 6 and BA 7).

Using these connectivity patterns, we have been able to simulate rhythm propagation fairly well in all trials, as documented by the good correlation coefficients achieved, although some significant discrepancies are also evident from time to time. These discrepancies are especially imputable to a lack of some rhythms in the simulated patterns, such as a lack of a few slow oscillations in the alpha band or of some gamma or ultra gamma bursts immediately after the impulse. However, it is worth noting that the quality of fitting might be significantly improved by assuming small changes in the internal parameters of each region from one subject to another (results not reported here for brevity). In fact, the frequency of the individual rhythms exhibits

small variations among subjects, and these may be better reproduced assuming a moderate internal variability. We decided to maintain internal parameters at the same value for all subjects, to generalize the model and reducing the number of estimated parameters.

In the present work, all 9 trials have been used to estimate model parameters, and generalization is simply based on the observation that inter-region connectivity remains quite stable for different TMS strengths and, moreover, exhibits moderate inter-subject variations. A more powerful generalization procedure (named "leave-one-out") would consists in using N-1 signals to estimate parameters (training set) and leave the remaining signal out to test the model (test set). In our case, this would mean to use 8 signals to estimate parameters and use the remaining signal to generalize. We did not use this procedure since "leave one out" implicitly assumes that all N signals carry a similar information content, hence estimation on N-1 of them allows prediction on the remaining one. Conversely, in our data each of the 9 signals carries a different piece of information, which may not be entirely deducible from the others. For instance, the activity measured on BA6 when BA19 is stimulated may provide information on the connection from BA19 to BA6, which cannot be entirely derived from the other signals (or can be derived only indirectly in a much less accurate way).

Our results, generalized on five subjects, suggest that TMS-EEG technique joined with neural mass models may represent a promising, non-invasive method in the field of engineering applied to the brain, in particular to assess inter-regional connectivity. This is a very important point for clinics, since connectivity can exhibit significant changes in pathological conditions such as multiple sclerosis, schizophrenia, etc. [Guye et al., 2010].

Furthermore, simulation of the overall model, with the assigned connectivity pattern, provides interesting indications on how cortical activity signals with a large frequency-band can be generated and modulated. Let us consider, for instance, the results displayed in Figure V.10, when different regions are assumed to receive independent white noise. The kind of spectra which are obtained exhibit complex changes in frequency, which cannot easily be predicted via a qualitative reasoning, but arise as a consequence of multiple information included in the model (connectivity, time constants, time delays, etc.). This is a good example of how a complex model may provide interesting scenarios which cannot be understood in simple qualitative terms. In perspective, this model capacity may have important implications for neuroscience, since the way a natural rhythm is transmitted from one region to another may play an important role in many perceptive, motor or cognitive brain functions [Fries et al., 2007; Kaiser & Lutzenberger, 2005; Steriade, 2006].

Results of Figure V.10 may become the subject of further ad hoc testable predictions. In particular, a connectivity pattern among ROIs can be estimated from TMS stimulation (perhaps including additional anatomical and physiological a priori constraints to improve the solution); then, the patterns of multimodal spectra predicted by the model when all (or some) regions are activated with white noise, can be compared with real EEG spectra obtained during ad hoc motor or cognitive tasks.

4.3. Comparison with other models

The model utilized in this work represents a good compromise between simplicity and completeness. As discussed in section 2. , and shown in the previous chapter, it contains the fundamental elements necessary to generate multiple alpha, beta and gamma rhythms and to transmit them robustly among regions.

Alternative models, of course, have been proposed in recent years, which should be taken in mind as possible candidates for future studies. These comprehend different neural mass models, mean field variational approaches, and models with spiking neurons.

While most neural mass models include three populations [David & Friston, 2003; Jansen & Rit, 1995; Moran et al., 2007], some of them include elements not present here. For instance, Sotero et al. [Sotero et al., 2007] incorporated a positive self-loop among pyramidal neurons, to take into account the fact that, at a large spatial scale, pyramidal-to-pyramidal connections become increasingly important. Moreover, they incorporated connections with thalamic relay nuclei, the latter described by means of two population models. Inclusion of thalamic connections may represent a fundamental further step for our model too. In a more recent work, Sotero et al. [Sotero et al., 2010] extended the complexity of the cortical column model, raising the number of populations to eight: four excitatory and four inhibitory populations in layers 2/3, 4, 5 and 6. Intrinsic connectivity were assigned on the basis of anatomical constraints and fitting to local field potentials recorded in rat area S1. Although this model carefully incorporate most aspects of a cortical column, it is certainly too complex to attempt parameter fitting from TMS-evoked EEG responses.

Of course, neural mass models, despite evident advantages in terms of synthesis and computational load, also represent a drastic simplification of the reality. Hence, comparison with more realistic model may be advantageous. In particular, NMMs consider only the average activity within a population, i.e., they neglect the second order statistics. A more rigorous mean-field approach is presented in [Deco et al., 2008; Hasegawa, 2003], where implications for analysis of brain connectivity are also discussed. At a greater complexity level, the overall characteristics of neuron dynamics is captured by models which make use of spiking neurons. Among the others, Esser et al. [Esser et al., 2005] developed a detailed model of a portion of the thalamo-cortical system to simulate the effect of a TMS pulse. The model has been recently extended to include three cortical areas and to study connectivity changes during sleep [Esser et al., 2009]. Indeed, these two types of model are complementary, and exhibit different advantages, objectives and limitations. While neural mass models are more oriented to the study of macroscopic quantities, and can implement complex connectivity patterns without excessive computational cost, detailed models are more oriented toward microscopic phenomena, such as the investigation of synaptic currents and the role of different neuromodulators.

4.4. Optimization technique

The present study makes use of a sophisticate genetic algorithm for parameter estimation. The reason why we used this rather complex optimization procedure instead of a traditional one, is that the problem tends to generate a huge amount of local minima associated to unacceptable solutions. Different global optimization methodologies (traditional Genetic Algorithm, Simulated Annealing and intensive Monte Carlo methods) have been implemented and tested, but they get caught in poor local minima, or at least require a lot of iterations (and time) to find a good solution. The procedure proposed in this chapter tries to cope with the problem of local minima by creating “ways of escape”: a method based on a single cost function would stop when it reaches a local minimum, unless it explores a portion of the parameters space large enough to contain a better solution: conversely, a method based on multiple cost functions uses a local minimum of one of those functions as a starting point rather than as a dead end. This procedure has proven to work well also in the study described in chapter III [Cona et al., 2009].

4.5. Limitations and future steps

Finally, it is worthwhile to point out limitations of the work presented in this chapter and lines for future investigation.

A first limitation consists in the possible existence of multiple set of parameters able to fit the same data. Although the GA exhibits an excellent capacity to discover a good solution, which can simulate all 9 signals simultaneously, it does not warrant the uniqueness of this solution. Hence, at the present stage, the connectivity pattern discovered by the algorithm represents just one possible scenario, i.e., we discovered just one possible connectivity pattern, able to explain the observed responses fairly well. Additional "a priori" information (such as anatomical and physiological knowledge, or connectivity values obtained from other tests) is required to drive the algorithm toward a unique solution, and this should represent the most important challenge for future studies.

The focus of the present study was on the response to a single TMS pulse, as a direct way to discover natural frequencies and identify model dynamics. Many recent studies, however, used repetitive TMS stimulation, to modulate cortical activity and to cause a transient frequency "entrainment" [Hamidi et al., 2009; Thut & Miniussi, 2009]. A further method to validate the model in future works, to test the possible effect of non-linearities, and generate new testable predictions may be the use of multiple TMS stimuli. A first stimulus, in fact, may lead the system into a different working point, on which a second stimulus may operate. This procedure may be the subject of further ad hoc empirical tests.

Moreover it is worth noting that while Rosanova et al. [Rosanova et al., 2009] showed that each region exhibits an endogenous, predominant rhythm with respect to the rhythms transmitted from the other regions, our model focuses on rhythm changes: as shown in our results, each region exhibits its endogenous rhythm when stimulated by TMS, but it significantly changes its frequency content when it receives the rhythms from another stimulated region.

Finally, in the present model we did not consider the crucial role played by the thalamus. Actually, the model does not include an explicit description of the thalamic nuclei nor includes connections between cortical and subcortical regions. Conversely, cortico-thalamic connections are known to play a pivotal role in generating brain oscillations [Steriade, 2006] as well as in the transmission of information among cortical regions. For instance, Van Der Werf and colleagues [Van Der Werf & Paus, 2006; Van Der Werf et al., 2006] observed that single pulses of TMS applied over the motor cortex elicit a brief beta oscillation and that the amplitude of these oscillations is strongly decreased in patients with Parkinson disease who underwent a surgical lesion of motor thalamic nuclei. The authors concluded that feedback loops between cortical and subcortical structures are involved in this process. The choice of not including subcortical (thalamic) regions in the model was motivated by a parsimony rationale: we wished to model a TMS stimulation experiment, with a reduced number of regions and of connectivity parameters. For this reason, in evaluating the fitting between model and real curves we filtered low-frequency rhythms, which are crucially dependent on the thalamus. Inclusion of an explicit description of the thalamus or of other subcortical regions may represent a possible model extension. However, this enlarged model will include additional parameters, and thus will require more data to fit all parameters in both cortical and thalamic regions altogether.

VI. BINDING AND SEGMENTATION IN MEMORY RELATED TASKS[4]

1. INTRODUCTION

The execution of complex cognitive tasks requires that the brain integrates a mosaic of scattered information, distributed across different cortical areas. A concept largely used for understanding the large-scale integration capacity of the brain is that of neural assembly; this is defined as a distributed network of neurons, whose activities participate to the realization of the same cognitive act, and which are reciprocally linked by dynamical connections [Damasio, 1990; Varela et al., 2001].

In order to understand the principles of brain functioning, much effort in modern neuroscience is devoted to explain how neural assemblies are formed, dissolved and how they exchange information reciprocally. Recent hypotheses emphasize the role of brain dynamics in the formation of neural assemblies, laying special emphasis on theta, beta and gamma rhythms [Buzsáki & Draguhn, 2004; Fries, 2009; Varela et al., 2001].

Oscillatory activity is a common property of neural populations. Data collected in past decades demonstrate that theta, beta and gamma rhythms are ubiquitous phenomena which occur throughout the neocortex in vivo [Buzsaki, 2006]; many studies suggest that these rhythms are not merely epiphenomena, resulting fortuitously from neural dynamics, but rather they play an important role in many cognitive tasks, such as in visual and auditory perception [Pulvermüller et al., 1997], associative learning [Düzel et al., 2010; Miltner et al., 1999], recognition of semantic features in words [Pulvermüller et al., 1996], face recognition [Rodriguez et al., 1999], representation of sequences [Siegel et al., 2009] and consciousness [Crick & Koch, 1990].

A popular hypothesis, named “binding by synchronization” [Singer & Gray, 1995; Singer, 1999; Varela et al., 2001], assumes that the formation of neural assemblies is realized by means of phase synchronization among neural groups oscillating in the high beta or in the gamma range. Binding by synchronization was originally proposed with reference to visual problems [Singer, 1999] but is now extended to several other higher cognitive tasks [Fries et al., 2007; Varela et al., 2001]. According to this hypothesis, neural assemblies can be formed rapidly in a highly dynamical way via synchronization of a gamma oscillation and can rapidly be disrupted under the influence of external or internal events, to make way for alternative assemblies. Furthermore, the recent observation that gamma rhythms are modulated by slower theta rhythms (4-7 Hz) suggested the idea that the construction and degradation of gamma rhythms is under the control of theta oscillations [Canolty et al., 2006; Doesburg et al., 2009; Schack et al., 2002]: according to this hypothesis, synchronization in the low-gamma frequency range allows the transient functional integration of neural populations involved in the same task or in the same perception; the theta rhythms governs the temporal aspects through which the individual gamma-oscillatory assemblies

[4] The contents of this chapter are accepted for publication in International Journal of Neural Systems.

are created or dissolved, i.e., they provide the slower temporal scaffold for the appearance of successive cognitive moments.

Within this theoretical framework, a lot of important questions are still on the table. A first problem concerns how these intrinsic rhythms are generated in the neocortex, and which mechanisms are used to synchronize oscillations among different neural groups to form assemblies. Of course, synchronization requires the existence of synaptic links among neurons involved in the same task: in case of perceptual problems these synapses may reflect basic Gestalt rules of perception organization (like proximity or smoothness), whereas in case of higher cognitive tasks (such as object recognition, semantic memory and associative learning) they may be the result of previous experience via Hebbian modifications. A problem is what kind of synapses may effectively favor a rapid synchronization of neural groups, as required by the binding hypothesis: these synapses should be the target of learning [Bartos et al., 2007; Jefferys et al., 1996]. Experimental and computational studies suggest that not only excitatory synapses from pyramidal neurons, but also synapses from interneurons (most inhibitory) are essential to achieve fast and robust synchronization [Bartos et al., 2007; Jefferys et al., 1996; Whittington & Traub, 2003]. Furthermore, electrical synapses (i.e., gap junctions) also contribute to rapid synchronization and desynchronization in networks of neurons [Traub et al., 2004].

A further essential issue, related with the binding through synchronization hypothesis, is segmentation. In many cognitive tasks the brain must deal with different neural assemblies simultaneously active (let us consider, for instance, the problem of segmentation of a visual scene, or the problem of multiple objects recognition in semantic memory, where each object is characterized by a different set of features). How can the brain assign a neural group to the correct assembly, while maintaining it separately from different neural groups which belong to other assemblies? To solve the segmentation problem, a common idea is that neural groups involved in different assemblies must desynchronize their phase, i.e. oscillate in time division. Experimental evidence exists that phase synchronization among some neural populations is accompanied by phase scattering vs. other neural groups [Varela et al., 2001].

The previous questions may represent important challenges not only for cognitive neuroscience but also for computational mathematical models. In particular, neural network models inspired by neurobiology are universally accepted nowadays as crucial tools to clarify how neural mechanisms operate in the brain, to check current hypotheses in rigorous quantitative terms and to suggest new ideas and make testable predictions [Rolls & Treves, 1998].

Several models inspired by neurobiology have been presented in the past decades to investigate the mechanisms of binding and segmentation of neural populations. Basically, these models can be subdivided into two major classes: models of individual neurons (such as those using Hodgkin-Huxley neurons or integrate-and-fire neurons) and models based on neural masses [Abbott & Nelson, 2000]. The first kind of model is essential to reach a deeper understanding of the mechanisms involved in synchronization at the cellular and subcellular level. Nevertheless, as explicitly stated in Varela et al. [Varela et al., 2001], the relevant variables to describe the dynamics of neural assemblies are not the individual neuron activities, but rather “the coordinated behavior of local neural groups through synaptic interactions”. Thus, an important insight into large-scale integration, which complements the study at the level of individual neurons, can be achieved through an analysis at the mesoscale level.

Models at a mesoscale level usually make use of state variables which represent activity of groups of neurons (or neural masses), and exhibit similar dynamics. Several works have appeared in recent years to analyze binding and segmentation with groups of oscillating neural populations linked via excitatory and inhibitory synapses. These make use of Wilson-Cowan oscillators [Campbell & Wang, 1996; von der Malsburg & Buhmann, 1992; Tagamets & Horwitz, 2000; Ursino & La Cara, 2004; Ursino et al., 2003, 2009; Wang, 1995; Wilson & Cowan, 1972], relaxation oscillators [Cesmeli & Wang, 2000; Wang & Terman, 1997], more complex spiking neurons [Knoblauch & Palm, 2002a, 2002b], or pulse-coupled oscillators [Wu & Chen, 2009] to investigate the formation of neural assemblies during different perceptual and cognitive problems. Synchronization between chaotic neural networks [Chakravarthy et al., 2008] and synchronization in small-world networks with synaptic plasticity [Han et al., 2011] have also been investigated recently.

These models, however, have several limitations: they produce waveforms, which are different from those observed through scalp EEG or via intracortical electroencephalography; do not consider the complexity of neural populations mixed up within a cortical column and their reciprocal links; and do not consider a realistic dynamics for the synapses. In particular, Wilson-Cowan and relaxation oscillators consider the feedback interaction of two populations only (one inhibitory and one excitatory) each described via a first-order non-linear differential equation, which is too simplistic to describe the neural dynamics.

A more realistic neural mass model (NMM), which simulates the population organization within a cortical column, was proposed by Jansen and Rit in the mid-nineties [Jansen & Rit, 1995], and then extended by Wendling et al. [Wendling et al., 2002]. The latter model includes four neural populations (pyramidal neurons, excitatory interneurons, inhibitory GABA-ergic interneurons with either slow or fast synaptic kinetics). These populations are reciprocally interconnected according to anatomical/physiological considerations, while the dynamics of each synapse is described via a second-order impulse response. Recently, we proposed a new version of the model as described in chapter IV, which incorporates a self-loop among fast inhibitory interneurons [Ursino et al., 2010]. Reciprocal connections among fast interneurons, in fact, have been documented in the neurophysiological literature [Kisvárday et al., 1993; Sik et al., 1995] and play a pivotal role in the generation of gamma rhythms [Moran et al., 2008]. The latter model is able to simulate realistic EEG time patterns and power spectra (with multiple peaks in the theta, alpha, beta and gamma ranges) whose shape vary depending on model parameters and on long-range connections among columns.

We are not aware that realistic models of cortical columns have been used so far to analyze the binding through segmentation hypothesis and to study the formation of neural assemblies. We deem that such an analysis can provide valuable new insights into the problem. In particular, such models may help to fill the gap between EEG/MEG measurements, detection of cortical rhythms, and their functional role in higher cognitive tasks.

The aim of this work is to simulate the formation of neural assemblies according to the binding and segmentation hypothesis using the cortical column model described in Ursino et al. [Ursino et al., 2010]. The simulations reproduce an associative learning task (i.e., a task in which elements of the assembly are learned from past experience using an Hebbian paradigm and then recovered from partial information). The following questions are investigated with the model: how can oscillatory activity in different bands (especially theta and low-gamma) be generated with the model? Which mechanisms are able to warrant rapid synchronization and desynchronization

among cortical columns and what kind of neural populations and synapses may be especially involved? How can these assemblies be learned from past experience to realize an autoassociative network? What is the role of different synaptic kinetics (for instance fast AMPA receptors)?

2. METHOD

The model is a neural network which consists of two layers. The two layers have the same structure: they are composed of N×M units, each described as a single cortical column. Layer 1 (L_1) receives inputs from the external environment and sends outputs to layer 2 (L_2). The network can learn patterns of features: each feature corresponds to a position ij (i=1,…,N; j=1,…,M) and is therefore associated to two columns, one in L_1 and one in L_2. Before learning, columns in each layer oscillate in the alpha range, if stimulated by white noise or by a constant external input. After learning, L_1 realizes an autoassociative network in the theta range, restoring previously memorized objects from lacking information. L_2 segments these objects in the gamma band, exploiting fast inhibitory interneurons. An overall activity in the theta + gamma band then originates from the interaction of the two layers.

In the following, an overview of the general model structure, and of the main hypotheses, is first presented. Then equations of a single cortical column (i.e., a single column in the model) are described. Later, the two layer model is built from these equations and learning mechanisms are put forward.

2.1. General aspects of the model

The network is based on the following general ideas:

1. L_1 receives the inputs and sends them to L_2. Columns in the same position in L_1 and L_2 communicate via one-by-one connections. Each column is described by means of a NMM of a single cortical column, developed recently [Ursino et al., 2010]. Parameters are given so that, if stimulated with white noise, columns in L_1 and L_2 oscillate in the low alpha range.
2. The overall output of the model is calculated as the firing rate of pyramidal neurons in L_2. A pattern (or a neural assembly) is represented by a set of columns which are firing in synchronism, but are out of phase (desynchronized) with respect to other columns in different patterns. An EEG signal is computed as the sum of post-synaptic membrane potentials of all pyramidal populations in L_2.
3. L_1 works as an autoassociative network, where previous experience is stored in the lateral excitatory synapses among columns (from pyramidal to pyramidal). Thanks to these synapses, a pattern can be restored in L_1 even in the presence of incomplete information.
4. A slower theta rhythm originates from the excitatory synapses within L_1, causing periods in which the networks are silent, alternated with periods of strong excitation.
5. Synapses in L_2 realize synchronization in the beta/gamma range. As suggested in previous work using Wilson-Cowan oscillators [Ursino et al., 2003], or spiking neurons [Bartos et al., 2002], in order to warrant good synchronization these synapses are directed toward inhibitory populations within the same pattern.
6. In order to segment different patterns simultaneously, L_2 must include a desynchronization mechanism. This is realized assuming that columns within a pattern send fast excitation to GABA-ergic populations in other patterns. Since this mechanism must be very rapid, we consider the possibility that this is realized via AMPA receptors with excitatory neurotransmission of the order of ms or less.
7. All synapses in the autoassociative network (both realizing restoration of incomplete information in L_1, and synchronization and desynchronization in L_2) are learned via

Hebbian (or anti-Hebbian) mechanisms, during a training phase in which complete patterns are individually presented to L_1.

2.2. Model of a single cortical column

The model of a single cortical column consists of four neural populations (Figure VI.1), which represent pyramidal neurons (subscript p), excitatory interneurons (subscript e), and inhibitory interneurons with slow and fast synaptic kinetics ($GABA_{A,slow}$ and $GABA_{A,fast}$, subscripts s and f,

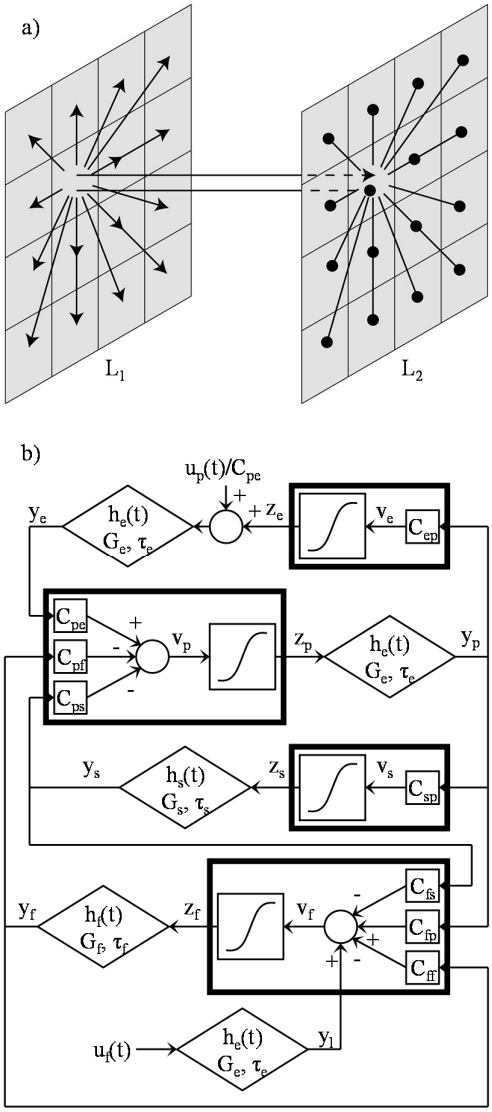

Figure VI.1: Network layout. Panel a shows the architecture of the two layers: arrows indicate connections toward pyramidal cells, while circles indicate connections toward $GABA_{A,fast}$ interneurons. Panel b shows the architecture of every column: boxes with bold contour represent (in descending order) excitatory interneurons, pyramidal cells, $GABA_{A,slow}$ and $GABA_{A,fast}$ interneurons.

respectively). All populations are described with a similar mathematical formalism. Briefly, each population receives an average postsynaptic membrane potential (v, in Eqs. VI.3, VI.7, VI.11 and VI.15) from other neural populations, and converts this membrane potential into an average

density of spikes fired by the neurons (z, in Eqs. VI.4, VI.8, VI.12 and VI.16). In order to account for the presence of inhibition (when potential is below a given threshold) and saturation (when potential is high) this conversion is simulated with a static sigmoidal relationship.

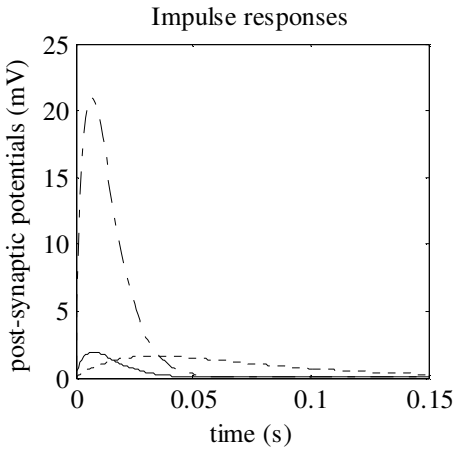

Figure VI.2: Impulse responses of the three kinds of synapses. The solid line indicates $h_e(t)$, the dotted line indicates $h_s(t)$, while the dotted/dashed line indicates $h_f(t)$.

To model a whole cortical column, the four populations are connected via excitatory and inhibitory synapses, with impulse response $h_e(t)$, $h_s(t)$ or $h_f(t)$, (Figure VI.2) assuming that synapses from pyramidal neurons and excitatory interneurons have similar dynamics. The kinetics of each synapse are described with a second order system, but with different parameter values. By denoting with z the input to a synapse, and with y the synapse output, its dynamics can be described through the following second order differential equation

$$\frac{d^2y(t)}{dt^2} = \frac{G}{\tau}z(t) - \frac{2}{\tau}\frac{dy(t)}{dt} - \frac{y(t)}{\tau^2} \qquad \text{VI.1}$$

where the G and τ have different values depending on the type of synaptic block (excitatory, slow inhibitory or fast inhibitory). It is worth noting that Eq. VI.1 corresponds to the following impulse response

$$h(t) = \frac{G}{\tau}t \cdot e^{-\frac{t}{\tau}} \qquad \text{VI.2}$$

In the following, Eq. VI.1 will be implemented with two first order differential equations (in Eqs. VI.5, VI.6, VI.9, VI.10, VI.13, VI.14, VI.17, VI.18, VI.19, VI.20). Differently from previous chapters (III, IV and V), here I use τ instead of $1/\omega$, even if they have exactly the same meaning, just because it is more convenient to refer to the time constants in this context.

The average numbers of synaptic contacts among neural populations are represented by eight parameters, C_{ij} (Figure VI.1), where the first subscript represents the target (post-synaptic) population and the second subscript refers to the pre-synaptic population. These connections agree with those proposed by Wendling et al. [Wendling et al., 2002] but with the addition of the new self-loop C_{ff}. As demonstrated in chapter IV this new loop ensures the occurrence of a strong gamma-rhythm which may coexist with other slower rhythms within the same column. The existence of significant synaptic contacts among fast inhibitory interneurons is well documented

in the literature [Kisvárday et al., 1993; Sik et al., 1995], and their role in the genesis of gamma rhythms has been demonstrated both via computational models [Ursino et al., 2010] and experimental studies [White et al., 2000].

Table VI.1: Description of parameters and variables of the model of a cortical column

Symbol	Description		Subscripts/Superscripts
$h_i(t)$	Impulse response of synapse of type i	i =	e for excitatory
G_i	Gain of synapse of type i		s for $GABA_{A,slow}$ inhibitory
τ_i	Time constant of synapse of type i		f for $GABA_{A,fast}$ inhibitory
v_i	Membrane potential of neural population i	i, j =	p for pyramidal cells
z_i	Spiking rate of neural population i		e for excitatory interneurons
x_i, y_i	State variables of neural population i		s for $GABA_{A,slow}$ interneurons
u_i	External input to neural population i		f for $GABA_{A,fast}$ interneurons
C_{ij}	Number of synaptic contacts from neural population j to population i		l for state variables of the external input to $GABA_{A,fast}$ interneurons
e_0	Maximum neural activation rate		
r	Steepness of neural activation rate	-	
s_0	Average activation threshold		

Cortical columns can receive inputs from other columns in the model or from external sources. Anatomical and neurophysiological considerations suggest that all populations can receive inputs, whereas only pyramidal neurons can send outputs toward other columns. In the work described in chapter IV [Ursino et al., 2010], we performed a sensitivity analysis on the role of these connections for rhythm propagation (i.e., how much a given connection is able to transmit rhythms) and found that the most influential connections are "from pyramidal to pyramidal" and "from pyramidal to fast inhibitory". The other two connections play a less important role. For this reason, in this work we decided to neglect the other two connection types and assumed that external inputs (coming from other columns) reach only pyramidal and fast-inhibitory populations.

The model of a column is displayed in Figure VI.1. The equations of a single column (both in L_1 or L_2) are written below, while the meaning of all symbols is reported in Table VI.1:

Pyramidal neurons

$$v_p(t) = C_{pe}y_e(t) - C_{ps}y_s(t) - C_{pf}y_f(t) + E(t) \quad \text{VI.3}$$

$$z_p(t) = \frac{2e_0}{1 + e^{r(s_0 - v_p)}} \quad \text{VI.4}$$

$$\frac{dy_p(t)}{dt} = x_p(t) \quad \text{VI.5}$$

$$\frac{dx_p(t)}{dt} = \frac{G_e}{\tau_e}z_p(t) - \frac{2}{\tau_e}x_p(t) - \frac{1}{\tau_e^2}y_p(t) \quad \text{VI.6}$$

Excitatory interneurons

$$v_e(t) = C_{ep}y_p(t) \quad \text{VI.7}$$

$$z_e(t) = \frac{2e_0}{1 + e^{r(s_0 - v_e)}} \quad \text{VI.8}$$

$$\frac{dy_e(t)}{dt} = x_e(t) \quad \text{VI.9}$$

$$\frac{dx_e(t)}{dt} = \frac{G_e}{\tau_e}\left(z_e(t) + \frac{u_p(t)}{C_{pe}}\right) - \frac{2}{\tau_e}x_e(t) - \frac{1}{\tau_e^2}y_e(t) \quad \text{VI.10}$$

Slow inhibitory interneurons

$$v_s(t) = C_{sp}y_s(t) \quad \text{VI.11}$$

$$z_s(t) = \frac{2e_0}{1 + e^{r(s_0 - v_s)}} \quad \text{VI.12}$$

$$\frac{dy_s(t)}{dt} = x_s(t) \quad \text{VI.13}$$

$$\frac{dx_s(t)}{dt} = \frac{G_s}{\tau_s}z_s(t) - \frac{2}{\tau_s}x_s(t) - \frac{1}{\tau_s^2}y_s(t) \quad \text{VI.14}$$

Fast inhibitory interneurons

$$v_f(t) = C_{fp}y_p(t) - C_{fs}y_s(t) - C_{ff}y_f(t) + y_l(t) + I(t) \quad \text{VI.15}$$

$$z_f(t) = \frac{2e_0}{1 + e^{r(s_0 - v_f)}} \quad \text{VI.16}$$

$$\frac{dy_f(t)}{dt} = x_f(t) \quad \text{VI.17}$$

$$\frac{dx_f(t)}{dt} = \frac{G_f}{\tau_f}z_f(t) - \frac{2}{\tau_f}x_f(t) - \frac{1}{\tau_f^2}y_f(t) \quad \text{VI.18}$$

Finally, two additional equations are needed to describe the external input to fast inhibitory interneurons, as commented below:

$$\frac{dy_l(t)}{dt} = x_l(t) \quad \text{VI.19}$$

$$\frac{dx_l(t)}{dt} = \frac{G_e}{\tau_e}u_f(t) - \frac{2}{\tau_e}x_l(t) - \frac{1}{\tau_e^2}y_l(t) \quad \text{VI.20}$$

The inputs to the model, $u_p(t)$ and $u_f(t)$ (in Eqs. VI.10 and VI.20) represent all exogenous contributions coming from external sources (i.e., input patterns from the environment) in terms of spikes per second; in particular, $u_p(t)$ is the input to pyramidal cells and $u_f(t)$ the input to $GABA_{A,fast}$ interneurons, respectively. These quantities are modeled as Gaussian white noise with mean value m_p, m_f and variance σ_p^2, σ_f^2 [Ursino et al., 2010]. The quantities E(t) and I(t) represent the excitation and inhibition coming from the other columns in the model. These terms will be described below. Eqs. VI.3, VI.7, VI.11 and VI.15 can be commented as follows: excitatory interneurons (Eq. VI.7) and slow inhibitory interneurons (Eq. VI.11) receive only an excitatory input from pyramidal neurons. Pyramidal neurons (Eq. VI.3) receive excitation from excitatory

interneurons, inhibition from both slow and fast inhibitory interneurons, and further external excitatory inputs. Fast interneurons (Eq. VI.15) receive excitation from pyramidal neurons, inhibition from themselves and from slow inhibitory interneurons, and further external excitatory inputs.

Eqs. VI.10, VI.19 and VI.20, which describe the effect of external noise, require a further comment. The external noise must affect the target neurons with the dynamics of excitatory synapses, since long-range connection in the brain are glutamatergic. As a consequence, noise must be filtered via the impulse response of excitatory synapses. For what concerns the noise to pyramidal neurons (i.e., u_p), this is realized by exploiting the same impulse response from excitatory interneurons to pyramidal neurons (i.e., Eqs. VI.9 and VI.10) to reduce the number of differential equations. Conversely, two additional differential equations have been introduced, (Eqs. VI.19 and VI.20), to describe the effect of noise (i.e., u_f). on fast inhibitory interneurons.

2.3. Model of two interconnected layers

L_1 represents is stimulated by external inputs ($u_p(t)$ and $u_f(t)$ as described above). The inputs excite a group of columns in L_1, thus generating a pattern of activity; the excitation is then sent to L_2, by means of a feed-forward connectivity.

In the following, we will use the subscripts ij to denote a quantity belonging to a column at position ij in a given layer, and the superscripts L1 or L2 to denote the individual layer. Hence, by way of example, the symbol $v^{L1}_{p,ij}$ denotes the membrane potential of a pyramidal population at position ij in L_1; $z^{L2}_{p,hk}$ denotes the average spike density of the pyramidal population at position hk in L_2.

The connectivity between L_1 and L_2 is one by one: this means that each column ij in L_1 is connected only with the corresponding ij column in L_2. With this organization, when a group of columns in L_1 is stimulated by an external input, it becomes active, and its excitation is sent to the corresponding columns in L_2. Moreover, columns within a layer may also be reciprocally interconnected; these connections are created on the basis of past experience.

We assumed that long-range connections (i.e., connections directed outside the cortical column) originate only from pyramidal neurons. Three groups of synapses are considered: Hebbian excitatory synapses from pyramidal to pyramidal (symbol W); Hebbian excitatory synapses from pyramidal to fast-inhibitory interneurons (symbol K); anti-Hebbian fast synapses (possibly mediated by AMPA receptors only) from pyramidal to fast inhibitory interneurons (symbol A). For each synapse, the following notation is used: the first superscript denotes the post-synaptic layer, and the second superscript the pre-synaptic layer. Moreover, the first two subscripts denote the position of the postsynaptic column, the last two subscripts denote the position of the presynaptic column. By way of example, the symbol $W^{L1\ L1}_{ij\ hk}$ denotes an excitatory pyramidal to pyramidal synapse linking the presynaptic column at position hk to the post-synaptic column at position ij, both in layer L_1.

In the following, connections to L_1 and L_2 will be separately described.

2.3.1. Layer 1

As specified above, the pyramidal population in L_1 receives the connectivity from other pyramidal populations in the same layer. Hence, the synaptic terms E_{ij} (Eq. VI.3) to a column at position ij in layer L_1 can be written as follows

$$E_{ij}^{L1}(t) = \sum_h \sum_k W_{ij,hk}^{L1L1} \cdot y_{p,hk}^{L1}(t) \qquad \text{VI.21}$$

where the sums are extended to all neurons hk in L_1.

Conversely, inhibitory interneurons in L1 do not receive connections, hence the term I(t) in Eq. VI.15 is

$$I_{ij}^{L1}(t) = 0 \qquad \text{VI.22}$$

It is worth noting that, in Eq. VI.21 we used quantities $y^{L1}{}_{p,hk}$ which represents the post-synaptic membrane potential induced by a pyramidal population at position hk in L_1 (Eqs. VI.5 and VI.6). This quantity originates from the spikes of the pyramidal population ($z^{L1}{}_{p,ij}$) passed through the second-order dynamics of a glutamatergic synapse.

2.3.2. Layer 2

The pyramidal populations in L_2 receive synapses from the pyramidal populations in L_1 at the same positions. Moreover, fast inhibitory interneurons in L_2 receive plastic synapses (learned via Hebbian mechanisms) from pyramidal neurons in the same layer. Furthermore, a third group of synapses, targeting fast-inhibitory interneurons, is necessary to desynchronize patterns.

Consequently, terms E_{ij} and I_{ij} (Eqs. VI.3 and VI.15) to a column at position ij in L_2 assume the following expressions

$$E_{ij}^{L2}(t) = W_{ij,ij}^{L2L1} \cdot y_{p,ij}^{L1}(t) \qquad \text{VI.23}$$

$$I_{ij}^{L2}(t) = K_{ij,ij}^{L2L1} \cdot y_{p,ij}^{L1} + \sum_h \sum_k K_{ij,hk}^{L2L2} \cdot y_{p,hk}^{L2}(t) + D_{ij}^{L2}(t) \qquad \text{VI.24}$$

where Eq. VI.23 and the first term in the right-hand member of Eq. VI.24 describe connections from L_1 to L_2. The second term in the right-hand member of Eq. VI.24 represents connections among columns at different positions within L_2 (where ij is the post-synaptic column and hk the pre-synaptic one) and the sums are extended to all neurons hk in L_2. Finally, the last term in the right-hand member of Eq. VI.24 represents a "desynchronization" term, necessary to segment different patterns simultaneously present in memory. This will be described in sub-sub-section 2.3.3. .

It is worth noting that $W^{L1}{}_{ij}{}^{L1}{}_{hk}$ and $K^{L2}{}_{ij}{}^{L2}{}_{hk}$ (i.e., synapses within a layer) are autoassociative matrices, which, after training, will contain information on stored patterns.

2.3.3. Desynchronization

As it will be shown in section 3. , the previous equations allow synchronization of columns belonging to the same pattern, by using learned expressions for the autoassociative arrays (i.e., a correct choice of the autoassociative arrays allows the solution of the "binding problem").

However, a fundamental advantage of gamma-band oscillations is the possibility to maintain different patterns simultaneously active ("segmentation problem") by using a temporal coding division [Canolty et al., 2006; von der Malsburg & Buhmann, 1992; Singer, 1999]. To this end, an additional inhibitory mechanism must be included in L_2, in order to avoid that two patterns are simultaneously active. Previous models which tried to segment multiple objects using gamma-band oscillators [Campbell & Wang, 1996; Ursino et al., 2003; Wang, 1995] used a sort of

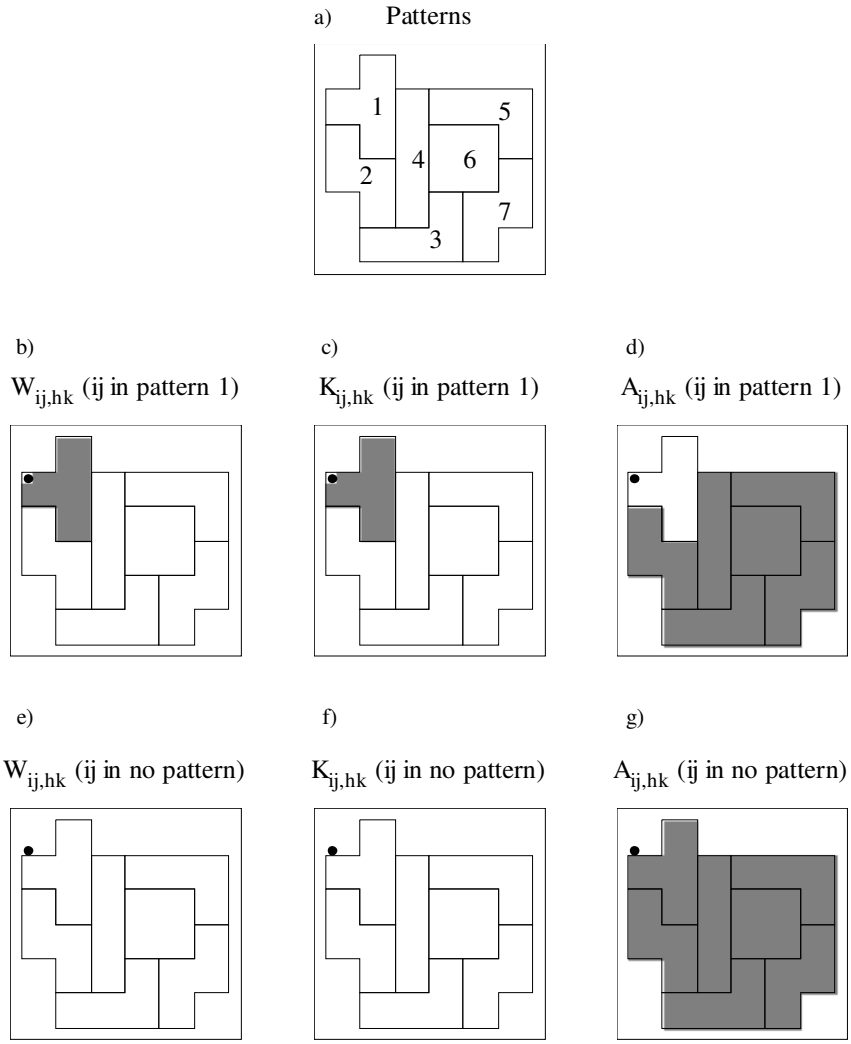

Figure VI.3: Patterns and connectivity in the two layers. Panel a shows the 7 patterns. In panels b to g, columns that send synapses of a specific type (indicated by the corresponding title) to the column marked with a dot, are colored in gray. All connections are within one layer, L_1 in panels b and e, L_2 in panels c, d, f and g.

"global inhibition" (not present in traditional autoassociative nets): as soon as a pattern of oscillators becomes active it momentarily inhibits all alternative patterns, to avoid that different patterns simultaneously pop out.

In the present work, this further inhibition is realized assuming that pyramidal populations which code for a given object can inhibit all columns in L_2 coding for different objects. Simulations (see section 3.) show that, in order to realize a correct desynchronization of different objects (i.e., to solve the segmentation problem) this inhibition must be very fast. Hence, we assumed that it

occurs via very fast AMPA receptors. Indeed, some authors observed that fast AMPA receptors especially reside on inhibitory GABA-ergic interneurons [Itazawa et al., 1997; Yin et al., 1999]. Since the rise time of these excitatory post-synaptic currents can be as small as 0.2-0.3 ms [Geiger et al., 1997; Kleppe & Robinson, 1999; Zhou & Hablitz, 1998] (i.e., of the same order of magnitude as the integration step used in these simulations, 0.1 ms), they are considered as instantaneous compared with the dynamics of the other synapses in the model. We have:

$$D_{ij}^{L2}(t) = \sum_{h}\sum_{k} A_{ij,hk}^{L2L2} \cdot z_{p,hk}^{L2}(t) \qquad \text{VI.25}$$

where Eq. VI.25 provides the desynchronization input to be used in Eq. VI.24. Parameters $A^{L2}{}_{ij}{}^{L2}{}_{hk}$ represent the strength of the synapse from the pre-synaptic column hk to the post-synaptic column ij in L_2. Accordingly, Eq. VI.25 computes the sum of the global inhibition which reaches column ij in L_2, as a consequence of activity in other objects which are in memory.

It is worth noting that the effect of a fast AMPA receptor is simulated using the spiking activity of pyramidal neurons, $z_p{}^{L2}{}_{hk}$, directly in Eq. VI.25, instead of using their post-synaptic potential, $y_p{}^{L2}{}_{hk}$. Hence, this activity acts instantaneously on the post-synaptic membrane potential.

2.4. Training the network

Training has been performed by providing individual patterns to L_1 (one pattern at a time) described as a subset of active columns. At the beginning of training, the synapses within L_1 and L_2 are set at zero; then, Hebbian and anti-Hebbian learning rules are used to train them. The input patterns used for the training are simulated by stimulating a group of columns in L_1 with Gaussian white noise with mean value m and variance σ ($m_p = 600$, $m_f = 0$, $\sigma_p{}^2 = \sigma_f{}^2 = 5$) whereas all the other columns in L_1 as well as columns in L_2 are stimulated with a zero mean Gaussian noise ($m_p = m_f = 0$, $\sigma_p{}^2 = \sigma_f{}^2 = 5$). Seven different patterns have been used, as illustrated in Figure VI.3. After training, the network is able to restore a pattern, even starting from a partial information, and to segment it from other objects simultaneously given as inputs.

It is worth noting that, in this work, we used connected patterns only. This choice has been done just to facilitate the visualization of results; however, since there is no spatial rule in our model (i.e., columns are connected only on the basis of past experience, independently of their position), objects can be composed of disconnected parts equally well, without any prejudice on model results.

Different training rules are used for slower connections directed to pyramidal neurons (W) and GABA-fast neurons (K) and for faster AMPA connections (A).

2.4.1. Training the excitatory connections to pyramidal populations within layer 1

Training is performed on the basis of a simple time-dependent Hebbian rule based on the activity of the pre-synaptic and post-synaptic columns. Recent experimental data suggest that synaptic potentiation occurs if the pre-synaptic inputs precede post-synaptic activity by 20 ms or less [Abbott & Nelson, 2000; Markram et al., 1997]. Hence, in our learning phase we assumed that the Hebbian rule depends on the present value of post-synaptic activity, $z_p{}^{L1}{}_{ij}(t)$ (where ij is the position of the post-synaptic column), and on the moving average of the pre-synaptic activity ($m_p{}^{L1}{}_{hk}(t)$, position hk) computed during the previous 20 ms. We define a moving average signal, reflecting the average activity during the previous 20 ms, as follows

$$m_{p,hk}^{L1}(t) = \frac{\sum_{l=0}^{Ns-1} z_{p,hk}^{L1}(t - l \cdot Ts)}{Ns} \qquad \text{VI.26}$$

where Ts is the sampling time (in milliseconds), and Ns is the number of samples contained within 20 ms (i.e., Ns = 20/Ts). The synapses linking two columns (ij and hk) are then modified as follows during the learning phase (it is worth noting that we do not consider self-connections, thus the following rules are used with $ij \neq hk$)

$$W_{ij,hk}^{L1L1}(t + Ts) = W_{ij,hk}^{L1L1}(t) + \gamma_W \cdot \left[z_{p,ij}^{L1}(t) - \vartheta_L\right]^+ \cdot \left[m_{p,hk}^{L1}(t) - \vartheta_L\right]^+ \cdot \left(W_{max} - W_{ij,hk}^{L1L1}(t)\right), ij \neq hk \qquad \text{VI.27}$$

where γ_W is a learning rate, and the symbol $[]^+$ denotes the positive part. Eq. VI.27 signifies that both the instantaneous activity of the post-synaptic column, and the moving average activity of the pre-synaptic column are compared with a lower threshold, ϑ_L, and the synapse is reinforced only when both columns overcome this threshold. Moreover, we assume that synapses cannot increase above a given saturation level, W_{max}; hence the learning rate is progressively reduced to zero when the synapse approaches this value.

2.4.2. Training the glutamatergic connections to fast inhibitory interneurons within layer 2

The glutamatergic connections to $GABA_{A,fast}$ inhibitory connections are trained with a rule very similar to Eq. VI.27: the only difference is that the post-synaptic activity of fast-GABA-ergic columns is used in the Hebb rule. Hence, we have

$$K_{ij,hk}^{L2L2}(t + Ts) = K_{ij,hk}^{L2L2}(t) + \gamma_K \cdot \left[z_{f,ij}^{L2}(t) - \vartheta_L\right]^+ \cdot \left[m_{p,hk}^{L2}(t) - \vartheta_L\right]^+ \cdot \left(K_{max} - K_{ij,hk}^{L2L2}(t)\right), ij \neq hk \qquad \text{VI.28}$$

where a different learning rate, γ_K, is used. In this case too, the learning rate is reduced to zero when the individual synapse reaches a saturation level, K_{max}.

2.4.3. Training fast AMPA synapses within layer 2

Fast AMPA synapses were trained thinking that columns active in one pattern must inhibit all columns in different patterns. Since, during the training phase, patterns have been presented individually, we used an anti-Hebbian rule: the synapse reinforces if activity of the pre-synaptic column is above ϑ_L, while activity in the post-synaptic column is below an upper threshold, ϑ_U. However, in order to avoid that a column inhibits another column in the same pattern, we used a moving average not only for the pre-synaptic activity but also for the post-synaptic one. We have

$$A_{ij,hk}^{L2L2}(t + Ts) = A_{ij,hk}^{L2L2}(t) + \gamma_A \cdot \left[\vartheta_U - m_{f,ij}^{L2}(t)\right]^+ \cdot \left[m_{p,hk}^{L2}(t) - \vartheta_L\right]^+ \cdot \left(A_{max} - A_{ij,hk}^{L2L2}(t)\right), ij \neq hk \qquad \text{VI.29}$$

where a moving average activity for $GABA_{A,fast}$ populations, $m_f^{L2}{}_{ij}$, is computed with an equation analogous to Eq. VI.26. Finally, these synapses saturate to a maximum level, A_{max}.

2.4.4. Parameters' assignment

All the parameters have been assigned values within physiological ranges as stated by literature on NMMs [Jansen & Rit, 1995; Wendling et al., 2002]. τ_e, τ_s, τ_f, have been set to fit rise and decay times of impulse responses experimentally observed [Wu et al., 2004]. The values used for G_e, G_s, G_f are the same used in works described in previous chapter [Cona et al., 2011; Ursino et al., 2010]. The intrinsic connectivity (C_{ij}) has been tuned to make the columns oscillate in specific

Table VI.2: Parameter' values and units

Parameter		Value
τ_e	(ms)	7.7
τ_s	(ms)	34
τ_f	(ms)	6.8
G_e	(mV)	5.17
G_s	(mV)	4.45
G_f	(mV)	57.1
C_{ep}		31.7
C_{pe}		17.3
C_{sp}		51.9
C_{ps}		100
C_{fp}		66.9
C_{fs}		100
C_{pf}		12.3
C_{ff}		18
e_0	(Hz)	2.5
r	(mV^{-1})	0.7
s_0	(mV)	10
N, M		20
m_p	(s^{-1})	See text
m_f	(s^{-1})	0
σ_p^2	(s^{-2})	5
σ_f^2	(s^{-2})	5
γ_W	(s)	0.005
γ_K	(s)	0.1
γ_A	(s)	0.1
ϑ_L	(s^{-1})	0.6
ϑ_U	(s^{-1})	0.3
$W^{L2L1}{}_{ij}$		196
$K^{L2L1}{}_{ij}$		186
W_{max}		10
K_{max}		20.8
A_{max}		6

frequency ranges depending on which neural loop prevails over the other ones due to the lateral connections. In particular, before training the columns oscillate in the alpha range and all the populations work in the linear region of their sigmoidal functions. After training, the columns oscillate in the theta range when the pyramidal-$GABA_{A,slow}$ loop prevails (L_1) and in the gamma range when the pyramidal-$GABA_{A,fast}$ loop prevails (L_2). The input noise (m_p) has been given a value sufficient to excite the columns in L_1. For what concerns the extrinsic connectivity, W_{max} has been tuned to warrant the recovery of missing information in L_1, K_{max} has been tuned to warrant good gamma synchronization in L_2, and A_{max} has been tuned to warrant desynchronization among different patterns in L_2. The parameters γ_W, γ_K, γ_A, ϑ_L, ϑ_U have been

assigned values so that, during training, the extrinsic connections reach their saturation values in less than 2 s. Actually the γ parameters can be seen as the ratio between the integration step and the time constant of the first order dynamics used to train the synapses, so those parameter have values that are consistent with synapse's plasticity dynamics.

2.4.5. Examples of trained synapses

Figure VI.3 shows exempla of synapses obtained after training the network with the Hebbian and anti-Hebbian rules described above, using seven patterns. In particular, each panel represents the array of synapses entering a given column in L_1 (pyramidal-pyramidal, array W) and entering a given column in L_2 (pyramidal-fast inhibitory, arrays K and A) from other columns in the same layer. The upper panels consider a target column which belongs to pattern 1, hence receives excitatory (in L_1) and inhibitory (in L_2) synchronization synapses from other columns in the same pattern, and receives desynchronization synapses (in L_2) from columns located in the other six patterns. Conversely, the bottom panels consider a column which do not belong to either object, hence it receives negligible synchronization synapses from all other columns, and desynchronization synapses (in L_2) from columns belonging to all seven objects. A complete list of model parameters and their values is given in Table VI.2.

3. RESULTS

This section presents the performance of the network under different conditions. First, model behavior is presented before training, i.e., when all columns exhibit their intrinsic rhythm and do not receive lateral synapses from other columns in the same layer. Results of a sensitivity analysis on the main parameters are also discussed. Then, network behavior is shown after training, first in the absence of any desynchronization mechanism, then assuming trained desynchronization synapses targeting fast inhibitory interneurons. Finally, the problem of robustness (influence of noise and recovery of lacking information) and segmentation capacity (number of objects simultaneously segmented in L_2) is analyzed.

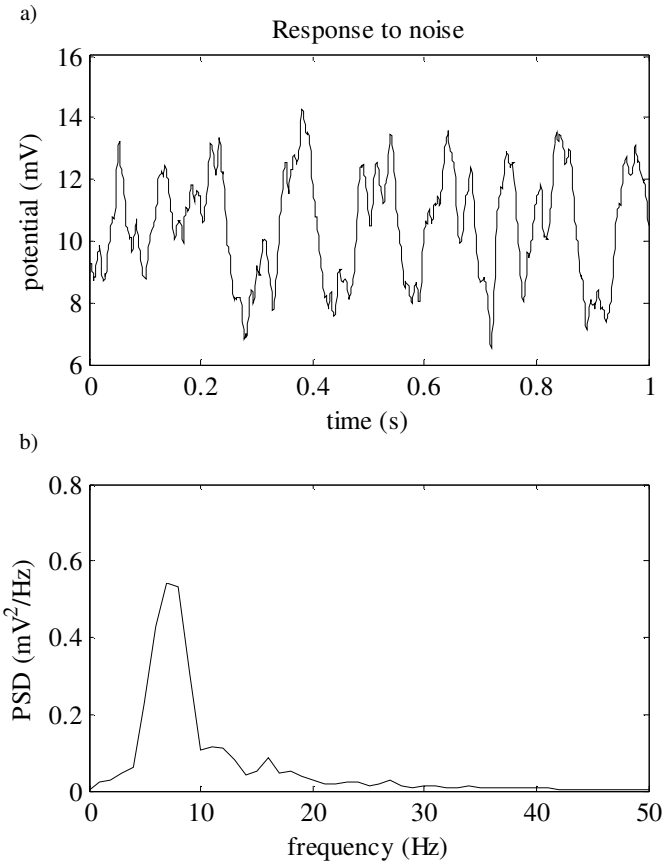

Figure VI.4: Output of a single cortical column when it is fed with non-zero mean white noise. Panel a shows the temporal course. Panel b shows the Power spectral density.

3.1. Simulation before training

The response of a typical column in L_1, stimulated with white noise (m_p=800, m_f=0, σ_p^2=10, σ_f^2=5) before training is presented in Figure VI.4. As can be observed, with the assigned parameter values, the column exhibits a significant rhythm in the lower alpha range (about 7-8 Hz), which is typical of a relaxed state, and some smaller activity also in the beta-gamma range (20-30 Hz). This behavior is quite robust, and can be observed even if the characteristic of noise are changed within a large range (the main oscillatory activity is in the 5-12 Hz range for almost

any combination of $0<m_p<1000$ and $0<\sigma_p^2<2500$). Moreover, a similar behavior occurs in L_2, whose columns receive excitation from columns in L_1.

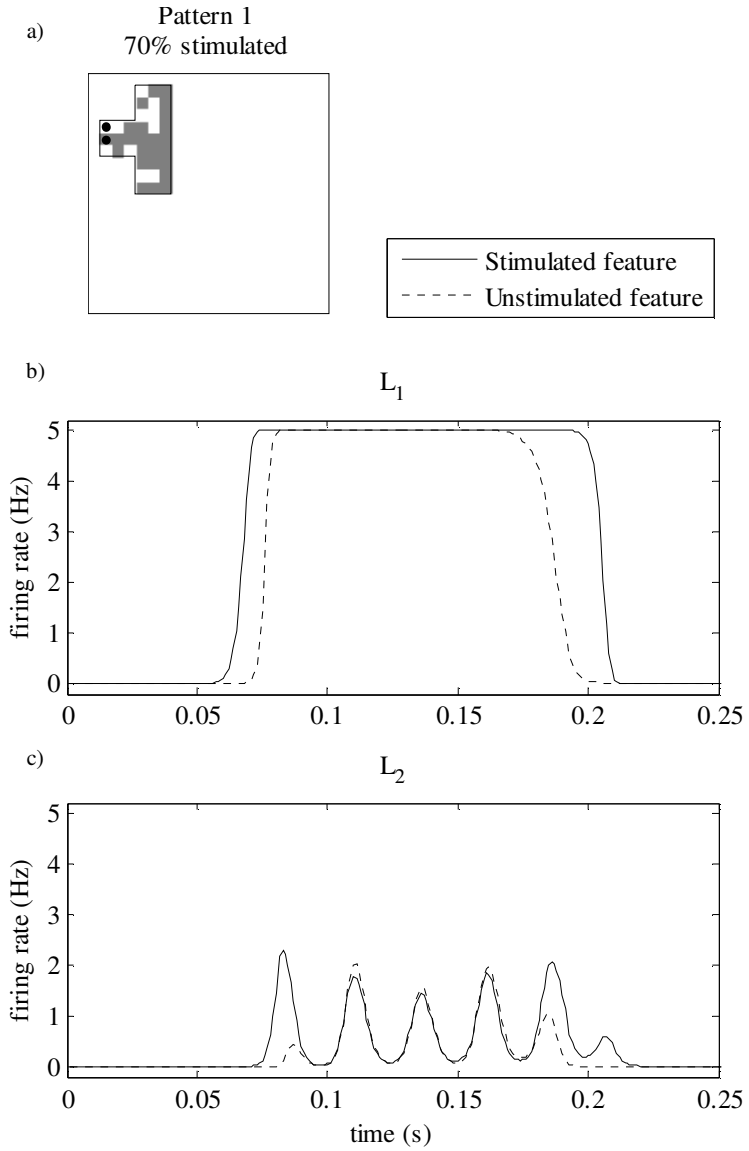

Figure VI.5: Reconstruction of a pattern. Panel a shows which features are stimulated (gray pixels). Panels b and c show the firing rates of two columns (marked in panel a with dots) in L_1 and of the corresponding columns in L_2; the solid lines represent the activities of the columns corresponding to the stimulated feature, while the dotted lines represent the activities of the columns corresponding to the unstimulated feature.

3.2. Simulation with a single partial pattern as input

Then, network behavior was simulated after training using a single pattern as input. In this condition, the role of the desynchronization mechanism is irrelevant. In particular, Figure VI.5 considers a case in which 70% of columns of pattern 1 in L_1 are stimulated by a non-zero mean external input ($m_p=600$, $m_f=0$, $\sigma_p^2=\sigma_f^2=5$) whereas the other columns in L_1 as well as columns in L_2 are stimulated with zero-mean external input ($m_p=m_f=0$, $\sigma_p^2=\sigma_f^2=5$). Results show that the

entire pattern is first recovered in L_1 (also the unstimulated 30%, see dashed line in the mid panel) and the overall object oscillates in the theta range. Moreover, all columns oscillate synchronously in L_2, with a frequency in the gamma band (bottom panel). It is worth noting that the theta rhythm

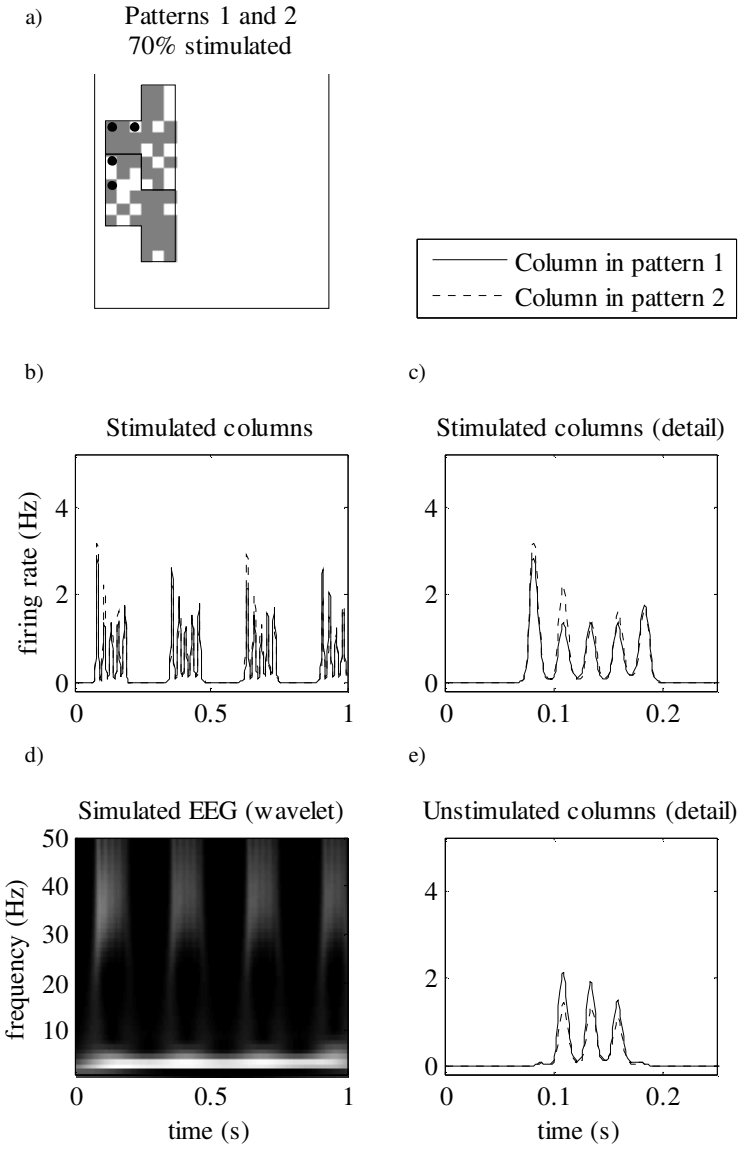

Figure VI.6: Reconstruction of two patterns without the desynchronization mechanism. Panel a shows the stimulated features (as in Figure VI.5). The other panels show the activity of 4 columns in L_2. Panel b shows the firing rate of two columns (one in pattern 1 and one in pattern 2) whose features are directly stimulated by the external input. Panel c shows a zoom of panel b, while panel d shows a wavelet map of the simulated EEG. Panel e shows the firing rate of two columns (one in pattern 1 and one in pattern 2) that are recovered by lateral synapses. The solid lines represent columns in pattern 1, the dotted lines represent columns in pattern 2.

originates from the excitatory connections in L_1, which lead pyramidal populations to saturation, followed by a slower inhibition induced by slow inhibitory interneurons. Conversely, the gamma rhythm in L_2 is caused by connection to fast inhibitory interneurons which, as shown in chapter IV, amplify the response in the gamma range.

3.3. Simulation with two partial patterns as input, without desynchronization mechanism

Figure VI.6 shows the behavior of four columns, when the network receives two partial patterns as input (each pattern is stimulated as in the previous simulation), but without any desynchronization mechanism. As in Figure VI.5, the average spike densities of the unstimulated columns become rapidly synchronized with the activity of columns stimulated by external inputs. Both patterns are well restored, however they are not segmented (i.e., they appear simultaneously). These results emphasize the need for a desynchronization mechanism to handle more than a single pattern at the same time. The time-frequency content shows that the EEG of L_2

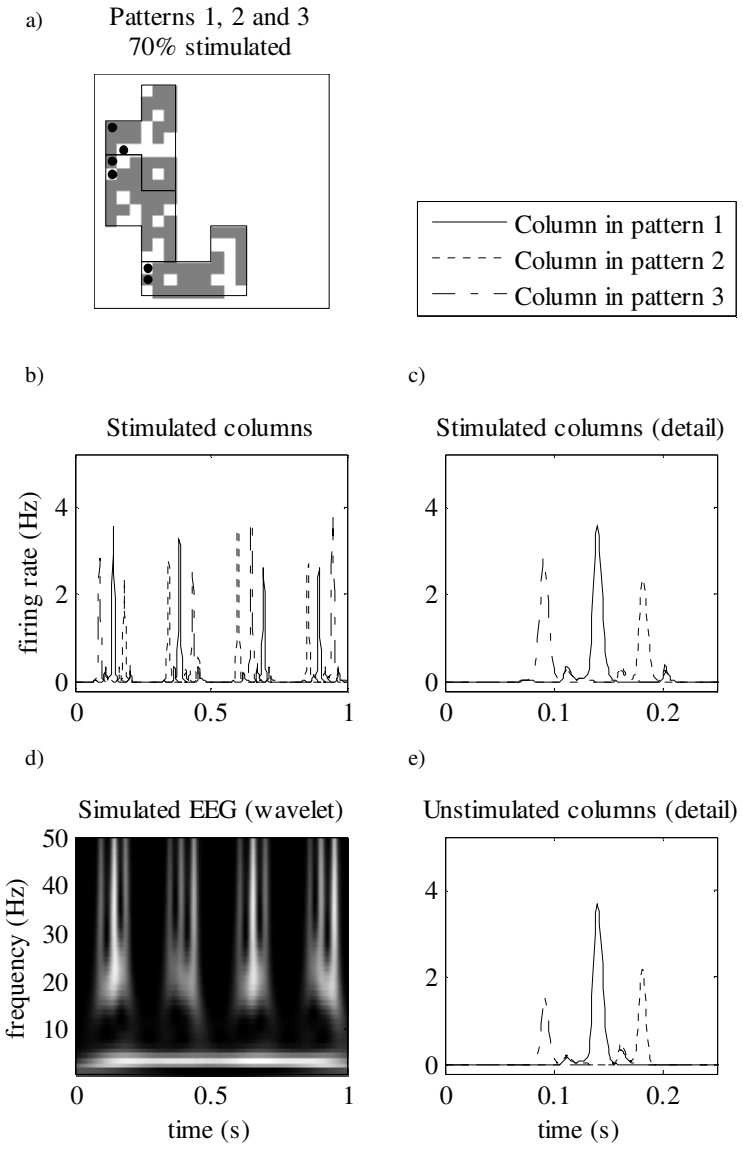

Figure VI.7: Reconstruction of three patterns with the desynchronization mechanism. Panel a shows the stimulated features (as in Figure VI.5). The other panels show the activity of 6 columns in L_2. Panel b shows the firing rate of three columns (one for each pattern) whose features are directly stimulated by the external input. Panel c shows a zoom of panel b, while panel d shows a wavelet map of the simulated EEG. Panel e shows the firing rate of three columns (one for each pattern) that are recovered by lateral synapses. The solid, dotted and dotted/dashed lines represent columns in pattern 1, 2 and 3 respectively.

exhibits a very strong activity in theta band (coming from L_1) and activity in the gamma band.

3.4. Simulation with two partial patterns as input, with desynchronization mechanism

A subsequent set of simulations were performed assuming the presence of desynchronizing synapses (trained with Eq. V.20) targeting $GABA_{A,fast}$ interneurons, with instantaneous dynamics (i.e., using the spike density, $z_p^{L2}{}_{hk}$ in Eq. VI.23), that simulate fast AMPA receptors with sub-millisecond rise time [Geiger et al., 1997].

Figure VI.7 shows the behavior of the network with three partial patterns as input and assuming fast trained synapses. Results show that the columns not stimulated by the external inputs are synchronized with the columns in the same pattern stimulated by external inputs. All patterns are well restored and segmented. As a consequence of the strong segmentation between patterns, the time-frequency content of the EEG in L_2 exhibits a significant rhythm in the beta-gamma band (>20 Hz) spaced out by a strong theta rhythm. However, it is worth noting that the frequency of oscillations in L_2 decreases, compared with the case of a single object (let us compare Figure VI.7 with Figure VI.6). The reason is that the three objects compete during a pause between one activation and the other, and this competition slows down the oscillatory rhythm (note the small activations between higher peaks in panels c and e of Figure VI.7).

3.5. Robustness of the object recovery

The network is able to completely recover the missing information when just 25% of object columns are stimulated. More particularly, if this percentage is higher than 60%, the lacking columns are fully excited by the stimulated ones; otherwise, the lacking columns are just partly excited by the others, and fully recover later thanks to their own reentrant activation. In the latter case, the theta rhythm is dilated (~3Hz, due to the dynamics with which the unstimulated columns slowly excite themselves).

We have also analyzed the robustness of the network to noise. We have stimulated the network with noise with different variances (σ_p^2 and σ_f^2 in the range 0-2500s^{-2}) and found that the network fails in recovering lacking information, and especially in segmenting patterns, when σ_p^2 and σ_f^2 are both 625s^{-2} or more. It is worth noting that this value is independent of the percentage of columns stimulated for each pattern.

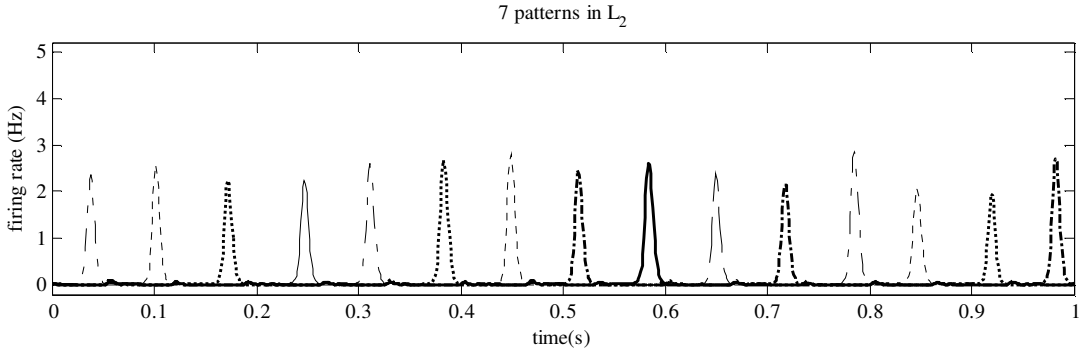

Figure VI.8: Stimulation of seven patterns. The figure shows the activity of seven columns which belongs to seven different patterns (different line styles represent different patterns) in L_2 when columns in L_1 are forced to fire continuously (thus neglecting the theta rhythm).

3.6. Segmentation capacity

To test the capacity of pattern recovery and segmentation we stimulated the network with all of the 7 patterns used during training. All the patterns are recovered successfully in L_1 if they are partially stimulated. However, they cannot all pop out in L_2, because half theta cycle cannot accommodate more than three beta-gamma cycles.

Indeed the only limitation is provided by the ratio between the theta period and the gamma period; i.e., if L_1 does not oscillate in the theta range, L_2 can segment a greater number of patterns. To show this, we forced the columns in L_1 to fire continuously toward columns in L_2 (i.e., we set $z^{L1}_{p,ij} \equiv 5\ s^{-1}$, for each column ij that belongs to one of the patterns), and verified that all the patterns were activated and correctly segmented in L_2. In this condition, however, the beta-gamma rhythm becomes even slower (~15 Hz), due to the harder competition of each pattern vs. all the other ones (Figure VI.8). Likely the network should work properly also with greater numbers of trained patterns.

4. DISCUSSION

The idea that synchronization of neural activity in the high beta and gamma bands plays a central role in many higher cognitive processes, as a putative mechanism for feature binding, has a long tradition in neuroscience [Pulvermüller et al., 1996; Singer, 1999] and has been exploited in several computational models in recent years [Cesmeli & Wang, 2000; von der Malsburg & Buhmann, 1992; Tagamets & Horwitz, 2000; Ursino & La Cara, 2004; Ursino et al., 2003, 2009; Wang & Terman, 1997; Wang, 1995]. However, despite these valuable studies on the subject, we are not aware that the problem has been modeled computationally using realistic neural mass models of a cortical column. This is a significant lack, since neural mass models are particularly suitable to simulate rhythm generation and rhythm propagation at a mesoscale level, and to provide reliable simulations of EEG whose spectra have multiple peaks [Moran et al., 2008; Zavaglia et al., 2006].

The present work was designed with the following main purposes:

1. to study the binding and segmentation problem using a recent improved version of a NMM, able to generate a variety of rhythms and to propagate them among interconnected cortical columns;
2. to investigate the possible synaptic mechanisms which allow fast synchronization and fast segmentation of objects;
3. to incorporate Hebbian rules within the model, to simulate high-level cognitive tasks involving previous experience and autoassociation;
4. to investigate the possibility to have two distinct rhythms within the model (one in the theta and the other in the beta-gamma range) and study the parameters which may affect the coexistence of these rhythms.

It is worth noting that the present model makes use only of previous knowledge to segment patterns, hence, it intends to simulate the recognition of complex objects, represented as a collection of features. Primary perception (such as segmentation of a visual scene) exploits different spatial rules (proximity, smoothness, common fate, etc…), and is not within the aim of the present model.

From the simulation results, some general conclusions can be drawn.

4.1. Synchronization

A NMM which reproduces the basic architecture of a cortical column can achieve a satisfactory synchronization of neural activity in the gamma band, using model glutamatergic synapses originating from pyramidal neurons and targeting other cortical columns coding for attributes of the same object. Moreover, in order to achieve robust synchronization, both excitation and inhibition among cortical columns should be used. In our model, this is realized via long-range synapses emerging from pyramidal neurons, which target pyramidal neurons in the first layer and fast-inhibitory interneurons in the second layer. The idea of using both excitation and inhibition to have strong synchronization is not new, and was exploited in previous models based on oscillating units [Ursino et al., 2009]. The observation that fast inhibitory interneurons play a relevant role in synchronization is also stressed in computational studies based on spiking neurons [Bartos et al., 2002].

4.2. Two rhythms in the model

A further aspect investigated with the model is the possible coexistence of the gamma rhythm with a slower theta rhythm. This is an interesting point, since the theta rhythm has been hypothesized to drive the formation and dissolution of patterns in autoassociative networks [Canolty et al., 2006; Doesburg et al., 2009; Schack et al., 2002], and to contribute to other important phenomena such as the precession of information in temporal sequences [Lisman & Idiart, 1995; Ward, 2003]. In particular, the presence of silent periods, in which the network does not show appreciable activity, alternated with periods of synchronized high frequency oscillations, can have a function to distinguish among moments in which information is recovered from the network and moments in which information is provided to the network [Ward, 2003].

The present model introduces an original element to improve synchronization and to generate robust coupled rhythms, i.e. a different role played by L_1 and L_2. Synapses to pyramidal columns in L_1 contribute to the recovery of lacking information. Thanks to these synapses, L_1 works as an autoassociative memory, which entirely recovers a previously stored information starting from a partial cue. In our model, with the present value of synaptic strengths, stimulating just 25% of the object features allows restoration of the remaining 75% of features. Moreover, the presence of autoassociative synapses in L_1 induces the theta rhythm. This rhythm originates from the feedback interaction between pyramidal populations and slow inhibitory interneurons within a column, and by trained excitation among pyramidal populations in different columns. Thanks to the strong reciprocal connections among pyramidal neurons, an initial excitation rapidly spreads among all columns in the same pattern, leading them to maximal excitation (i.e., to the upper saturation of the sigmoidal relationship). This strong excitation, in turn, causes the excitation of inhibitory interneurons with slow synaptic kinetics within the same column, which strongly inhibit the pyramidal neurons. The presence of a sigmoidal relationship (with upper saturation and sub-threshold silence) explains the long plateaus of the theta waves.

Conversely, synapses to fast inhibitory interneurons in the L_2 induce a gamma-rhythm, which is superimposed on the previous theta rhythm. Excitation in L_2 rapidly spreads to fast inhibitory interneurons within the same pattern. Since these interneurons exhibit a strong inhibitory self-loop, they tend to inhibit themselves inducing a fast oscillation, which is rapidly synchronized with oscillations in other columns in the same pattern.

In the present work we do not provide any indication of the possible neurophysiological or anatomical dispositions of these layers; the model wishes to have a general validity, i.e., it represents a proof of principle. By way of example, L_1 may represent a sub-cortical structure (such as the thalamus or the hippocampus) connected with a cortical layer; alternatively, the two layers may represent a first stage and a second stage of the same local circuitry (such as layers CA1 and CA3 in the hippocampus).

4.3. Learning mechanism for autoassociation

The previous mechanism for synchronization and autoassociation can be learned from past experience using realistic Hebbian rules. In particular, we used a time-dependent version of the Hebb rule, based on correlation between the instantaneous post-synaptic activity and the pre-synaptic activity in a previous 20 ms time window [Abbott & Nelson, 2000; Markram et al., 1997]. In this way, previous knowledge on objects can be stored in the network and subsequently

exploited to synchronize the properties of the object in the gamma band and to recover lacking information from incomplete cues.

4.4. Segmentation

A difficult problem, faced with the model, concerns the segmentation of multiple objects. This implies the possibility to have different objects simultaneously present, exploiting a time division (i.e., phase shift) of their oscillation activity. Previous models which used simpler oscillating units (such as Wilson Cowan oscillators [Ursino et al., 2003, 2009; Wang, 1995], or relaxation oscillators [Cesmeli & Wang, 2000; Ursino & La Cara, 2004]) solved the segmentation problem with the use of a "global inhibitor", i.e., a unit which calculates the overall activity in the network and sends back an inhibitory signal.

In the present work we did not use a global inhibitor, owing to its scarce physiological reliability, rather we assumed the presence of a further inhibitory mechanism within L_2, which works to ensure desynchronization among different objects. We argued that the time course of excitatory synapses (10-20 ms) was too slow to allow fast desynchronization among different objects. Hence, we adopted an alternative hypothesis: connections that provide fast and efficient desynchronization originate from pyramidal neurons and target fast inhibitory interneurons in other columns through faster synapses with a sub-millisecond rise time [Geiger et al., 1997]. Indeed, fast AMPA receptors are especially encountered at a pyramidal neuron-inhibitory interneuron synapse [Geiger et al., 1997; Itazawa et al., 1997; Yin et al., 1999; Zhou & Hablitz, 1998]; some authors hypothesized that their fast kinetics enables interneurons to detect synchronous activity of principal neurons [Geiger et al., 1997]. In our model, these synapses have been simulated assuming that their time constant is negligible (at least compared with that of other synapses in the model). Simulations demonstrate that these connections between pyramidal and fast inhibitory interneurons have the dynamical properties to favor pattern desynchronization, as required to solve the segmentation problem.

A strong assumption of this work is that these synapses are trained with an anti-Hebbian mechanism, i.e., they reinforce when the pre-synaptic activity is high but the post-synaptic activity is low (both mediated over a time window, to account for the presence of oscillatory activity). According to this assumption, inhibition is directed selectively only to cortical columns in different objects, i.e., an object cannot inhibit itself. This mechanism allows a stronger separation among oscillating patterns, as illustrated in Figure VI.7 and Figure VI.8. The possibility to reinforce a fast AMPA synapse to detect the anticorrelation among cortical columns, and the emphasis on their role in segmentation, represents a new hypothesis of the model, requiring ad hoc validation, and constitutes testable predictions for future studies.

4.5. Model limitations and future lines

It is difficult with the present model to segment more than three patterns simultaneously within a theta cycle. The fundamental reason is that the frequency of the gamma rhythm decreases with the number of objects simultaneously present, as a consequence of their competition realized by fast AMPA inhibitory synapses. This is evident by comparing Figure VI.5 with Figure VI.7 and Figure VI.8. The competition among three objects in Figure VI.7 causes some silent periods which slow down the frequency. The phenomenon is even more evident when seven patterns are simultaneously present (Figure VI.8). Of course, this model limitation is evident only if the theta rhythm is present. In the case of a constant input activity, the model can segment seven patterns

without problem, although with slower oscillation frequency. Hence, the model may segment many patterns if the theta rhythm is artificially slowed down.

Two improvements can be introduced in the model to overcome this problem

1. The use of neural populations with a higher oscillation rate may favor the presence of a greater number of patterns segmented during the theta cycle. This may be realized using a smaller time constant for synapse kinetics within the column. However, in these conditions synchronization and recovery of lacking features may become more difficult;
2. Segmentation in this model is achieved using only a "previous knowledge" rule, stored within trained synapses. This is a high-level Gestalt rule. It is expected that, at an earlier processing stage, before reaching the present network, part of the input information is already segmented using low-level Gestalt rules (such as proximity, smoothness, common fate, etc…). This is true if previous information derives, for instance, from visual, tactile or auditory processing. Conversely, in our model all inputs are given simultaneously without any pre-segmentation procedure.

A further limitation is that the present model cannot segment patterns with common features. To segment superimposed objects, we should introduce further learning rules which allow long term depression of some previously created synapses. For instance, if two objects (A and B) have a common feature f, when object A is used in the learning phase, AMPA synapses are created from f to desynchronize all features in B. These synapses must be withdrawn when B is used in the learning phase, to allow synchronization of f with the features of B. Some preliminary simulations (not presented here) indicate that segmentation of superimposed objects may be possible with additional rules. This may represent the target of future model improvements.

In the cortex pyramidal neurons are self-connected. Indeed, some authors in recent years [Sotero et al., 2010] included a self-loop of pyramidal neurons in their model. However, many other studies do not consider this loop explicitly [Jansen & Rit, 1995; Wendling et al., 2002]. We did not include this loop to limit the number of parameters in the model. Actually, the self-excitation among pyramidal populations can be introduced in L_1 by maintaining the main diagonal of the lateral synapses matrix $W^{L1}{}_{ij}{}^{L1}{}_{hk}$ (ij = hk in Eq. VI.27); if we do so the overall behavior of the network does not change in an appreciable way. However, the issue of how the inclusion of a self-loop in pyramidal populations can affect the behavior of the network should be addressed with a sensitivity analysis in future studies. It is possible that the inclusion of a self-loop among pyramidal neurons makes the presence of excitatory interneurons unnecessary, thus leading to a simplification of the model.

Finally, the mechanism for the generation of the theta rhythm is quite simple. More sophisticate mechanisms exist in the brain and may be included in future work: they might comprehend a more detailed description of thalamic dynamics, including a loop between thalamic nuclei and the reticular formation, and a description of thalamic neural populations which incorporates the burst firing modality: both mechanisms are known to participate to the genesis of low-frequency rhythms, as those occurring during sleep [Huguenard & McCormick, 2007; Steriade, 2006].

VII. CONCLUSIONS

The study of cortical rhythms and connectivity, of their mutual interaction and of their role in the realization of motor and cognitive tasks is a huge issue that cannot be (and is not intended to be) fully covered in a Ph.D. thesis. The aim of this work has rather been to explore the capabilities of a neural model to help the research in the field of quantitative neuroscience. In these years we used different versions of a NMM to simulate experimental data and to reproduce physiological phenomena in order to fathom the ability of the model to describe the spectrum of expressions of the cortical activity, look at which conclusions can be drawn and estimate how reliable they are on the basis of scientific literature and previous knowledge on the subject.

In particular at the beginning of my Ph.D. our NMM could be used to reproduce the spectra of experimental EEGs in order to infer the connectivity patterns between different cortical areas, however it had some intrinsic limitations that narrowed down its possible applications. The model has been modified on the basis of experimental evidence to overcome these limitations and its new characteristics have been analyzed in detail. The new model has been successfully employed to reproduce the time courses of data recorded with the TMS-EEG technique, allowing to quantify the extrinsic connectivity of the areas involved in the task. Finally, the model has been used to reproduce some qualitative characteristics of the cortical electrical activity related to the memory recovery, suggesting how the brain can realize such a function.

At the end of this dissertation we can conclude that NMMs can greatly help the interpretation of experimental data from a physiological and functional point of view. Indeed, this augmented insight is not given for free since a model inversion is not a trivial operation. As has been shown in the previous chapters, the fitting of features of experimental data (time courses, spectra, etc.) with models that are neither linear nor low-dimensional in the parameters space, requires the use of advanced optimization tools and strategies. Some ways to obtain automatic fittings have been presented, but they require a great load of work to be developed, are usually to be preceded by some mandatory preprocessing steps and are often suitable only for ad hoc applications. However, if these fittings can be achieved after a bit of struggling, the model provides a kind of information that is almost immediately interpretable, parameters and variables have a clear physiological meaning and thus conclusions can be drawn quite straightforwardly.

Actually the analysis of physiological phenomena with mathematical models can not only provide information on the specific topic that is being studied, but can also suggest new paths of investigation, by pointing out issues that simply were not taken into consideration in the first place. For example, the network described in chapter VI used to recover pieces of information from memory, suggests that much more neural assemblies can be recalled if they are related to one another, as in a chain of events, rather than completely uncorrelated. Indeed, our future research is devoted also to the development of that network, in order to accommodate for the learning of patterns that are linked together in an ordered sequence.

It is clear that many efforts have to be done yet. In my opinion, a very important goal would be the development of optimization methods that could fit neural models to experimental data

automatically, without the need to adapt the procedure for new experiments and new data. Important results have already been achieved in this direction (let's consider for example the Statistical Parametric Mapping framework developed at the Wellcome Trust Center for Neuroimaging of London), but I think that an automatic fitting procedure, or at least a set of algorithms, that gives satisfying results when models are non-linear, have very high or very low sensitivity on some parameters, and high-dimensional research spaces, is still lacking.

Future lines of research will surely include the development of models that employ both cortical and thalamic modules, in order to study phenomena that are strictly correlated with the activity of the thalamus and its interaction with the cortex (sleep, processing of sensory information). Such networks would be priceless in clinics to help the diagnosis of different states of unconsciousness and to estimate the effectiveness of treatments by inferring the connectivity between different areas in the cortex and the thalamus, and following the changes in these parameters.

REFERENCES

1. L.F. Abbott and S.B. Nelson, Synaptic plasticity: taming the beast, *Nat. Neurosci.* **3** (2000) 1178-1183.

2. S. Achard and E. Bullmore, Efficiency and cost of economical brain functional networks, *PLoS. Comput. Biol.* **3**(2) (2007) e17.

3. L. Astolfi, F. Cincotti, D. Mattia, S. Salinari, C. Babiloni, A. Basilisco, P.M. Rossini, L. Ding, Y. Ni, B. He, M.G. Marciani and F. Babiloni, Estimation of the effective and functional human cortical connectivity with structural equation modeling and directed transfer function applied to high-resolution EEG, *Magn. Reson. Imaging.* **22**(10) (2004) 1457-1470.

4. L. Avitan, M. Teicher and M. Abeles, EEG generator—a model of potentials in a volume conductor, *J. Neurophysiol.* **102**(5) (2009) 3046-3059.

5. A. Babajani and H. Soltanian-Zadeh, Integrated MEG/EEG and fMRI model based on neural masses, *IEEE. T. Bio-Med. Eng.* **53**(9) (2006) 1794-1801.

6. F. Babiloni, F. Cincotti, C. Babiloni, F. Carducci, D. Mattia, L. Astolfi, A. Basilisco, P.M. Rossini, L. Ding, Y. Ni, J. Cheng, K. Christine, J. Sweeney and B. He, Estimation of the cortical functional connectivity with the multimodal integration of high-resolution EEG and fMRI data by directed transfer function, *Neuroimage.* **24**(1) (2005) 118-131.

7. L.A. Baccalá and K. Sameshima, Partial directed coherence: a new concept in neural structure determination, *Biol. Cybern.* **84**(6) (2001) 463-474.

8. M.I. Banks, J.A. White and R.A. Pearce, Interactions between distinct GABAA circuits in hippocampus, *Neuron.* **25**(2) (2000) 449-457.

9. M. Bartos, I. Vida, M. Frotscher, A. Meyer, H. Monyer, J.R.P. Geiger and P. Jonas, Fast synaptic inhibition promotes synchronized gamma oscillations in hippocampal interneuron networks, *P. Natl. Acad. Sci. USA.* **99**(20) (2002) 13222-13227.

10. M. Bartos, I. Vida and P. Jonas, Synaptic mechanisms of synchronized gamma oscillations in inhibitory interneuron networks, *Nat. Rev. Neurosci.* **8**(1) (2007) 45-56.

11. E. Başar, C. Başar-Eroğlu, S. Karakaş and M. Schürmann, Brain oscillations in perception and memory, *Int. J. Psychophysiol.* **35**(2-3) (2000) 95-124.

12. E. Başar, C. Başar-Eroglu, S. Karakaş and M. Schürmann, Gamma, alpha, delta, and theta oscillations govern cognitive processes, *Int. J. Psychophysiol.* **39**(2-3) (2001) 241-248.

13. P. Berg and M. Scherg, A fast method for forward computation of multiple-shell spherical head models, *Electroen. Clin. Neuro.* **90**(1) (1994) 58-64.

14. H. Berger, Über das elektrenkephalogramm des menschen, *Arch. Psychiat. Nerven.* **87**(1) (1929) 527-570.

15. G. Buzsaki, *Rhythms of the brain* (Oxford University Press, USA, 2006).

16. G. Buzsáki and A. Draguhn, Neuronal oscillations in cortical networks, *Science.* **304**(5679) (2004) 1926-1929.

17. S. Campbell and D. Wang, Synchronization and desynchronization in a network of locally coupled Wilson-Cowan oscillators, *IEEE. T. Neural. Networ.* **7**(3) (1996) 541-554.

18. R.T. Canolty, E. Edwards, S.S. Dalal, M. Soltani, S.S. Nagarajan, H.E. Kirsch, M.S. Berger, N.M. Barbaro and R.T. Knight, High gamma power is phase-locked to theta oscillations in human neocortex, *Science.* **313**(5793) (2006) 1626-1628.

19. E. Cesmeli and D. Wang, Motion segmentation based on motion/brightness integration and oscillatory correlation, *IEEE. T. Neural. Networ.* **11**(4) (2000) 935-947.

20. V.S. Chakravarthy, N. Gupte, S. Yogesh and A. Salhotra, Chaotic synchronization using a network of neural oscillators, *Int. J. Neur. Syst.* **18**(02) (2008) 157-164.

21. S.R. Cobb, E.H. Buhl, K. Halasy, O. Paulsen and P. Somogyi, Synchronization of neuronal activity in hippocampus by individual GABAergic interneurons, *Nature.* **378**(6552) (1995) 75-78.

22. S.R. Cobb, K. Halasy, I. Vida, G. Nyíri, G. Tamás, E.H. Buhl and P. Somogyi, Synaptic effects of identified interneurons innervating both interneurons and pyramidal cells in the rat hippocampus, *Neuroscience.* **79**(3) (1997) 629-648.

23. F. Cona, M. Zavaglia, L. Astolfi, F. Babiloni and M. Ursino, Changes in EEG power spectral density and cortical connectivity in healthy and tetraplegic patients during a motor imagery task, *Comput. Intell. Neurosci.* **2009** (2009) 1-12.

24. F. Cona, M. Zavaglia, M. Massimini, M. Rosanova and M. Ursino, A neural mass model of interconnected regions simulates rhythm propagation observed via TMS-EEG, *Neuroimage.* **57**(3) (2011) 1045-1058.

25. F. Crick and C. Koch, Towards a neurobiological theory of consciousness, *Semin. Neurosci.* **2** (1990) 263-275.

26. M.O. Cunningham, C.H. Davies, E.H. Buhl, N. Kopell and M.A. Whittington, Gamma oscillations induced by kainate receptor activation in the entorhinal cortex in vitro, *J. Neurosci.* **23**(30) (2003) 9761-9769.

27. A.R. Damasio, Synchronous activation in multiple cortical regions: a mechanism for recall, *Semin. Neurosci.* **2** (1990) 287-296.

28. O. David, D. Cosmelli and K.J. Friston, Evaluation of different measures of functional connectivity using a neural mass model, *Neuroimage.* **21**(2) (2004) 659-673.

29. O. David, L. Harrison and K.J. Friston, Modelling event-related responses in the brain, *Neuroimage.* **25**(3) (2005) 756-770.

30. O. David, S.J. Kiebel, L.M. Harrison, J. Mattout, J.M. Kilner and K.J. Friston, Dynamic causal modeling of evoked responses in EEG and MEG, *Neuroimage.* **30**(4) (2006) 1255-1272.

31. O. David and K.J. Friston, A neural mass model for MEG/EEG: coupling and neuronal dynamics, *Neuroimage.* **20**(3) (2003) 1743-1755.

32. P. Dayan and L.F. Abbott, *Philosophical psycology* (The MIT Press, 2001).

33. G. Deco, V.K. Jirsa, P.A. Robinson, M. Breakspear and K. Friston, The dynamic brain: from spiking neurons to neural masses and cortical fields, *PLoS. Comput. Biol.* **4**(8) (2008) e1000092.

34. J. DeFelipe, L. Alonso-Nanclares and J.I. Arellano, Microstructure of the neocortex: comparative aspects, *J. Neurocytol.* **31**(3-5) (2002) 299-316.

35. Y.D. Van Der Werf, A.F. Sadikot, A.P. Strafella and T. Paus, The neural response to transcranial magnetic stimulation of the human motor cortex. II. Thalamocortical contributions, *Exp. Brain. Res.* **175**(2) (2006) 246-255.

36. Y.D. Van Der Werf and T. Paus, The neural response to transcranial magnetic stimulation of the human motor cortex. I. Intracortical and cortico-cortical contributions, *Exp. Brain. Res.* **175**(2) (2006) 231-245.

37. S.M. Doesburg, J.J. Green, J.J. McDonald and L.M. Ward, Rhythms of consciousness: binocular rivalry reveals large-scale oscillatory network dynamics mediating visual perception, *PLoS. ONE.* **4**(7) (2009) e6142.

38. E. Düzel, W.D. Penny and N. Burgess, Brain oscillations and memory, *Curr. Opin. Neurobiol.* **20**(2) (2010) 143-149.

39. A.K. Engel and W. Singer, Temporal binding and the neural correlates of sensory awareness, *Trends. Cogn. Sci.* **5**(1) (2001) 16-25.

40. S.K. Esser, S.L. Hill and G. Tononi, Modeling the effects of transcranial magnetic stimulation on cortical circuits, *J. Neurophysiol.* **94**(1) (2005) 622-639.

41. S.K. Esser, S. Hill and G. Tononi, Breakdown of effective connectivity during slow wave sleep: investigating the mechanism underlying a cortical gate using large-scale modeling, *J. Neurophysiol.* **102**(4) (2009) 2096-2111.

42. B. Feige, K. Scheffler, F. Esposito, F. Di Salle, J. Hennig and E. Seifritz, Cortical and subcortical correlates of electroencephalographic alpha rhythm modulation, *J. Neurophysiol.* **93**(5) (2005) 2864-2872.

43. D.J. Felleman and D.C. Van Essen, Distributed hierarchical processing in the primate cerebral cortex, *Cereb. Cortex.* **1**(1) (1991) 1-47.

44. W.J. Freeman, *Mass action in the nervous system* (Academic Press, New York, 1975).

45. W.J. Freeman, Models of the dynamics of neural populations, *Electroencephalogr. Clin. Neurophysiol. Suppl.* (34) (1978) 9-18.

46. W.J. Freeman, Simulation of chaotic EEG patterns with a dynamic model of the olfactory system, *Biol. Cybern.* **56**(2-3) (1987) 139-150.

47. T.F. Freund and G. Buzsáki, Interneurons of the hippocampus, *Hippocampus.* **6**(4) (1996) 347-470.

48. P. Fries, D. Nikolic and W. Singer, The gamma cycle, *Trends. Neurosci.* **30**(7) (2007) 309-316.

49. P. Fries, Neuronal gamma-band synchronization as a fundamental process in cortical computation, *Annu. Rev. Neurosci.* **32** (2009) 209-224.

50. K.J. Friston, W. Penny, C. Phillips, S. Kiebel, G. Hinton and J. Ashburner, Classical and bayesian inference in neuroimaging: theory, *Neuroimage.* **16**(2) (2002) 465-483.

51. K.J. Friston, L. Harrison and W. Penny, Dynamic causal modelling, *Neuroimage.* **19**(4) (2003) 1273-1302.

52. K.J. Friston, Models of brain function in neuroimaging, *Annu. Rev. Psychol.* **56**(1) (2005) 57-87.

53. K. Friston, R. Henson, C. Phillips and J. Mattout, Bayesian estimation of evoked and induced responses, *Hum. Brain. Mapp.* **27**(9) (2006) 722-735.

54. J.R.P. Geiger, J. Lübke, A. Roth, M. Frotscher and P. Jonas, Submillisecond AMPA receptor-mediated signaling at a principal neuron-interneuron synapse, *Neuron.* **18**(6) (1997) 1009-1023.

55. C.M. Gómez, J. Marco-Pallarés and C. Grau, Location of brain rhythms and their modulation by preparatory attention estimated by current density, *Brain. Res.* **1107**(1) (2006) 151-160.

56. G. Gómez-Herrero, M. Atienza, K. Egiazarian and J.L. Cantero, Measuring directional coupling between EEG sources, *Neuroimage.* **43**(3) (2008) 497-508.

57. G. González-Burgos, L.S. Krimer, N.V. Povysheva, G. Barrionuevo and D.A. Lewis, Functional properties of fast spiking interneurons and their synaptic connections with pyramidal cells in primate dorsolateral prefrontal cortex, *J. Neurophysiol.* **93**(2) (2005) 942-953.

58. F. Grimbert and O. Faugeras, Bifurcation analysis of Jansen's neural mass model, *Neural. Comput.* **18**(12) (2006) 3052-3068.

59. Y. Gutfreund, Y. yarom and I. Segev, Subthreshold oscillations and resonant frequency in guinea-pig cortical neurons: physiology and modelling., *J. Physiol.* **483**(Pt 3) (1995) 621-640.

60. M. Guye, G. Bettus, F. Bartolomei and P.J. Cozzone, Graph theoretical analysis of structural and functional connectivity MRI in normal and pathological brain networks, *Magn. Reson. Mater. Phy.* **23**(5-6) (2010) 409-421.

61. M. Hamidi, H.A. Slagter, G. Tononi and B.R. Postle, Repetitive transcranial magnetic stimulation affects behavior by biasing endogenous cortical oscillations, *Front. Integr. Neurosci.* **3**(14) (2009) 1-12.

62. F. Han, M. Wiercigroch, J.A. Fang and Z. Wang, Excitement and synchronization of small-world neuronal networks with short-term synaptic plasticity, *Int. J. Neur. Syst.* (2011) 21-25.

63. H. Hasegawa, Dynamical mean-field theory of spiking neuron ensembles: Response to a single spike with independent noises, *Phys. Rev. E.* **67**(4) (2003) 041903.

64. J.H. Holland, *Adaptation in natural and artificial systems* (University of Michigan Press, 1975).

65. J.C. Horton and D.L. Adams, The cortical column: a structure without a function, *Philos. Trans. R. Soc. Lond. B. Biol. Sci.* **360**(1456) (2005) 837-862.

66. B. Horwitz, The elusive concept of brain connectivity, *Neuroimage.* **19**(2) (2003) 466-470.

67. J.R. Huguenard and D.A. McCormick, Thalamic synchrony and dynamic regulation of global forebrain oscillations, *Trends. Neurosci.* **30**(7) (2007) 350-356.

68. S.I. Itazawa, T. Isa and S. Ozawa, Inwardly rectifying and Ca2+-permeable AMPA-type glutamate receptor channels in rat neocortical neurons, *J. Neurophysiol.* **78**(5) (1997) 2592-2601.

69. B.H. Jansen, G. Zouridakis and M.E. Brandt, A neurophysiologically-based mathematical model of flash visual evoked potentials, *Biol. Cybern.* **68**(3) (1993) 275-283.

70. B.H. Jansen and V.G. Rit, Electroencephalogram and visual evoked potential generation in a mathematical model of coupled cortical columns, *Biol. Cybern.* **73**(4) (1995) 357-366.

71. J.G.R. Jefferys, R.D. Traub and M.A. Whittington, Neuronal networks for induced «40 Hz» rhythms, *Trends. Neurosci.* **19**(5) (1996) 202-208.

72. O. Jensen, J. Kaiser and J.-P. Lachaux, Human gamma-frequency oscillations associated with attention and memory, *Trends. Neurosci.* **30**(7) (2007) 317-324.

73. J. Kaiser and W. Lutzenberger, Human gamma-band activity: a window to cognitive processing, *Neuroreport.* **16**(3) (2005) 207-211.

74. M. Kaminski, M. Ding, W.A. Truccolo and S.L. Bressler, Evaluating causal relations in neural systems: Granger causality, directed transfer function and statistical assessment of significance, *Biol. Cybern.* **85**(2) (2001) 145-157.

75. M. Kamiński, K. Blinowska and W. Szelenberger, Investigation of coherence structure and EEG activity propagation during sleep, *Acta. Neurobiol. Exp.* **55**(3) (1995) 213-219.

76. M. Kamiński, K. Blinowska and W. Szelenberger, Topographic analysis of coherence and propagation of EEG activity during sleep and wakefulness, *Electroen. Clin. Neuro.* **102**(3) (1997) 216-227.

77. M.J. Kaminski and K.J. Blinowska, A new method of the description of the information flow in the brain structures, *Biol. Cybern.* **65**(3) (1991) 203-210.

78. S.J. Kiebel, M.I. Garrido, R.J. Moran and K.J. Friston, Dynamic causal modelling for EEG and MEG, *Cog. Neurodyn.* **2**(2) (2008) 121-136.

79. Z.F. Kisvárday, C. Beaulieu and U.T. Eysel, Network of GABAergic large basket cells in cat visual cortex (area 18): Implication for lateral disinhibition, *J. Comp. Neurol.* **327**(3) (1993) 398-415.

80. I.C. Kleppe and H.P.C. Robinson, Determining the activation time course of synaptic AMPA receptors from openings of colocalized NMDA receptors, *Biophys. J.* **77**(3) (1999) 1418-1427.

81. W. Klimesch, R. Freunberger and P. Sauseng, Oscillatory mechanisms of process binding in memory, *Neurosci. Biobehav. R.* **34**(7) (2010) 1002-1014.

82. A. Knoblauch and G. Palm, Scene segmentation by spike synchronization in reciprocally connected visual areas. II. Global assemblies and synchronization on larger space and time scales, *Biol. Cybern.* **87** (2002a) 168-184.

83. A. Knoblauch and G. Palm, Scene segmentation by spike synchronization in reciprocally connected visual areas. I. Local effects of cortical feedback, *Biol. Cybern.* **87** (2002b) 151-167.

84. A. Korzeniewska, M. Mańczak, M. Kamiński, K.J. Blinowska and S. Kasicki, Determination of information flow direction among brain structures by a modified directed transfer function (dDTF) method, *J. Neurosci. Meth.* **125**(1-2) (2003) 195-207.

85. H. Laufs, K. Krakow, P. Sterzer, E. Eger, A. Beyerle, A. Salek-Haddadi and A. Kleinschmidt, Electroencephalographic signatures of attentional and cognitive default modes in spontaneous brain activity fluctuations at rest, *Proc. Natl. Acad. Sci. U.S.A.* **100**(19) (2003) 11053-11058.

86. D.T.J. Liley and I. Bojak, Understanding the transition to seizure by modeling the epileptiform activity of general anesthetic agents, *J. Clin. Neurophysiol.* **22**(5) (2005) 300-313.

87. J. Lisman and M. Idiart, Storage of 7 +/- 2 short-term memories in oscillatory subcycles, *Science.* **267**(5203) (1995) 1512-1515.

88. R.R. Llinás, A.A. Grace and Y. Yarom, In vitro neurons in mammalian cortical layer 4 exhibit intrinsic oscillatory activity in the 10- to 50-Hz frequency range, *Proc. Natl. Acad. Sci. U.S.A.* **88**(3) (1991) 897-901.

89. F.H. Lopes da Silva, A. Hoeks, H. Smits and L.H. Zetterberg, Model of brain rhythmic activity, *Kybernetik.* **15**(1) (1974) 27-37.

90. F.H. Lopes da Silva, A. van Rotterdam, P. Barts, E. van Heusden and W. Burr, Models of neuronal populations: the basic mechanisms of rhythmicity, *Prog. Brain Res.* **45** (1976) 281-308.

91. F.H. Lopes da Silva, J.E. Vos, J. Mooibroek and A. van Rotterdam, Relative contributions of intracortical and thalamo-cortical processes in the generation of alpha rhythms, revealed by partial coherence analysis, *Electroen. Clin. Neuro.* **50**(5-6) (1980) 449-456.

92. R. Maex and E. De Schutter, Mechanism of spontaneous and self-sustained oscillations in networks connected through axo-axonal gap junctions, *Eur. J. Neurosci.* **25**(11) (2007) 3347-3358.

93. C. von der Malsburg and J. Buhmann, Sensory segmentation with coupled neural oscillators, *Biol. Cybern.* **67**(3) (1992) 233-242.

94. D. Mantini, M.G. Perrucci, C. Del Gratta, G.L. Romani and M. Corbetta, Electrophysiological signatures of resting state networks in the human brain, *Proc. Natl. Acad. Sci. U.S.A.* **104**(32) (2007) 13170-13175.

95. H. Markram, J. Lübke, M. Frotscher and B. Sakmann, Regulation of synaptic efficacy by coincidence of postsynaptic APs and EPSPs, *Science.* **275**(5297) (1997) 213-215.

96. D. Mattia, F. Cincotti, L. Astolfi, F. de Vico Fallani, G. Scivoletto, M.G. Marciani and F. Babiloni, Motor cortical responsiveness to attempted movements in tetraplegia: Evidence from neuroelectrical imaging, *Clin. Neurophysiol.* **120**(1) (2009) 181-189.

97. C.M. Michel, D. Lehmann, B. Henggeler and D. Brandeis, Localization of the sources of EEG delta, theta, alpha and beta frequency bands using the FFT dipole approximation, *Electroen. Clin. Neuro.* **82**(1) (1992) 38-44.

98. R. Miles, K. Tóth, A.I. Gulyás, N. Hájos and T.F. Freund, Differences between somatic and dendritic inhibition in the hippocampus, *Neuron.* **16**(4) (1996) 815-823.

99. W.H.R. Miltner, C. Braun, ArnoldMatthias, H. Witte and E. Taub, Coherence of gamma-band EEG activity as a basis for associative learning, *Nature.* **397**(6718) (1999) 434-436.

100. R.J. Moran, S.J. Kiebel, K.E. Stephan, R.B. Reilly, J. Daunizeau and K.J. Friston, A neural mass model of spectral responses in electrophysiology, *Neuroimage.* **37**(3) (2007) 706-720.

101. R.J. Moran, K.E. Stephan, S.J. Kiebel, N. Rombach, W.T. O'Connor, K.J. Murphy, R.B. Reilly and K.J. Friston, Bayesian estimation of synaptic physiology from the spectral responses of neural masses, *Neuroimage.* **42**(1) (2008) 272-284.

102. R.J. Moran, K.E. Stephan, T. Seidenbecher, H.-C. Pape, R.J. Dolan and K.J. Friston, Dynamic causal models of steady-state responses, *Neuroimage.* **44**(3) (2009) 796-811.

103. L. Neltner, D. Hansel, G. Mato and C. Meunier, Synchrony in heterogeneous networks of spiking neurons, *Neural. Comput.* **12**(7) (2000) 1607-1641.

104. C. Neuper, M. Wörtz and G. Pfurtscheller, ERD/ERS patterns reflecting sensorimotor activation and deactivation, *Prog. Brain Res.* **159** (2006) 211-222.

105. C. Neuper and G. Pfurtscheller, Evidence for distinct beta resonance frequencies in human EEG related to specific sensorimotor cortical areas, *Clin. Neurophysiol.* **112**(11) (2001) 2084-2097.

106. P.L. Nunez, *Neocortical dynamics and human EEG rhythms* (Oxford University Press, USA, 1995).

107. P.L. Nunez and R. Srinivasan, *Electric fields of the brain: the neurophysics of EEG* (Oxford University Press, 2006).

108. T. Paus, Primate anterior cingulate cortex: where motor control, drive and cognition interface, *Nat. Rev. Neurosci.* **2**(6) (2001) 417-424.

109. T. Paus, P.K. Sipila and A.P. Strafella, Synchronization of neuronal activity in the human primary motor cortex by transcranial magnetic stimulation: An EEG study, *J. Neurophysiol.* **86**(4) (2001) 1983-1990.

110. N. Picard and P.L. Strick, Motor areas of the medial wall: A review of their location and functional activation, *Cereb. Cortex.* **6**(3) (1996) 342-353.

111. M. Pirini and M. Ursino, A mass model of interconnected thalamic populations including both tonic and burst firing mechanisms, *Int. J. Bioelectromagn.* **12**(1) (2010) 26-31.

112. M.I. Posner, M.K. Rothbart, B.E. Sheese and Y. Tang, The anterior cingulate gyrus and the mechanism of self-regulation, *Cogn. Affect. Behav. Ne.* **7**(4) (2007) 391-395.

113. F. Pulvermüller, H. Preissl, W. Lutzenberger and N. Birbaumer, Brain rhythms of language: Nouns versus verbs, *Eur. J. Neurosci.* **8**(5) (1996) 937-941.

114. F. Pulvermüller, N. Birbaumer, W. Lutzenberger and B. Mohr, High-frequency brain activity: Its possible role in attention, perception and language processing, *Prog. Neurobiol.* **52**(5) (1997) 427-445.

115. C.J. Rennie, J.J. Wright and P.A. Robinson, Mechanisms of cortical electrical activity and emergence of gamma rhythm, *J. Theor. Biol.* **205**(1) (2000) 17-35.

116. C.J. Rennie, P.A. Robinson and J.J. Wright, Unified neurophysical model of EEG spectra and evoked potentials, *Biol. Cybern.* **86**(6) (2002) 457-471.

117. P.J. Roback and R.A. Askins, Judicious use of multiple hypothesis tests, *Conserv. Biol.* **19**(1) (2005) 261-267.

118. P.A. Robinson, C.J. Rennie, J.J. Wright, H. Bahramali, E. Gordon and D.L. Rowe, Prediction of electroencephalographic spectra from neurophysiology, *Phys. Rev. E.* **63**(2) (2001) 021903.

119. E. Rodriguez, N. George, J.P. Lachaux, J. Martinerie, B. Renault and F.J. Varela, Perception's shadow: long-distance synchronization of human brain activity, *Nature.* **397**(6718) (1999) 430-433.

120. E. Rolls and A. Treves, *Neural networks and brain function* (Oxford University Press, USA, 1998).

121. M. Rosanova, A. Casali, V. Bellina, F. Resta, M. Mariotti and M. Massimini, Natural frequencies of human corticothalamic circuits, *J. Neurosci.* **29**(24) (2009) 7679-7685.

122. D.L. Rowe, P.A. Robinson and C.J. Rennie, Estimation of neurophysiological parameters from the waking EEG using a biophysical model of brain dynamics, *J. Theor. Biol.* **231**(3) (2004) 413-433.

123. J.B. Rowe, K.E. Stephan, K. Friston, R.S.J. Frackowiak and R.E. Passingham, The prefrontal cortex shows context-specific changes in effective connectivity to motor or visual cortex during the selection of action or colour, *Cereb. Cortex.* **15**(1) (2005) 85-95.

124. H. Sakoe and S. Chiba, Dynamic programming algorithm optimization for spoken word recognition, *IEEE. T. Acoust. Speech.* **26**(1) (1978) 43-49.

125. S. Salenius and R. Hari, Synchronous cortical oscillatory activity during motor action, *Curr. Opin. Neurobiol.* **13**(6) (2003) 678-684.

126. B. Schack, N. Vath, H. Petsche, H.G. Geissler and E. Möller, Phase-coupling of theta-gamma EEG rhythms during short-term memory processing, *Int. J. Psychophysiol.* **44**(2) (2002) 143-163.

127. H. Shibasaki and M. Hallett, What is the bereitschaftspotential?, *Clin. Neurophysiol.* **117**(11) (2006) 2341-2356.

128. M. Siegel, M.R. Warden and E.K. Miller, Phase-dependent neuronal coding of objects in short-term memory, *P. Natl. Acad. Sci. USA.* **106**(50) (2009) 21341-21346.

129. A. Sik, M. Penttonen, A. Ylinen and G. Buzsaki, Hippocampal CA1 interneurons: an in vivo intracellular labeling study, *J. Neurosci.* **15**(10) (1995) 6651-6665.

130. W. Singer, Neuronal synchrony: a versatile code for the definition of relations, *Neuron.* **24** (1999) 49-65.

131. W. Singer and C.M. Gray, Visual feature integration and the temporal correlation hypothesis, *Annu. Rev. Neurosci.* **18**(1) (1995) 555-586.

132. R.C. Sotero, N.J. Trujillo-Barreto, Y. Iturria-Medina, F. Carbonell and J.C. Jimenez, Realistically coupled neural mass models can generate EEG rhythms, *Neural. Comput.* **19**(2) (2007) 478-512.

133. R.C. Sotero, A. Bortel, R. Martínez-Cancino, S. Neupane, P. O'Connor, F. Carbonell and A. Shmuel, Anatomically-constrained effective connectivity among layers in a cortical column modeled and estimated from local field potentials, *J. Integr. Neurosci.* **9**(4) (2010) 355-379.

134. A. Stancák Jr. and G. Pfurtscheller, Event-related desynchronisation of central beta-rhythms during brisk and slow self-paced finger movements of dominant and nondominant hand, *Cognitive. Brain. Res.* **4**(3) (1996) 171-183.

135. K.E. Stephan, L.M. Harrison, S.J. Kiebel, O. David, W.D. Penny and K.J. Friston, Dynamic causal models of neural system dynamics: current state and future extensions, *J. Bioscience.* **32**(1) (2007) 129-144.

136. M. Steriade, R.C. Dossi and D. Contreras, Electrophysiological properties of intralaminar thalamocortical cells discharging rhythmic (≈40 HZ) spike-bursts at ≈1000 HZ during waking and rapid eye movement sleep, *Neuroscience.* **56**(1) (1993) 1-9.

137. M. Steriade, Grouping of brain rhythms in corticothalamic systems, *Neuroscience.* **137**(4) (2006) 1087-1106.

138. M.A. Tagamets and B. Horwitz, A model of working memory: bridging the gap between electrophysiology and human brain imaging, *Neural. Networks.* **13**(8-9) (2000) 941-952.

139. C. Tallon-Baudry, O. Bertrand, C. Delpuech and J. Pernier, Stimulus specificity of phase-locked and non-phase-locked 40 Hz visual responses in human, *J. Neurosci.* **16**(13) (1996) 4240-4249.

140. J.C. Tamraz and Y.G. Comair, *Atlas of regional anatomy of the brain using MRI* (Springer, 2005).

141. A.M. Thomson, D.C. West, J. Hahn and J. Deuchars, Single axon IPSPs elicited in pyramidal cells by three classes of interneurones in slices of rat neocortex., *J. Physiol.* **496**(Pt 1) (1996) 81-102.

142. G. Thut and C. Miniussi, New insights into rhythmic brain activity from TMS–EEG studies, *Trends. Cogn. Sci.* **13**(4) (2009) 182-189.

143. P.H. Tiesinga and J.V. José, Robust gamma oscillations in networks of inhibitory hippocampal interneurons, *Network* **11**(1) (2000) 1-23.

144. G. Tinguely, L.A. Finelli, H.-P. Landolt, A.A. Borbély and P. Achermann, Functional EEG topography in sleep and waking: State-dependent and state-independent features, *Neuroimage.* **32**(1) (2006) 283-292.

145. R.D. Traub, A. Bibbig, A. Fisahn, F.E.N. LeBeau, M.A. Whittington and E.H. Buhl, A model of gamma-frequency network oscillations induced in the rat CA3 region by carbachol in vitro, *Eur. J. Neurosci.* **12**(11) (2000) 4093-4106.

146. R.D. Traub, A. Bibbig, F.E.N. LeBeau, E.H. Buhl and M.A. Whittington, Cellular mechanisms of neuronal population oscillations in the hippocampus in vitro, *Annu. Rev. Neurosci.* **27**(1) (2004) 247-278.

147. R.D. Traub, D. Contreras, M.O. Cunningham, H. Murray, F.E.N. LeBeau, A. Roopun, A. Bibbig, W.B. Wilent, M.J. Higley and M.A. Whittington, Single-column thalamocortical network model exhibiting gamma oscillations, sleep spindles, and epileptogenic bursts, *J. Neurophysiol.* **93**(4) (2005) 2194 -2232.

148. M. Ursino, G.E. La Cara and A. Sarti, Binding and segmentation of multiple objects through neural oscillators inhibited by contour information, *Biol. Cybern.* **89**(1) (2003) 56-70.

149. M. Ursino, M. Zavaglia, L. Astolfi and F. Babiloni, Use of a neural mass model for the analysis of effective connectivity among cortical regions based on high resolution EEG recordings, *Biol. Cybern.* **96**(3) (2006) 351-365.

150. M. Ursino, E. Magosso and C. Cuppini, Recognition of abstract objects via neural oscillators: Interaction among topological organization, associative memory and gamma band synchronization, *IEEE. T. Neural. Networ.* **20**(2) (2009) 316-335.

151. M. Ursino, F. Cona and M. Zavaglia, The generation of rhythms within a cortical region: Analysis of a neural mass model, *Neuroimage.* **52**(3) (2010) 1080-1094.

152. M. Ursino and G.E. La Cara, Modeling segmentation of a visual scene via neural oscillators: fragmentation, discovery of details and attention, *Network. Comp. Neural.* **15** (2004) 69-89.

153. F. Varela, J.P. Lachaux, E. Rodriguez and J. Martinerie, The brainweb: Phase synchronization and large-scale integration, *Nat. Rev. Neurosci.* **2**(4) (2001) 229-239.

154. F. De Vico Fallani, L. Astolfi, F. Cincotti, D. Mattia, A. Tocci, S. Salinari, M.G. Marciani, H. Witte, A. Colosimo and F. Babiloni, Brain network analysis from high-resolution EEG recordings by the application of theoretical graph indexes, *IEEE. T. Neur. Sys. Reh.* **16**(5) (2008) 442-452.

155. J. Virtanen, J. Ruohonen, R. Näätänen and R.J. Ilmoniemi, Instrumentation for the measurement of electric brain responses to transcranial magnetic stimulation, *Med. Biol. Eng. Comput.* **37**(3) (1999) 322-326.

156. D. Wang, Emergent synchrony in locally coupled neural oscillators, *IEEE. T. Neural. Networ.* **6**(4) (1995) 941-948.

157. X.J. Wang and G. Buzsáki, Gamma oscillation by synaptic inhibition in a hippocampal interneuronal network model, *J. Neurosci.* **16**(20) (1996) 6402-6413.

158. D. Wang and D. Terman, Image segmentation based on oscillatory correlation, *Neural. Comput.* **9**(4) (1997) 805-836.

159. L.M. Ward, Synchronous neural oscillations and cognitive processes, *Trends. Cogn. Sci.* **7**(12) (2003) 553-559.

160. P. Welch, The use of fast Fourier transform for the estimation of power spectra: A method based on time averaging over short, modified periodograms, *IEEE. T. Acoust. Speech* **15**(2) (1967) 70-73.

161. F. Wendling, J.J. Bellanger, F. Bartolomei and P. Chauvel, Relevance of nonlinear lumped-parameter models in the analysis of depth-EEG epileptic signals, *Biol. Cybern.* **83**(4) (2000) 367-378.

162. F. Wendling, F. Bartolomei, J.J. Bellanger and P. Chauvel, Epileptic fast activity can be explained by a model of impaired GABAergic dendritic inhibition, *Eur. J. Neurosci.* **15**(9) (2002) 1499-1508.

163. F. Wendling, A. Hernandez, J.J. Bellanger, P. Chauvel and F. Bartolomei, Interictal to ictal transition in human temporal lobe epilepsy: insights from a computational model of intracerebral EEG, *J. Clin. Neurophysiol.* **22**(5) (2005) 343-356.

164. J.A. White, C.C. Chow, J. Ritt, C. Soto-Trevino and N. Kopell, Synchronization and oscillatory dynamics in heterogeneous mutually inhibited neurons, *J. Comput. Neurosci.* **5**(1) (1998) 5-16.

165. J.A. White, M.I. Banks, R.A. Pearce and N.J. Kopell, Networks of interneurons with fast and slow gamma-aminobutyric acid type A (GABAA) kinetics provide substrate for mixed gamma-theta rhythm, *Proc. Natl. Acad. Sci. U.S.A.* **97**(14) (2000) 8128-8133.

166. M.A. Whittington, R.D. Traub and J.G. Jefferys, Synchronized oscillations in interneuron networks driven by metabotropic glutamate receptor activation, *Nature.* **373**(6515) (1995) 612-615.

167. M.A. Whittington and R.D. Traub, Interneuron diversity series: Inhibitory interneurons and network oscillations in vitro, *Trends. Neurosci.* **26**(12) (2003) 676-682.

168. H.R. Wilson and J.D. Cowan, Excitatory and inhibitory interactions in localized populations of model neurons, *Biophys. J.* **12**(1) (1972) 1-24.

169. J.J. Wright, C.J. Rennie, G.J. Lees, P.A. Robinson, P.D. Bourke, C.L. Chapman, E. Gordon and D.L. Rowe, Simulated electrocortical activity at microscopic, mesoscopic, and global scales, *Neuropsychopharmacol.* **28 Suppl 1** (2003) S80-93.

170. S.H. Wu, C.L. Ma and J.B. Kelly, Contribution of AMPA, NMDA, and GABAA receptors to temporal pattern of postsynaptic responses in the inferior colliculus of the rat, *J. Neurosci.* **24**(19) (2004) 4625-4634.

171. W. Wu and T. Chen, Impossibility of asymptotic synchronization for pulse-coupled oscillators with delayed excitatory coupling., *Int. J. Neur. Syst.* **19**(06) (2009) 425-435.

172. H.Z. Yin, S.L. Sensi, S.G. Carriedo and J.H. Weiss, Dendritic localization of Ca2+-permeable AMPA/kainate channels in hippocampal pyramidal neurons, *J. Comp. Neurol.* **409**(2) (1999) 250-260.

173. M. Zavaglia, L. Astolfi, F. Babiloni and M. Ursino, A neural mass model for the simulation of cortical activity estimated from high resolution EEG during cognitive or motor tasks, *J. Neurosci. Meth.* **157**(2) (2006) 317-329.

174. M. Zavaglia, L. Astolfi, F. Babiloni and M. Ursino, The effect of connectivity on EEG rhythms, power spectral density and coherence among coupled neural populations: Analysis with a neural mass model, *IEEE. T. Bio-Med. Eng.* **55**(1) (2008a) 69-77.

175. M. Zavaglia, L. Astolfi, F. Babiloni and M. Ursino, A model of rhythm generation and functional connectivity during a simple motor task: preliminary validation with real scalp EEG data, *Int. J. Bioelectromagn.* **10**(1) (2008b) 68-75.

176. M. Zavaglia, F. Cona and M. Ursino, A neural mass model to simulate different rhythms in a cortical region, *Comput. Intell. Neurosci.* **2010** (2010).

177. F.M. Zhou and J.J. Hablitz, AMPA receptor-mediated EPSCs in rat neocortical layer II/III interneurons have rapid kinetics, *Brain. Res.* **780**(1) (1998) 166-169.

SCIENTIFIC WRITING

1. PUBLICATIONS IN INTERNATIONAL JOURNALS

1. F. Cona, M. Zavaglia, M. Ursino, *"Binding and Segmentation via a Neural Mass Model Trained with Hebbian and Anti-Hebbian Mechanisms"*, accepted for publication in **International Journal of Neural Systems**.

2. F. Cona, M. Zavaglia, M. Massimini, M. Rosanova, M. Ursino, *"A neural mass model of interconnected regions simulates rhythm propagation observed via TMS-EEG",* published in **Neuroimage**, Agosto 2011, Volume 57 (3), pag 1045-1058.

3. M. Ursino, F. Cona, M. Zavaglia, *"The generation of rhythms within a cortical region: Analysis of a neural mass model",* published in **Neuroimage**, September 2010, Volume 52 (2010), pag 1080-1094.

4. M. Zavaglia, F. Cona, M. Ursino, *"A neural mass model to simulate different rhythms in a cortical region"*, published on-line in **Computational Intelligence and Neuroscience,** Volume 2010 (2010), Article ID 456140, doi: 10.1155/2010/456140.

5. F. Cona, M. Zavaglia, L. Astolfi, F. Babiloni, and M. Ursino, *"Changes in EEG power spectral density and cortical connectivity in healthy and tetraplegic patients during a motor imagery task"*, published on-line in **Computational Intelligence and Neuroscience**, 2009 June 24. doi: 10.1155/2009/279515.

2. CHAPTERS IN INTERNATIONAL BOOKS

1. F. Cona, M. Zavaglia., M. Massimini, M. Rosanova, M. Ursino "Computational Study of Rhythm propagation Induced by TMS stimuli in Different Brain Regions", in **Studies in Computational Intelligence**, in press.

3. CHAPTERS IN NATIONAL BOOKS

1. M. Ursino, F. Cona, M. Zavaglia. "Modelli di popolazioni e strutture neuronali, aree funzionali e loro connettività", in **Bioingegneria per le neuroscienze cognitive**, a cura di F. Babiloni, G. Baselli, A. Bertoldo, E. Biondi, C. Cobelli, pp. 129-152, Patron editore, Bologna 2009.

4. PUBLICATIONS IN PROCEEDINGS OF INTERNATIONAL CONFERENCES

1. M. Zavaglia, F. Cona, M. Ursino. *"Rhythms generation in a population of neurons simulated by a neural mass model"*, **Proceedings of 7th International Symposium on Noninvasive**

Functional Source Imaging of the Brain and Heart & 7th International Conference on Bioelectromagnetism, 29-31 May 2009, Rome (Italy).

5. ABSTRACTS IN PROCEEDINGS OF INTERNATIONAL CONFERENCES

1. F. Cona, M. Zavaglia, M. Rosanova, M. Ursino, *"Cortical rhythms induced by TMS stimulation: Analysis with a neural mass model",* **Proceedings of the 2nd International Conference on Neural Computation**, 24-26 October 2010, Valencia, Spain.

2. F. Cona, M. Zavaglia, M. Mirri, M. Rosanova, M. Ursino, *"Estimation of TMS by means of a neural mass model",* **Proceedings del Secondo Congresso Nazionale di Bioingegneria**, 8-10 July 2010, Torino, Italy.

3. F. Cona, M. Zavaglia, L. Astolfi, F. Babiloni, M. Ursino, *"Assessment of effective connectivity in healthy and tetraplegic subjects by using a neural mass model"*, **Proceedings of the IV International Conference on Computational Bioengineering**, 16-18 September 2009, Bertinoro (Forlì-Cesena), Italy.

4. M. Zavaglia, F. Cona, L. Astolfi, F. Babiloni, M. Ursino, *"Cortical connectivity estimation in healthy and tetraplegic patients during a motor imagery task"*, **Proceedings of the 15th Annual Meeting Human Brain Mapping**, 18–23 June 2009, San Francisco, USA, **NEUROIMAGE**, vol. 47, Suppl. 1, ISSN: 1053-8119.

6. AWARDS

1. Best Student Paper Award for *"Cortical rhythms induced by TMS stimulation: Analysis with a neural mass model"*, **2nd International Conference on Neural Computation,** 24-26 October 2010, Valencia, Spain.